Implementation of GFDM Transceiver using SDR for 5G Communication Systems

Submitted in partial fulfilment of the requirements
for the award of the degree
of

Doctor of Philosophy

by

Siva Prasad Valluri

(Roll No: 716142)

Under the supervision of

Dr. V. Venkata Mani

Associate professor

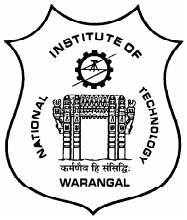

Department of Electronics & Communication Engineering

National Institute of Technology Warangal

Telangana, India - 506004

2020

Dedicated

To

My Family,

Teachers & Friends

Approval Sheet

This thesis entitled **Implementation of a GFDM Transceiver using SDR for 5G Communication Systems** by **Siva Prasad Valluri** is approved for the degree of **Doctor of Philosophy**.

Examiners

Research Supervisor

Dr. V. Venkata Mani
Associate professor
Department of ECE
NIT Warangal, India-506004

Chairman & Head

Prof. L. Anjaneyulu
Department of ECE
NIT Warangal, India-506004

Place:

Date:

Declaration

This is to certify that the work presented in this thesis entitled **Implementation of a GFDM Transceiver using SDR for 5G Communication Systems** is a bonafied work done by me under the supervision of **Dr. V. Venkata Mani** and was not submitted elsewhere for the award of any degree.

I declare that this written submission represents my own ideas and even considered others ideas which are adequately cited and further referenced the original sources. I understand that any violation of the above will cause disciplinary action by the institute and can also evoke panel action from the sources or from whom proper permission has not been taken when needed. I also declare that I have adhered to all principles of academic honesty and integrity and have not misrepresented or fabricated or falsified any idea or data or fact or source in my submission.

Place:

Date:

Siva Prasad Valluri
Research Scholar
Roll No.: 716142

NATIONAL INSTITUTE OF TECHNOLOGY

WARANGAL, INDIA-506004

Department of Electronics & Communication Engineering

CERTIFICATE

This is to certify that the thesis work entitled **Implementation of GFDM Transceiver using SDR for 5G Communication Systems** is a bonafide record of work carried out by **Siva Prasad Valluri** submitted to the faculty of **Electronics & Communication Engineering** department, in partial fulfilment of the requirements for the award of the degree of **Doctor of Philosophy** in **Electronics and Communication Engineering, National Institute of Technology Warangal, India-506004**. The contributions embodied in this thesis have not been submitted to any other university or institute for the award of any degree.

Dr. V. Venkata Mani
Research Supervisor
Associate Professor
Department of ECE
NIT Warangal, India-506 004.

Place:
Date:

Acknowledgements

First and foremost, I want to thank my research supervisor, Dr. V. Venkata Mani for her continuous guidance, encouragement and constant support throughout my research work. I feel very happy, privilege and pleased to be work with her, who is having lot of knowledge, energy, passion and potential in the area of wireless communication, which helped me to develop fundamental concepts on multicarrier techniques. She is the one whom I look up to as a role model, for inspiration, admiration and seek suggestions at various stages of this duration, at both technical and personal level. She always boosts my confidence, extends my wings in understanding the concepts, foresees my capabilities, spends countless hours and adds every little information to extend my boundary limits. I couldn't imagine a better supervisor than her to complete successfully my PhD work. My sincere thanks to chairman of the Doctoral Scrutiny Committee (DSC) and Head of the department Prof. L. Anjaneyulu for his invaluable advices, motivation and insightful comments at various stages of this work. I would also like to thank the DSC members, Prof.D. Srinivasacharya (Department of Mathematics) and Prof. N. Bheema Rao (Department of Electronics & Communication Engineering) who has always driven me with their constructive suggestions, fruitful discussions and thought provoking words through out my doctoral studies. I extend my thanks to all the faculty members of the Department of ECE and non-teaching staff for their support.

I have been extremely happy to have some of the incredible people in Wireless Communication Research Laboratory, Dr. Sai Krishna Kondoju, Dr. Shravan kumar bandari, Kishore Vejandla, Ganesh Miriyala and Suseela Vappangi whose friendship is truly valuable, always having a healthy technical debates and having enjoyable non-technical aspects as a refreshment. My deepest thanks to all the teachers having their blessings and school friends who are constantly in touch with me, wishes me to achieve great heights,

giving financial help and supporting all events in my life. I also want to acknowledge anonymous reviewers for taking their valuable time to evaluate this thesis and suggesting improvements.

Whatever I accomplish its only because of my parents everlasting love, blessings, support and care. A simple 'thank you' is not just good enough to show my immense love, gratitude towards them and no words to express my gratefulness to them, I wish them a good healthy life ahead. I want to thank my grandfather Siva Prasad Valluri, grandmother Venkata Lakshmi, brother Sai Kiran, father Bapiraju and other family members for there unwavering support throughout my education, endless love, understanding my goals and for being my side throughout my ups and downs, which kept me to move forward. Finally, thanks to God for giving me an opportunity to meet all this wonderful people and giving me this life with warm memories

Siva Prasad Valluri

Abstract

Nearly sixty two percent of today's population worldwide are inhabitants with mobile phones, which clearly indicates it's influence on human life. Interestingly, more than half of the used handsets are '*smart*' devices too, so the demand for fast internet experience is increasing day by day. Apart from high data rate, fascinating applications without human interaction like Machine Type Communication (MTC), Internet of Things (IoT) are envisioned for the next generation of wireless communication. These applications demand low power, low latency and asynchronous data transfer. This lead to the investigation of new physical-layer waveforms where plethora of alternative waveforms are investigated.

Generalized Frequency Division Multiplexing (GFDM) is one of the primary contender with flexible block structured multicarrier scheme featuring with low Out Of Band (OOB) radiation and high spectrum efficiency. The key idea of GFDM is to filter every subcarrier with a well-localized user desired prototype filter to reduce the effect of OOB. There are various approaches suggested for its analysis via simulations but testing in real time environments is necessary for its standardization. Traditional data aided methods of synchronization directly adopted from fourth generation avoid the effect of egress noise in pilot preamble, destroying its spectral advantage. To safeguard this advantage, preamble needs to be pulse shaped. In this thesis, the derivation for generalized Maximum Likelihood (ML) estimation of frequency and time offsets for receiver synchronization in GFDM systems, using the modified preamble by the application of matrix inversion lemma is derived. The dependency of the choice of the filter on Cramer Rao Lower Bound (CRLB) of frequency offset estimation is also emphasized. After preamble aided synchronization, this thesis enlightens various aspects in real-time implementation of blind GFDM signal transceiver using oversampling for Carrier Frequency Offset (CFO)

correction in indoor environments. It is observed that, the phase shift between neighbouring sample points in an oversampled GFDM symbol is constant throughout the symbol duration. This phase shift is found to be unassociated with either subcarrier or subsymbol indices. Using this property, the ML estimate of the CFO is deduced and is analysed in various channel environments. The CRLB for the oversampling based GFDM signal model is derived and we demonstrate through simulation that, the proposed algorithm results in a little error floor. The results obtained in simulations have been validated with real-time test bed built with USRP 2953R as hardware and LabVIEW as software.

Additionally, the flexible nature of GFDM leads to superimposition of multiple subsymbols in time domain, the consequence of which is high Peak-to-Average-Power Ratio (PAPR). Selected Mapping (SLM) is one of the prominent PAPR reduction techniques in GFDM, which uses bank of modulation matrices to generate a set of alternative signal representations. This procedure increases the complexity of the GFDM system enormously. In this contribution, we utilize the concepts of conversion matrices and linearity to achieve low complexity with respect to the modulation matrices in the conventional SLM method. By using the proposed conversions we evolve at three modified SLM schemes which have much lower complexity. SLM procedure requires mandatory Side Information (SI) estimation or transmission which in turn decreases data reliability or efficiency. To address these issues, this thesis presents a modified approach of pilot-assisted GFDM SLM system without the need of SI transmission and estimation to enable joint PAPR reduction and data recovery. In the proposed approach, we utilize a common modulating phase to modulate all subcarriers in a subsymbol assuming that each subsymbol consists of at least two pilots. This creates an inherent SI cancellation mechanism using the pilots which are employed for channel estimation.

Recently the usage of deterministic sequence, named as Unique Word (UW), instead of well known cyclic prefix (CP) is introduced for one of the promising contenders of 5G physical layer i.e., GFDM. The primary motive behind introduction of UW is to exploit the correlations in frequency domain which results in coding gain. However, perfect Symbol Time Offset (STO) compensation is a prerequisite and is the first task to be done. A blind metric for the estimation of STO using the structure of UW-GFDM system without requirement of pilot symbols presence in UW positions, is proposed in this work. The

developed algorithm can blindly estimate the block duration, symbol duration, number of redundant subcarriers and number of subcarriers. The obtained simulation results verify the feasibility of the proposed algorithm in various channel conditions. The real time transmission of Multi-taper Generalized Frequency Division Multiplexing (MGFDM) is carried out using Software Defined Radio (SDR) by implementing various channel estimation and synchronization algorithms. We employed all the correction algorithms using a windowed preamble to satisfy low OOB requirements. However, the high speed performance of MGFDM system is heavily effected by jitter noise, since it results in improper sampling instances. This contribution underlines the jitter noise power reduction using oversampling with the supported mathematical expressions and simulations. We observed that the integer oversampling would mitigate the noise power in linear fashion by increasing the sampling rate. In short, this thesis deals with the important physical layer issues associated with GFDM and its variants using simulations, analysis and experiments.

Contents

List of Figures

List of Tables

List of Abbreviations / Acronyms

ACLR Adjacent Channel Leakage Ratio

ADC Analog to Digital Converter

AMC Adaptive Modulation and Coding

AWGN Additive White Gaussian Noise

BER Bit Error Rate

CA Carrier Aggregation

CFO Carrier Frequency Offset

CMOS Complementary Metal Oxide Semiconductor

CP Cyclic Prefix

CP-OFDM Cyclic Prefix Orthogonal Frequency Division Multiplexing

CRLB Cramer Rao Lower Bound

CRS Cell-Specific Reference Signals

CoMP Coordinated Multi Point

DAB Digital Audio Broadcasting

DAC Digital to Analog Converter

DPSS Discrete Prolate Spheroidal Sequence

DSP Digital Signal Processing

DVB-T DVB-Terrestrial

FBMC Filter Bank Multi-Carrier

FDD Frequency Division Duplexing

FFT Fast Fourier Transform

FPGA Field Programmable Gate Array

GFDM Generalized Frequency Division Multiplexing

ICI Inter Carrier Interference

IF Intermediate Frequency

IFFT Inverse Fast Fourier Transform

IoT Internet of Things

ISI Inter Symbol Interference

LTE Long term Evolution

LTE-A Long term Evolution Advanced

MC Multicarrier

MCS Modulation and Coding scheme

MGFDM Multi-taper Generalized Frequency Division Multiplexing

MHz Mega Hertz

MIMO Multiple Input Multiple Output

ML Maximum Likelihood

MSE Mean Square Error

MTC Machine Type Communication

NI National Instruments

OFDM Orthogonal Frequency Division Multiplexing

OFDMA Orthogonal Frequency Division Multiple Access

OOB Out Of Band

OQAM Offset Quadrature Amplitude Modulation

PAPR Peak-to-Average-Power Ratio

PLC Power-Line Communication

PLL Phase Lock Loops

PRBs Physical Resource Blocks

PSS Primary Synchronization Signal

PTS Partial Transmit Sequence

RF Radio frequency

RN Relay Nodes

RRC Root Raised Cosine

SC-FDMA Single Carrier-Frequency Division Multiple Access

SDR Software Defined Radio

SI Side Information

SISO Single Input Single Output

SLM Selected Mapping

SSS Secondary Synchronization Signal

STO Symbol Time Offset

TDD Time Division Duplexing

TV Television

UHF Ultra high frequency

USRP universal software radio peripheral

UW Unique Word

UW-GFDM Unique Word Generalized Frequency Division Multiplexing

VDSL Very-high-bit-rate DSL

VI Virtual Instrument

VNI Visual Network Index

WLAN Wireless Local Area Network

WiMAX Worldwide Interoperability for Microwave Access

WRAN Wireless Regional Area Network

ZP-OFDM Zero Padded Orthogonal Frequency Division Multiplexing

3G Third Generation

4G Fourth Generation

5G Fifth Generation

Chapter 1

Introduction

To satisfy everlasting human needs, various generations of wireless communication provided improved performance in terms of data rates, connection density, security and latency. In earlier generations of communication, the primary issue with mobile radio transmission is to combat the channel induced distortions in the received signal in a frequency-selective propagation environments [1]. This occurs because the transmitted radio waves not only travels over a line of sight but also in scattering, reflections in the vicinity of the receiving antenna. Reflected waves may add destructively, causing the received signal to disappear or become heavily attenuated at certain locations. This effect is often termed as fading. Moreover, waves excessively delayed by remote reflections cause distortion of the shape of transmitted waveforms.

Historically, single carrier modulation can be noted as a well known way of transmitting data serially. It is an important choice specially in uplink transmission due to its low Peak to Average Power Ratio (PAPR) when compared to Multicarrier (MC). However, over the past two decades there is an enormous development in both wireline and wireless communication applications especially with the usage of MC modulation schemes. MC modulation systems are the systems that split up a wideband signal at a high symbol rate into a number of lower rate signals through the use of suitable pulse-shaping filters. Each one of the lower rate signals occupies a narrower bandwidth and has its own associated carrier [2]. In other words, a MC system splits a total bandwidth into chunks of narrow sub-channels whose bandwidth is much lesser than coherence bandwidth of the channel. This allows the channel to be relatively flat fading and hence immune to Inter Symbol

Interference (ISI) [3].

The Fourth Generation (4G) communication systems used the MC and the concept of single tap equalization for combating frequency selective channels. As a result, nowadays the most quoted critical issues of wireless systems are no longer directly related to multipath fading, but are

- The scarcity of radio spectrum and the resulting mutual interference among users
- The power consumption of portable terminals and the inadequacy of existing battery and other energy storage technologies
- The complexity of the software needed to support user mobility, e.g. from cell to cell or from operator to operator.

In applications perspective, the first four generations of wireless communications concentrated on improving the human interaction in terms of voice and data. As a first step, this chapter introduces the evolution of wireless communication and will define the problem statements one of the 5G physical layer waveform named Generalized Frequency Division Multiplexing (GFDM) [4].

1.1 Review of physical layer for 4G communication systems

In 2009, 4G wireless standard was introduced with a peak speed of 100 Mbps. The Long term Evolution (LTE) service was opened in Stockholm and Oslo in December 14, 2009 [5]. LTE supported both Time Division Duplexing (TDD) and Frequency Division Duplexing (FDD) with the possibility to have carrier bandwidths varying between 1.4 Mega Hertz (MHz) and 20MHz by supporting six different modes ($1.4, 3, 5, 10, 15$ or 20MHz) with utilized frequency bands ranging from 700MHz to 2600MHz [6]. LTE used Orthogonal Frequency Division Multiple Access (OFDMA) technique (for downlink) and Single Carrier-Frequency Division Multiple Access (SC-FDMA) (for uplink) for communication. Additionally, sophisticated scenarios like Adaptive Modulation and Coding (AMC) and spatial multiplexing are used for adverse channel conditions. LTE systems could achieve high data rates of 75Mbps for uplink communication and a data rate of 300Mbps for

downlink scenarios. With usage of Digital Signal Processing (DSP) chips the bandwidth utilization is maximised in the available radio frequency spectrum [7]. In order to achieve this, lot of credit should be given for the adopted physical layer multi-carrier technique. This is because Orthogonal Frequency Division Multiplexing (OFDM) uses the concept of division of high baud rate signals into multiple signals with the usage of simple Inverse Fast Fourier Transform (IFFT) implementation. By using this approach scientists were able to achieve spectral efficiency and scheduling in the available precious time-frequency resources.

The fundamental idea of OFDM is to chunk the available RF spectrum into small parts such that each part experience flat fading. This leads to easy channel equalization at the receiver [8]. In order to obtain high spectral efficiency the frequency response of all the overlapping sub carriers are adjusted with maintaining the orthogonality, hence the name OFDM. Various versions of OFDM are available in the literature but the Cyclic Prefix Orthogonal Frequency Division Multiplexing (CP-OFDM) is the commercially used as a physical layer technique in 4G systems. The Cyclic Prefix (CP) is nothing but the part of the OFDM signal appended at the start of the transmission packet. The introduction of CP makes the OFDM signal periodic and in turn aids the receiver with the possibility of single tap equalization. Two main aspects which attracted industries to consider OFDM as the foremost technique are easy implementation and single tap equalization [9]. The first advantage is achieved due to utilization of simple DSP chips which can process Fast Fourier Transform (FFT) operations at both transmitter and the receiver. Secondly, due to the presence of concept of CP the complexity present in the channel equalization is minimized and thereby reducing the complexity at the receiver which was a serious concern in Third Generation (3G) communication [10].

1.2 Introduction to OFDM

A Pseudo noise generator is used for obtaining a random bit stream which are mapped into complex symbols using a QAM modulator. In OFDM modulator, the serial input complex QAM data is converted into parallel followed an N-IFFT operation [11]. After performing IFFT, the parallel data is converted back to serial data to obtain OFDM

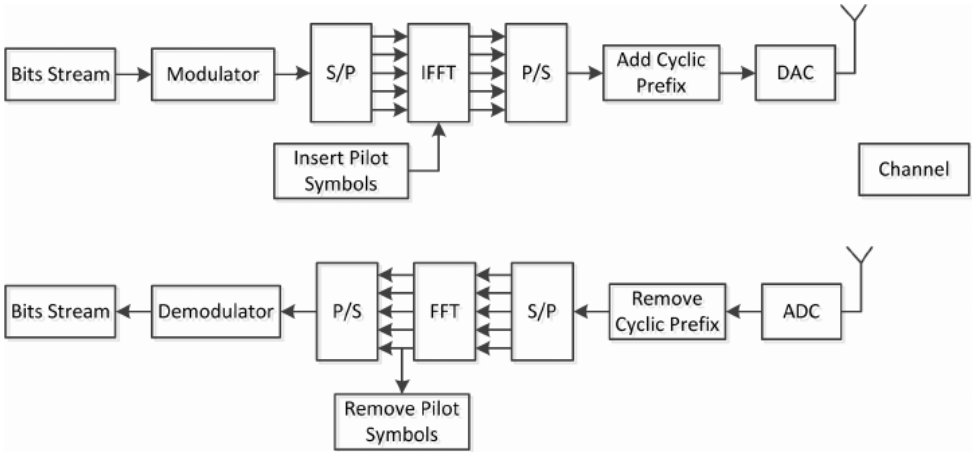

Figure 1.1: Block diagram of OFDM transmission System

signal. Mentioned earlier, for converting the linear convolution into circular an extra CP ia added at the start of the OFDM packet [12]. This reduces the effect of ISI and Inter Carrier Interference (ICI) [13]. For estimation of the channel response and the synchronization errors like STO and Carrier Frequency Offset (CFO) pilots are added at the transmitter as shown in Figure 1.1. The OFDM signal can be formulated as,

$$x(n) = \sum_{k=0}^{N-1} \mathbf{X}(k) e^{\frac{j2\pi kn}{N}} \tag{1.1}$$

for $n = 0 \leq n \leq N-1$ and k is denoting the subcarrier index and n is showing the time index. $X(k)$ is showing the QAM modulated signal generated after bit mapping.

Another important advantage of OFDM is, its easy adaptiveness to Multiple Input Multiple Output (MIMO) environments. The extension of Long term Evolution Advanced (LTE-A) focussed on increasing capacity range for achieving better data rates to end users. Various approaches like Carrier Aggregation (CA), MIMO, Relay Nodes (RN) and Coordinated Multi Point (CoMP) are utilized. As an example, CA introduced the feature of aggregating different sub carriers with intelligent spacing. This idea provided the network operators not only with higher mobile data transmission speed but also helped in increasing the capacity of the network. Practically, a maximum bandwidth of 100MHz is achieved in FDD transmission by aggregation of 5 carriers with each carrier extending up to 20MHz. To further improve the performance a decisive adjustment with introduction of spatial multiplexing is present in LTE-A standard. Typically, 8×8 MIMO and 4×4 MIMO are allowed for uplink and downlink communication. Due to

effective exploitation of the spatial dimension the desired target of 100 Mbps is reached at the cost of size and complexity. An effective implementation using the DSP chips by avoiding the traditional bank of modulators and demodulators droved the researchers to adopt OFDM in main wireless standards like Wireless Local Area Network (WLAN) (IEEE 802.11a/g), Wireless Regional Area Network (WRAN) (IEEE 802.22), Worldwide Interoperability for Microwave Access (WiMAX) (IEEE802.16), LTE, Very-high-bit-rate DSL (VDSL), Power-Line Communication (PLC), Digital Audio Broadcasting (DAB) and DVB-Terrestrial (DVB-T).

1.3 Summarizing pros of OFDM

- Eliminates complex oscillators with simple FFT blocks to implement modulation and demodulation.
- Immune to frequency selective channels
- Good protection to interferences using guard intervals
- Simpler channel equalization techniques.
- Efficient use of spectrum.
- Allows pilot subcarriers for channel estimation
- Efficient Broadcasting: Multiple base stations can synchronize to combine their transmitted signals enabling higher broadcast data rates.

More importantly, OFDM utilizes the scarce spectrum resource more efficiently by allowing to overlap the frequency spectrum of every subcarriers of the transmitted signal as shown in the Figure 1.2. After the advent of OFDM, a predominant technique, widely accepted in 4G uses simple FFT algorithms for its generation and created a single tap equalization scenario and adds some part of the data packet as CP to combat interference resulted from frequency selective channels.

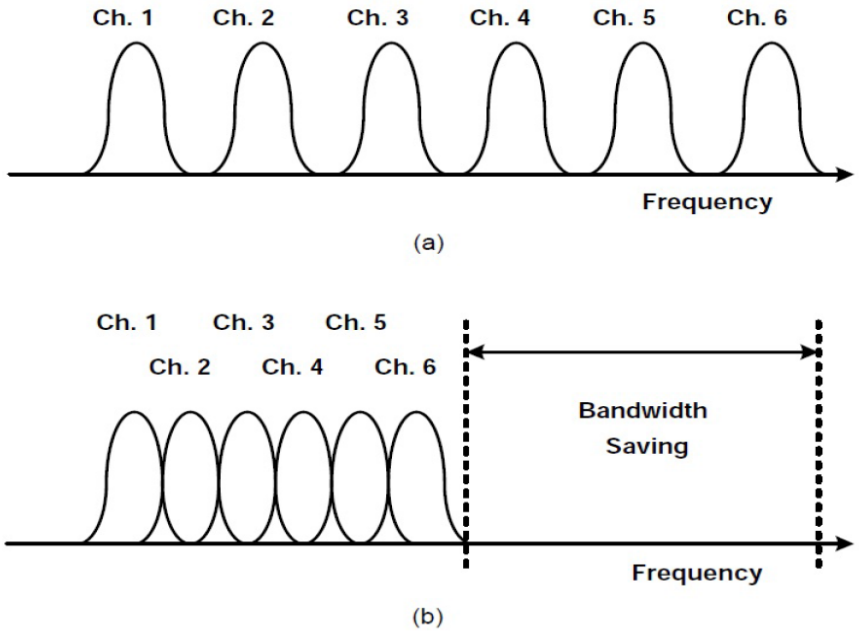

Figure 1.2: Spectral advantage of OFDM System

1.4 Demerits of OFDM

Despite of the above mentioned advantages of OFDM, it cannot be used for the next generation wireless standards. It is a irony that the every advantage of OFDM is achieved at the snag of another requirement of the 5G systems [14]. The exact reasons are detailed below:

- The simple implementation is achieved by FFT algorithms at both the transmitter and receiver. For IFFT of large size, summation of several in phase subcarriers would lead to a high peak in the resultant OFDM signal. This would lead to high PAPR, which would require a high power amplifier. This demerit provides transmitter with option to either allow amplitude distortion or to have high power amplifier to compensate the effect. This is prominent especially in uplink scenarios when the user equipment is transmitting data to the mobile station. This is main hurdle for various 5G applications [15].

- The above mentioned advantages of OFDM occur at the cost of strict orthogonality, which forces the subcarriers components to utilize rectangular filters. This scenario result in Ingress (In band) and Egress (out of band) noises. Though Ingress noise is a concern for long distance transmission modern receiver structures were able to

combat this impairments to a large extent. However, the Egress noise is a serious concern and is the major reason for not achieving low latency and high bandwidth efficiency by using OFDM as physical layer technique. Let us consider LTE release 10 as an use case to explain the above scenario. In the 20 MHz bandwidth mode LTE will perform 2048 IFFT at the transmitter where only 1200 subcarriers considered as active since OOB radiation may cause Egress noise to neighbouring symbols. In fact, the remaining subcarriers are kept to recompense these unnecessary emissions. All the 1200 subcarrier are further divided into 100 Physical Resource Blocks (PRBs), where every PRBs has 12 subcarriers. Ingress noise occurs among these PRB would result in ICI and has to be compensated with complex procedures in the receiver. The power spectral density comparisons between the OFDM and GFDM is depicted in the Figure 1.3. We can clearly observe that, an minimum OOB of 38dB occurs due to the circular prototyping filters in the GFDM system. This is around 20dB less when compared with the traditional OFDM system. This characteristic of GFDM system makes it suitable technique for scrambled spectrum applications. Hence, with the scarcity of RF spectrum, we need to shift our focus to GFDM instead of OFDM for effective spectrum utilization.

- Another concern is, maintenance of strict orthogonality would require significant amount of payroll data for Primary Synchronization Signal (PSS), Cell-Specific Reference Signals (CRS), Secondary Synchronization Signal (SSS) etc.,. This motivated, the next generation communication system to envision non-orthogonal waveforms with prototype filtering (to avoid rectangular filtering) for handling the above mentioned errors.

- Typically 25 percent of the signal is added as CP in the traditional CP-OFDM. Hence the power used for transmitting CP would decrease in power efficiency. To handle this issue another idea is to insert zeros, which was named as Zero Padded Orthogonal Frequency Division Multiplexing (ZP-OFDM). In addition, adding a CP for every OFDM signal would reduce the spectral efficiency since CP doesn't carry any useful information.

Figure 1.3: Spectrum comparison between OFDM and GFDM

1.5 Introduction to 5G

Fifth Generation (5G) shall be necessary globally owing to the accumulating market of data and video streaming in present time. The available 4G technology cannot satisfy the requirements of the increasing needs of mobile internet. As such, 5G has no specific definition [16], but, we consider 5G in actual terms and attain clarity of definition of 5G in technological sense. Basically, the first four generations of communication can be summarized in a shortly as "*improvements in human interaction in terms data and video traffic*". 5G probably can be considered a new way for thinking about communication. It comprises of many "dream projects" like performing machine to machine communication which is broader sense can be called as IoT [10]. 5G also aims at providing an organised applications for installing services in order increase its elasticity. It includes the capability to provide services at any place, time, and anything, for meeting the changing requirements of public and businesses organisations.

5G technology intend to improve the achieved technological progress by utilizing the present wireless communication systems. The reciprocal ideas like utilization of cloud and core technologies in order to serve higher data transmission rates is an key aspect for this generation. The estimated requirements of 5G technology are:

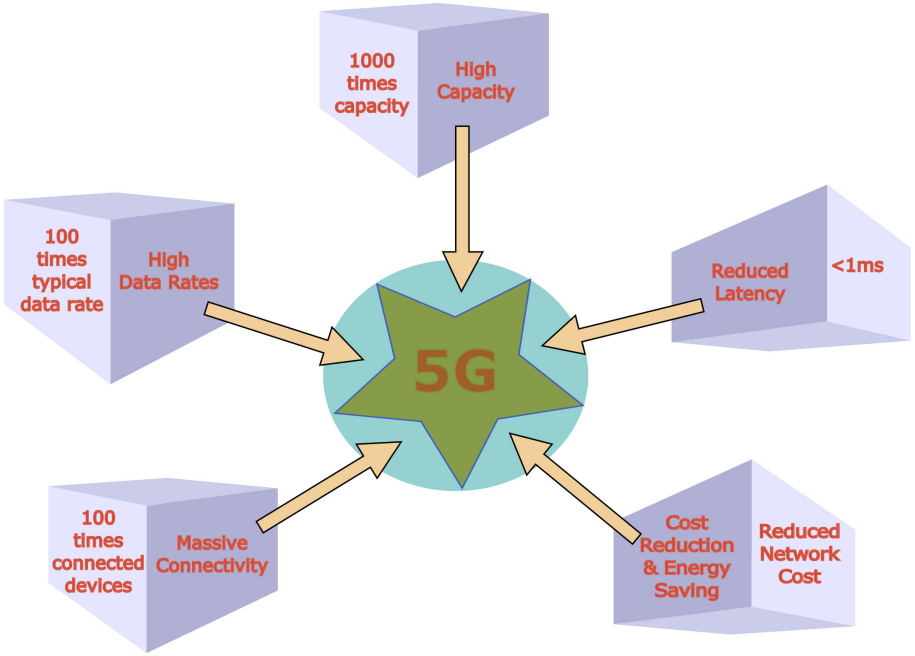

Figure 1.4: 5G Requirements

- 10-100 times higher practical data rate
- 1000 times of mobile data volume per area
- 10-100 times increment in the number of devices connected
- 10 times battery life for low-power devices
- Five times reduction in latency

To attain the above target, the physical layer of next generation communication is expected to have the succeeding attributes:

- Flexible and smart
- Intelligent spectrum management
- Reduction in cost and efficiency
- Ability to connect billions of devices
- Amalgamate with antecedent and contemporary technologies

5G networks need to include various previous generation features like LTE and also support high number of users than previous networks as shown in Figure 1.4. Some researchers argue that, considering the simple implementation strategy of LTE, there is no need for an obsessive desire of going to new generation. However, the summit Visual Network Index (VNI) has denied this argument and suggested depending on advances of 4G shall not meet the everlasting need of the mobile users. This lead to discovery of various technologies for 5G communication [17].

1.6 Key Technologies for 5G

1.6.1 Architectural Innovation

One idea for next generation communication is to develop device centric architecture to truncate the load used for establishing links. It is envisaged to utilize minimal control signals for improving the routing capability and in turn reducing the base stations. By reducing the base stations the amount of overhead on the payroll data decreases leading to better performance. These organised networks would provide efficient usage of spectrum and energy. On the other side, an intelligent cellular networking with careful management of radio resource has to be done to achieve the gains as discussed. The primary issues in developing these networks are

- User cooperation
- Handling crowded environments
- Channel estimation for different devices
- Hardware complexity

1.6.2 Millimetre wave

The terahertz (THz) band is described with the frequency between 0.3 and 10 THz. However, due to expensive signal generation sources for radiation, this band was not considered for transmission. With the emergence of optical technology and Complementary

Metal Oxide Semiconductor (CMOS) as generation sources interest toward THz band communication has escalated. The Radio frequency (RF) technologies developed until the 4G concentrated at a maximum frequency ranges of 6GHz. A fair amount of researchers argue that to increase in bandwidth can be achieved by shifting this range to around 60Ghz [18]. Rapport, supported this argument by demonstrating the transmission system from 800 MHz to 2 GHz. Primarily, (28-30)GHz and (37-40)GHz are considered as for testing its capability for 5G communication [19]. The main challenges in its implementation are,

- Skin depth becomes a challenge for waveform transmission at this high frequency
- Blockage due to skyscrapers, moving objects make the channel design very difficult when compared with traditional RF design
- Complex methodologies like Modulation and Coding scheme (MCS) will be mandatory for small distance communication since for Millimetre wave transmission line of sight transmission becomes very important.

1.6.3 Massive MIMO

Massive MIMO systems is one of the next generation alternative whose implementation involves with substantial increment in the number of antennas when compared to the available LTE-standard. This strategy would increase the directivity and eventually the probability of occurance of interference is reduced [20]. Massive MIMO technology is growing technology due to its better performance over conventional especially for point to point communication [21]. The base stations are inserted with many antennas in Massive MIMO systems for proving productive energy even across the boundaries of the cell. Massive MIMO is massive in terms gain, and is intended to provide flexibility. However, the main implementation issues are

- Sophisticated antenna transmission strategies
- Size miniaturization
- System complexity

1.6.4 Physical layer waveforms

Although Moore's Law in its basic form is running to the limits of device sizes, other techniques are being developed that mean the spirit of Moore's Law is able to continue and to further increase the processing capability. As such new 5G waveforms that require additional processing power, but are able to provide additional advantages are still viable. The potential applications for 5G including high speed video downloads, gaming, car-to-car / car-to-infrastructure communications, general cellular communications, IoT/M2M communications and the like, all place requirements on the form of 5G waveform scheme that can provide the required performance. Some of the key requirements that need to be supported by the modulation scheme and overall waveform include: Capable of handling high data rate wide bandwidth signals, able to provide low latency transmissions for long and short data bursts, i.e. very short Transmission Tine Intervals are needed. There is a lot of exploration in the research community for the search of an alternate and flexible multicarrier waveform where plethora of waveforms are proposed. The objective of all the waveforms is to address the shortcomings of OFDM without disturbing its advantages. We can broadly categorize them as Filter Bank Multi-Carrier (FBMC) systems. To detail, the researchers have come to a conclusion that, filtering is a mandatory for avoiding the unnecessary OOB emissions. Fundamentally the pulse shaping is done in two ways, namely linear pulse shaping and circular pulse shaping.

The principle of FBMC is to perform linear pulse shaping across every subcarrier and these systems relies on the fact that filter can span over all the symbols. FBMC systems are not only resistant to time and frequency misalignments but also achieve high suppression of OOB emission. On the other side, due to the linear nature of pulse shaping, ramp up and ramp down are required compulsorily at the start and the end of the packet. This results in high loss of latency and resources. Additionally, due to pulse shaping an self interference occurs between the subcarriers and subsymbols leading to high Bit Error Rate (BER). By using the techniques like Offset Quadrature Amplitude Modulation (OQAM) this can be reduced and the orthogonality can be improved. Interestingly, the circular prototyping filters use the concept of tail biting by which they don't require the transients and hence can achieve low latency. In this thesis we analyse the analysis of this circular FBMC, which was proposed with the name GFDM [22].

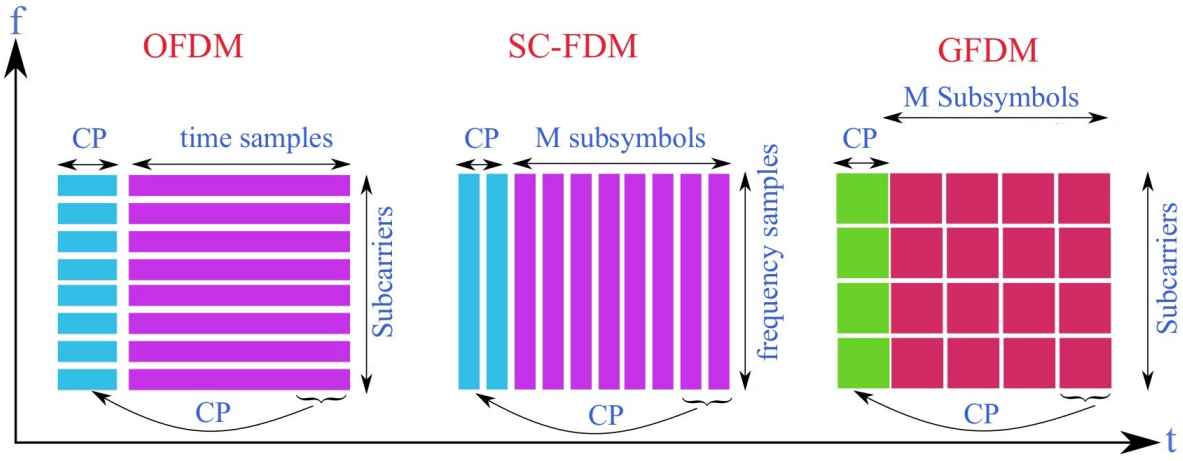

Figure 1.5: Generalized nature of GFDM

GFDM, a non-orthogonal multi carrier transmission and is one of the befitting replacement of OFDM proposed by Fettweis et al. [23]. It used a prototype filter with more time and frequency containment for pulse shaping with circular convolution. GFDM is a rectangular grid structure with M subsymbols in time and K subcarriers across frequency axis. Hence a flexible time frequency grid structure will be available for the design of GFDM systems. The pulse shaping filter in GFDM is appropriately chosen in such a manner that, it is having better decaying nature in frequency domain in contrast to OFDM which results in the larger OOB emission due to the usage of rectangular filtering. By the removal of tail in the circular pulse shaping mechanism low latency is achieved. As stated in the cons of OFDM, inclusion of CP for each symbol in an OFDM frame will lead to spectral inefficiency, whereas, in GFDM single CP is appended for the whole GFDM frame which consists of several symbols. In this context, GFDM reduces the CP overhead and poses to feature a better spectral efficiency and the same includes CP for a complete frame. GFDM is a special block based multicarrier technique covering both OFDM and Single Carrier (SC)-Frequency Division Multiplexing (FDM) as corner cases. Hence, GFDM can be reduced to the present 4G communication system as special cases. GFDM reduces to OFDM with $M = 1$ and rectangular pulse shaping, and to SC-FDM with $K = 1$ as shown in Figure 1.5. Hence, the generalized FDM is given for GFDM. Notationally, $\mathbf{d_k} = [d_k(0) \cdots d_k(M-1)]$ symbolizes the data on the k^{th} subcarrier, while $\mathbf{d} = [\mathbf{d_1}\ \mathbf{d_2}\ \cdots\ \mathbf{d_k}]$ represents the data vector of length MK [22]. Upon clear observation, the data which is to be GFDM modulated using subcarrier representation can be

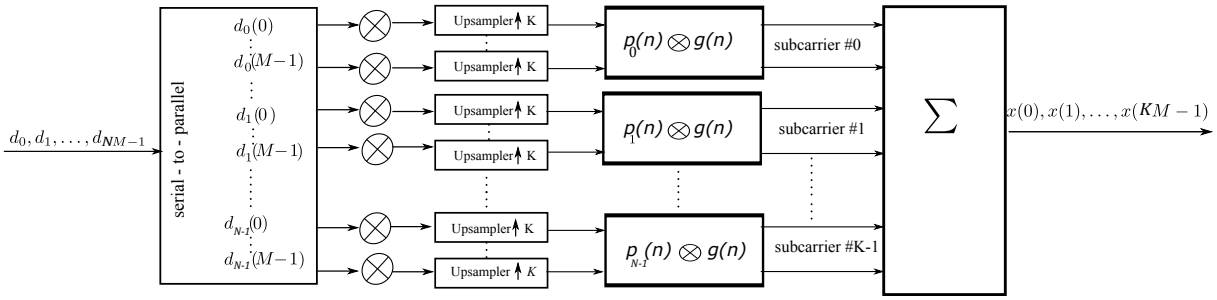

Figure 1.6: The steps involved in the design of GFDM transmitter

interchangeably used as,

$$\mathbf{d_k}(n) = \mathbf{d}(kM + n) \tag{1.2}$$

In the first step the data on every k^{th} subcarrier is upsampled by an amount of K.

$$p_k(n) = \sum_{m=0}^{M-1} d_k(m)\delta(n - mK) \tag{1.3}$$

In other words, (1.3) can be alternatively represented as,

$$p_k(n) = \begin{cases} d_k(m) & n = Km \\ 0 & \text{otherwise} \end{cases} \tag{1.4}$$

where $m = 0 \cdots M-1$. The obtained upsampled data on every subcarrier using the above step is circularly convolved with a user desired prototype filter of choice (generally RRC), $g(n)$ which extends to a long length of KM. Next, the circularly convolved data of every subcarrier is unconverted to its corresponding frequency and finally, amalgamating all the signal processing operations the GFDM symbol is given by,

$$\begin{aligned} x(n) &= \sum_{k=0}^{K-1} (p_k(n) \odot g(n)) e^{j\frac{2\pi kn}{K}} \\ &= \sum_{k=0}^{K-1} \sum_{m=0}^{M-1} d_k(m) g\left\{(n - mK) \text{mod} MK\right\} e^{j\frac{2\pi kn}{K}} \end{aligned} \tag{1.5}$$

where $\odot$ represents the circular convolution utilized to obtain the GFDM signal $x(n)$ as shown in the Figure 1.6. The simplified matrix form of generation of the GFDM system is given is given by [24],

$$\mathbf{x} = \mathbf{Ad}. \tag{1.6}$$

The matrix $\mathbf{A}$ is modulation matrix of size $N \times N$ representing all the necessary signal processing operations. The data vector $\mathbf{d} = [d_0(0) \cdots d_0(M-1) \cdots d_{K-1}(M-1)]^T$ consists of all the QAM modulated data symbols. Here, T in superscript represents the transpose of a matrix.

$$\mathbf{A} = [\mathbf{G} \quad \epsilon_\mathbf{1}\mathbf{G} \quad \cdots \quad \epsilon_{\mathbf{N-1}}\mathbf{G}] \tag{1.7}$$

where $\mathbf{G}$ is an $MK \times M$ matrix with its first column containing all the samples of the pulse shaping filter g. Remaining columns are obtained by circularly shifting its previous column by an amount of N. $\epsilon_\mathbf{1} = \text{diag}\{[\mathbf{e_i}^T, \cdots \quad \mathbf{e_i}^T]^T\}$ is an $MK \times MK$ diagonal matrix which consists of M concatenation of the vector $\mathbf{e_i} = [1, e^{\frac{2\pi i}{N}}, \cdots e^{\frac{2\pi(N-1)}{N}}]$. For understanding the concept, let us consider the number of subcarriers and subsymbols then the modulation matrix can be reduced into

$$\mathbf{A} = [\mathbf{G} \quad \epsilon_\mathbf{1}\mathbf{G}] \tag{1.8}$$

$$\mathbf{G} = \begin{bmatrix} g_0 & g_2 \\ g_1 & g_3 \\ g_2 & g_0 \\ g_3 & g_1 \end{bmatrix} \tag{1.9}$$

Hence, the modulation matrix $\mathbf{A}$ is having block circulant nature due to the usage of circular prototyping filter in its generation. On the other side, the presence of flexible structure increases the complexity of GFDM system. However, with the evolution in electronics technology, the GFDM scheme can be implemented by using a customizable Field Programmable Gate Array (FPGA) with lesser effort.

1.6.5 Variants of GFDM

Due to circular prototyping, all the drawbacks of the OFDM are addressed but at the cost of destroying the orthogonality of the system. This introduced the self interference between the subcarriers of the GFDM signal which lead to high BER [25]. Additionally, the rectangular grid structure offered flexibility to the GFDM system by increasing receiver complexity. Hence, self interference and high computational complexity are the

main disadvantages of GFDM system. To solve this problem two variants of the GFDM are proposed which are described in the following sub sections.

MGFDM

The MGFDM aimed at improving the orthogonality of the system by using Discrete Prolate Spheroidal Sequence (DPSS) or multitapers as prototype filters. multitapers are an orthogonal basis function with better localization in time and frequency than the traditional RRC filters. These filters feature lower OOB, PAPR, BER when compared with the traditional GFDM as described in [26].

UW-GFDM

The purpose of introduction of CP in transmission packet is to combat the ISI which is highly prevalent in multipath channels. After channel equalization CP has no purpose and is simply removed at the receiver [27]. To increase the bandwidth efficiency along with BER the concept of using deterministic sequence named as UW instead of CP was introduced. In OFDM, CP is appended at the start of the packet but the mandatory guard interval (UW) is an integral part of the frequency samples of the IFFT block. Hence, certain number of subcarriers can't be used for transmitting data, but will transmit the redundant information. The subcarriers which are sacrificed are named as redundant subcarriers. By designing these redundant subcarriers would improve the synchronization, channel estimation requirements and in turn improve system performance metrics. The modulation matrix $\mathbf{A}$ is $\mathbb{C}^{N\times N}$ which is a block circulant matrix with every sub block of size $\mathbb{C}^{K\times K}$. The block diagonalization of $\mathbf{A}$ would result as [28],

$$\mathbf{A} = \begin{bmatrix} \mathbf{A_0} & \mathbf{0} & \cdots & \mathbf{0} \\ \mathbf{0} & \mathbf{A_1} & \cdots & \mathbf{0} \\ \vdots & \vdots & \ddots & \vdots \\ \mathbf{0} & \mathbf{0} & & \mathbf{A_{M-1}} \end{bmatrix} \tag{1.10}$$

where each $\mathbf{A_m}$ is an approximated sub matrix of size $\mathbb{C}^{K\times K}$. Mentioned earlier, for obtaining correlations in frequency domain between the subcarriers named as redundant subcarriers must be scarified. Let us represent K_r as redundant subcarriers and K_d

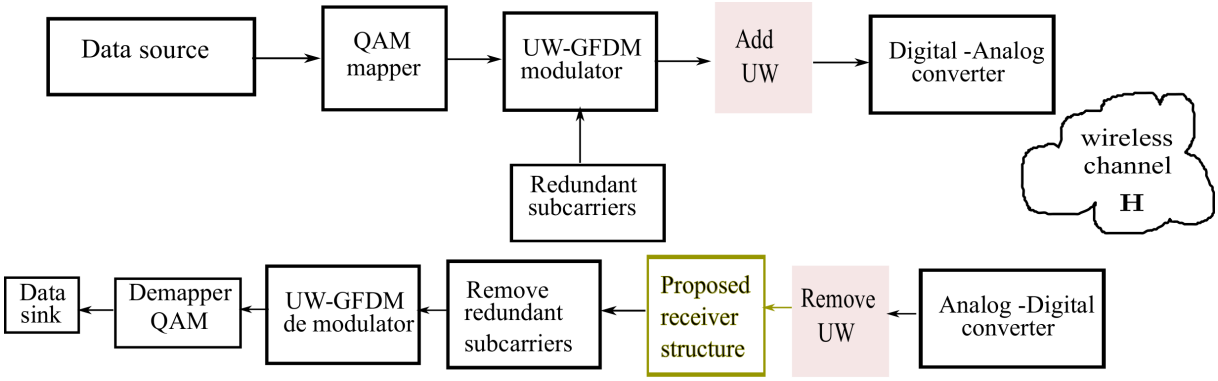

Figure 1.7: Block diagram of the UW-GFDM system

data subcarriers such that $K = K_r + K_d$. Hence, the data on subsymbol of Unique Word Generalized Frequency Division Multiplexing (UW-GFDM) symbol is shown as $\mathbf{d_m} = [\mathbf{d_{md}}\ \mathbf{d_{mr}}]$, where $\mathbf{d_{md}} = [d_m(0) \cdots d_m(K_d - 1)]$ is representing the data carriers and $\mathbf{d_{mr}} = [d_m(K_d) \cdots d_m(K - 1)]$ is denoting the redundant carriers of a subsymbol m. The block diagram for the generation of UW-GFDM signal is shown in the Fig.1.7. For determining redundant subcarriers of the UW-GFDM signal the following procedure is performed across each subsymbol:

$$\mathbf{x_m} = \mathbf{A_m P} \begin{bmatrix} \mathbf{d_{md}} \\ \mathbf{d_{mr}} \end{bmatrix} = \begin{bmatrix} \mathbf{x_{md}} \\ \mathbf{0} \end{bmatrix} \tag{1.11}$$

where the index $m = 0 \cdots M - 1$ is the data on it corresponding subsymbol and $\mathbf{P}$ is permutation matrix for finding the positions of the redundant subcarriers. The conversion matrix of every subsymbol m, denoted by $\mathbf{M_m} = \mathbf{A_m P}$ can be decomposed as,

$$\mathbf{M_m} = \begin{pmatrix} \mathbf{M_m}^{11} & \mathbf{M_m}^{12} \\ \mathbf{M_m}^{21} & \mathbf{M_m}^{22} \end{pmatrix} \tag{1.12}$$

where the sub matrices of $\mathbf{M_m}^{11}$ is $\mathbb{C}^{K_d \times K_d}$, $\mathbf{M_m}^{12}$ is $\mathbb{C}^{K_d \times K_r}$, $\mathbf{M_m}^{21}$ is $\mathbb{C}^{K_r \times K_d}$ and $\mathbf{M_m}^{22}$ $\mathbb{C}^{K_r \times K_r}$. The last K_r samples arrested to zero as,

$$\mathbf{M_m}^{21}\mathbf{d_{md}} + \mathbf{M_m}^{22}\mathbf{d_{mr}} = 0 \tag{1.13}$$

The redundant subcarriers $\mathbf{d_{mr}}$ in (1.13) coincidentally results into minimum average redundant energy.

$$\begin{aligned} \mathbf{d_{mr}} &= \mathbf{M_m}^{21+}\mathbf{M_m}^{22}\mathbf{d_{md}} \\ &= \mathbf{T(m)}\mathbf{d_{md}} \end{aligned} \tag{1.14}$$

where $\mathbf{M_m}^{21+}$ is representation pseudo inverse obtained. We can verify by substituting (1.14) in (1.11) minimum energy can be obtained. In conventional GFDM systems precoding is generally performed in order to obtain coding gain. This coded GFDM will require the availability of channel state information (CSI) which is not possible [29]. In UW-GFDM no CSI will be required and hence can be the best for multipath channel environments. The redundant subcarriers across every subsymbol are present in the indices from K_d to $K-1$. This results in a high coding gain when compared with the traditional GFDM. This gain can be used to counteract the deep fades in fading channel situations. This credit of UW-GFDM is attributed for redundancy in frequency domain of every subsymbol. This advantage is achieved by UW-GFDM by using a slight loss in throughput efficiency. The UW-GFDM after the step 1 can be simplified as,

$$\mathbf{x} = [\mathbf{x_{1d}}\ \mathbf{0}\ \mathbf{x_{2d}}\ \mathbf{0} \cdots \mathbf{x_{Md}}\ \mathbf{0}] \tag{1.15}$$

Every $\mathbf{0}$ in (1.15) is of length K_r and are present at a distance of K. In the step 2, an user desired pilots or UW can be inserted as $\mathbf{x_u(m)}$. In IEEE 802.11 WLAN will consist of barker sequences in the place of 0 in $\mathbf{x}$. UW-GFDM signal for a subsymbol m is,

$$\mathbf{c(m)} = \mathbf{P}\begin{bmatrix}\mathbf{d_{md}}\\ \mathbf{d_{mr}}\end{bmatrix} = \mathbf{P}\begin{bmatrix}\mathbf{I}\\ \mathbf{T(m)}\end{bmatrix}\mathbf{d_{md}} = \mathbf{Z(m)d_{md}} \tag{1.16}$$

In the receiver, after performing channel equalization we can represent the received data vector as,

$$\hat{\mathbf{d}}_\mathbf{m} = \hat{\mathbf{c}}(\mathbf{m}) + \hat{\mathbf{x}}_\mathbf{u}(\mathbf{m}) + \mathbf{w}(\mathbf{m}) \tag{1.17}$$

The self interference due to the UW is subtracted by $\hat{\mathbf{d}}_\mathbf{md} = \hat{\mathbf{d}}_\mathbf{m} - \hat{\mathbf{x}}_\mathbf{u}(\mathbf{m})$. For the conventional LMMSE estimator, the data can be estimated as [28],

$$\hat{\mathbf{c}}(\mathbf{m}) = \mathbf{C_{c(m)c(m)}}\left(\mathbf{C_{c(m)c(m)}} + \mathbf{C_{ww}}\right)^{-1}\hat{\mathbf{d}}_\mathbf{m} \tag{1.18}$$

where $\mathbf{C_{ww}} = K\sigma_w^2\mathbf{I}$ is the noise covariance matrix and $\mathbf{C_{c(m)c(m)}} = \sigma_d^2\mathbf{Z(m)Z(m)}$. The authors have used Weiner filter for estimating the data symbols as,

$$\hat{\mathbf{d}}_\mathbf{md} = \left(\mathbf{Z^H(m)Z(m)} + K\frac{\sigma_n^2}{\sigma_d^2}\right)^{-1}\mathbf{Z^H(m)}\hat{\mathbf{d}}_\mathbf{m} \tag{1.19}$$

The Weiner smoothing operation in (1.19) exploits the correlations created by redundant subcarrier and leads to better BER gain.

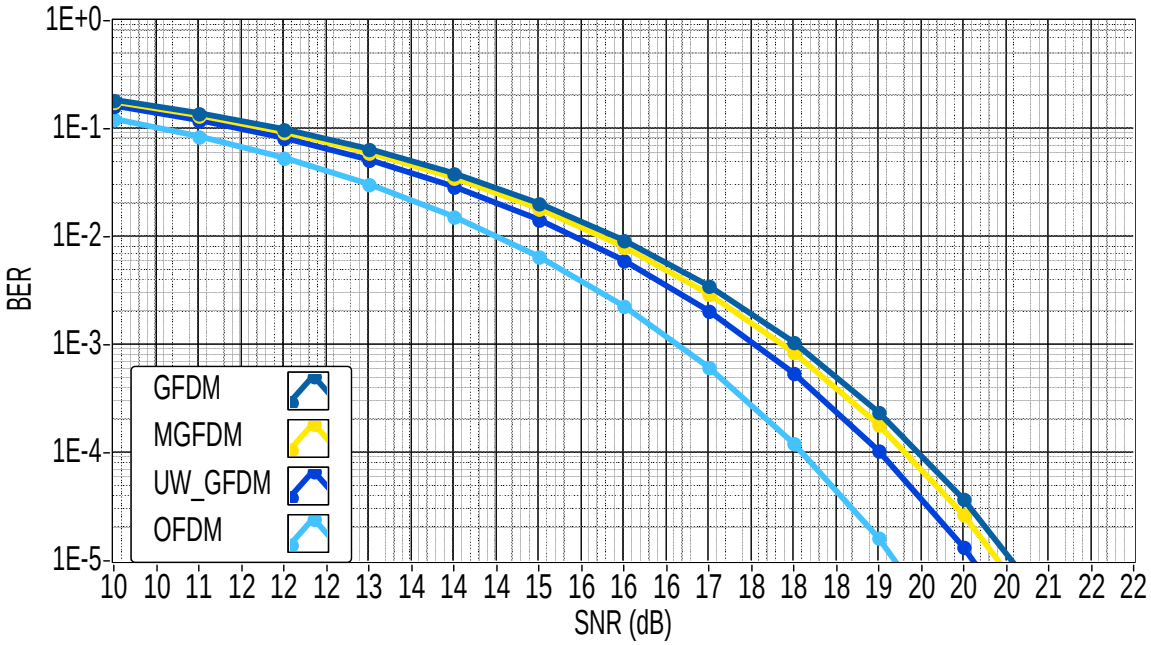

Figure 1.8: Comparison of all variants of GFDM systems in AWGN channels

To illustrate the concept we present the Figure. 1.8 where comparison of BER between various variants of GFDM can be observed. It can be clearly understood from the figure that, UW-GFDM outperforms the methods in the literature. However, it is to be remembered that this performance is achieved at the cost of throughput efficiency and hence can useful for those applications. The usage of multi tapers as prototype filters lead to implementation of MGFDM system, which improved the BER performance by making system more orthogonal [26]. The increase in strictness of orthogonality would require a relatively strict synchronization when compared with GFDM. Another important inference from the figure is, the performance of all three systems is inferior when compared with well accepted OFDM system.

1.7 Literature survey

In 2009, GFDM is introduced with the concept of spectrum aggregation for Television (TV) for Ultra high frequency (UHF) bands . In this work, the properties of GFDM in comparison to OFDM is explained, in which some of them are ultra low OOB radiation due to filtering giving flexibility in choosing prototype of choice, block based structure

using one CP for whole block and efficient utilization of FFT equalization. Comparisons of GFDM and OFDM by using GFDM as a secondary system in cognitive radio was explored in [30]. The results analysis depicts that the setup using GFDM secondary system will produce less interference to the primary system compared to the OFDM secondary system. The prototype filter used for pulse shaping the subcarriers will create a small spread in frequency of operation. Orthogonality loss between the subcarriers leads to inherent self ICI. Double sided serial interference was proposed in [31] to reduce this effect and showed significant improvement in the GFDM bit error rates. The cyclostationary detection of spectrum sensing in cognitive radio using GFDM modulation was presented in [32] and a good comparison of cyclostationary properties of OFDM is also investigated. In addition, spectrum sensing using energy detection is also studied [33]. With the motive of eliminating the ISI and ICI, the authors in [34] proposed instead of the DFT as used in traditional GFDM system. Furthermore, for the purpose of reducing the complexity caused by the channel equalization, the authors proposed the frequency domain DGT for the received GFDM signal in order to enable its perfect recovery. The authors in [35] analyse the impacts of STO, CFO and phase noise in OFDM and GFDM systems.

In addition, a novel receiver filter that is optimized to maximize SIR in the presence of CFO under AWGN channel is proposed for GFDM system. Upon comparison with OFDM, the simulated result analysis confirms the sensitivity of GFDM to CFO. In [36], authors have proposed discrete Fourier transform spreading based GFDM transmission to reduce the PAPR. Two subcarrier mapping schemes are considered, namely, localised frequency division multiple access and interleaved frequency division multiple access. The observations from [36] are that interleaved frequency division multiple access subcarrier mapping is more effective than localised frequency division multiple access. In addition, bit error rate performance is developed and supported by the analytical expressions. The analytical performance of MMSE receiver along with the proposed precoding techniques is studied in [37]. The precoding techniques proposed in [37] reduces the complexity of the MMSE receiver without compromising the error rate performance. Also, a thorough analysis on the complexity analysis of different transmitters and receivers of both precoded and uncoded GFDM are well presented. Since GFDM requires receivers with high computational complexity, authors in [38] have proposed a novel low-complexity joint MMSE receiver for GFDM by harnessing circulant properties of the matrices involved in

the demodulation process.

1.7.1 Synchronization for GFDM and its variants

In general, all the mentioned synchronization techniques use rectangle pulse shaping filter for pilot preamble which create non negligible OOB radiations. Further, employing rectangular filtering for standard IEEE 802.11 preamble with multiple identical data leads to spikes and slow decaying of side lobes which in turn leads to destruction of the advantage of GFDM. To circumvent this problem, the data aided synchronization is performed after limiting the pilot preamble with an arbitrary pulse shape. The non orthogonal nature it is still prone to severe ICI and ISI which results in STO and CFO. This makes synchronization the hardest problem in real channel environments [39]. These misalignments are estimated either by using data aided methods or by using the redundant CP. In [40], ML estimate using correlation with CP was proposed, but the main drawback involved with this method is that, it would be difficult to locate actual data because training symbols and actual symbols look alike. Another drawback associated with CP based synchronization methods is that, they rely on channel behaviour and are not ideal for multipath environments. Most popular pilot aided methods estimate STO by searching for two same halves, which present in training signal [41]. However this metric has a plateau shape which causes large STO varience. STO estimation can be further improved by considering different metrics as proposed in [42], [43] , [44]. A similar extensions to GFDM systems are presented in [45], [46], highlighting the performance degradation than traditional OFDM systems.

The authors have suggested a two step process for the UW generation [28]. The first step involves in introduction of correlations in the frequency domain by replacing the data part of time domain signal with block of zeros at UW positions. The purpose of introducing correlations in frequency domain is to obtain coding gain. In the second step, application desired UW can be inserted in the position of zeros to satisfy requirements like synchronization, channel estimation which leads to improvement in system BER. In short, UW is a deterministic sequence obtained by replacing the zeros in time domain for a UW-GFDM signal which sacrifices certain subcarriers named as redundant subcarriers in every subsymbol inorder to obtain coding gain.

It is important to note that, even for the case of null UW sequence, a systematic code is present within the sequence of subcarriers of every subsymbol. The coding gain in the UW-GFDM is achieved at the cost of strict synchronization. If the received data is not in the range of GFDM window due to improper time offset, we may destroy the purpose of design of the system. In literature we find many methods employing preamble aided synchronization [47], [48]. But they rely on the fact that the probability of false alarm or probability of not receiving the preamble is minimum. Instead, in this thesis, we propose a metric by avoiding the step 2 in generation of UW-GFDM system. The proposed scheme uses the fact that the energy in the locations of UW is minimum. The suggested scenario would result in low power consumption along with STO estimation.

Considering this as motivation, in contribution 1 we present the way in which synchronization must be performed for GFDM systems. In particular, this contribution has:

- Derivation of ML estimation algorithm for time and frequency offset estimation for any number of sets of identical data for the preamble after employing pulse shaping. CRLB for CFO and the influence of choice of filters on it is discussed.
- We propose a metric by avoiding the step 2 in generation of UW-GFDM system for STO estimation. The proposed scheme uses the fact that the energy in the locations of UW is minimum for timing synchronization.

1.7.2 Oversampling for CFO estimation and Jitter noise reduction

The above mentioned advantages of GFDM are largely dependent on its synchronization capability [49]. STO and CFO are the firmest problems, which lead to ISI and ICI [39]. Several methods [40], [50] have already been presented to compensate the effect for OFDM. Nevertheless, all misalignments cannot be precisely estimated as suggested in [51]. Blind methods for estimation are of significant interest, since they provide better bandwidth and power efficacy. ML estimate by using the redundant CP was presented in [40]. The performance of this method degrades in multipath channels due to consumption of CP to combat ISI. The extension of this method for GFDM systems evidenced good performance even in the presence of self interference [45]. The blind method in [41] has a plateau structure in its preamble leading to STO variance. This problem is solved

by dividing preamble into multiple parts and using different metrics in order to reduce variance in estimation as proposed in [42], [43], [52]. The severity of synchronization errors for GFDM systems was presented in [53], which was estimated by using pseudo noise and pseudo circular preambles in [54] and [46] respectively. There has been not much literature for blind synchronization in GFDM system, so, we use [45] for comparison in this work. For the above mentioned theoretical analysis, several approaches have been proposed. However, less work has been done so far to evaluate the performance considering by real time channel conditions.

This chapter in the thesis attempts to implement the GFDM system on real time hardware named universal software radio peripheral (USRP) for testing the realtime capability in the perspective of blind synchronization for the first time. For multipath channels, channel equalization on unsynchronized data would lead to improper selection of GFDM block, which causes erroneous effects [55]. After examining the importance of this phenomenon, we implement synchronization algorithms before channel estimation. The numerical value of CFO is independent of subcarrier and subsymbol indices i.e., the effect of change in frequency is same for all subcarriers and doesn't depend on the subsymbol location in the GFDM block. In this chapter, we exploit the constant phase obtained from difference of phase shift between neighbouring samples in twice oversampled signal for CFO estimation. The CRLB for the oversampling based GFDM signal model is derived. Also, we prove through simulation that, the proposed algorithm results in a little error floor. More importantly, the proposed method is data efficient because of the fact that, it utilizes only one GFDM symbol using reliable ML estimation in the presence of noise and multipath channels. Moreover, the constellation diagrams received in USRP validate the result by showing a good agreement with simulations.

1.7.3 Reduction of Complexity in GFDM-SLM system

The flexible nature of nature of GFDM allows it to contain multiple symbols whose superimposition in time leads to PAPR. This problem leaves the transmitter front-end with a choice to either allow signal distortion or to include a costly high power amplifier to compensate the effect. Simplest form of PAPR reduction techniques use signal distortion schemes like clipping, companding etc for power reduction, but these techniques results in

inevitable degradation of error performance [56]. Alternative idea of using efficient codes for reducing peak power, is efficient for few subcarriers to keep its complexity at permissible limit [57]. Probabilistic methods like SLM and Partial Transmit Sequence (PTS) are most befitting for PAPR reduction for block structured systems like GFDM. We considered SLM technique in this work, since it requires reduced computational complexity over PTS scheme to achieve similar performance in important performance metrics like Adjacent Channel Leakage Ratio (ACLR) and BER [58].

The probabilistic methods like SLM and PTS have received considerable recognition for multicarrier transmission [58]. We consider SLM technique in this work, because the available literature suggest efficient PAPR reduction gain is achieved by SLM at low complexity when compared with PTS [58]. In SLM approach, one GFDM signal with lowest PAPR is selected from a set of different candidate signals generated in the transmitter [59]. For generation of every alternative signal, the data vector which is to be GFDM modulated, is modified by multiplying with a different phase sequence vector [60]. Later, the candidate signal is generated by multiplying modulation matrix with its corresponding modified data sequence. As the name suggests, the signal which has the lowest PAPR among all generated GFDM signals is selected for transmission. Unlike clipping method, SLM do not create adverse effects on transmitted signal spectrum and can be considered as distortion less transmission scheme. The main issue with SLM technique is, it requires a bank of modulation matrices to generate the required set of candidate GFDM signals leading to high computational complexity. Therefore, reduction in complexity can be achieved by minimizing the number of alternative symbols. However, this scenario may decrease the PAPR reduction gain. To address this issue, in this contribution we propose three methods to alleviate high complexity associated with GFDM system .

1.7.4 Joint channel mitigation and SI estimation for GFDM system

In the conventional SLM technique, a combination of phase rotation vectors are generated to obtain modified form of GFDM signals. Among them, the signal corresponding to minimum PAPR is selected for transmission. As a result, the phase sequence vector which yields the low PAPR must be transmitted to the receiver, this extra information is popularly referred as SI. This customary SI is necessary for detection of the exact payroll

data and it's necessity in conventional methodologies reduces the throughput efficiency and makes the system unattractive for real time applications.

For that reason, statistical estimation of SI for data decoding are introduced for OFDM system [61]. These methods hypothesize the phase rotation sequence to follow a sequence easily understandable by the receiver and hence can be retrieved in the receiver without the need of any memory. A Blind ML detection is proposed in [60] using the method of extended subcarrier symbol. This algorithm would require many computations which are reduced by [62], [63]. The principle idea of SI estimation in these methods lies in using pilots in the transmitted signal for performing joint SI estimation and channel estimation. For this purpose, highly complex procedures are adopted which may require heavy detection algorithms. [62] uses a pilot based ML detection by forcing OFDM system to follow a clustered architecture, while [63] utilizes a frequency-domain correlation algorithm for enabling joint estimation for conventional SLM. However, all these algorithms cannot be applied straight forward manner to the conventional GFDM system due to it's non orthogonal nature. In this work, authors implement a real time prototype of the GFDM system focussing on PAPR reduction and channel estimation using USRP. To address the practically encountered challenges, joint SI and channel estimation is performed with the assistance of pilot symbols.

The choice of phase sequence vector makes a significant impact on achievable PAPR reduction gain. Traditionally, SLM technique was implemented by using phase sequences which are randomly generated from the set $\{+1, +j\}$ [55]. For traditional OFDM systems, usage of Neumann, monomial, cubic phase sequences are found to offer better PAPR reduction gain [64]. It is found in literature that the cubic phase sequences have superior performance at the cost of computational complexity [65]. The utilization of rows of the Hadamard matrix as phase sequence vectors was found to yield a good compromise for PAPR reduction and computational complexity for OFDM systems [65]. However, all the above mentioned algorithms cannot be applied directly to the GFDM system due to fundamental non orthogonal nature.

Figure 1.9: Experimental setup illustrating real time transmission

1.8 Introduction to the Experimental set up

In digital communication the idea of using software for implementing the algorithms is popularly refereed as SDR. In this thesis, we have built a experimental set up using hardware and software supplied by National Instruments (NI). The main advantage by using SDR lies in obtaining a clear understanding on various design issues in the implementation of the real time wireless communication. LabVIEW is used as software interface to transceiver hardware due to its easy implementation using graphical programming. Every routine developed in LabVIEW is referred as Virtual Instrument (VI) which is similar to function of MATLAB. LabVIEW can give support a simple interface for conjuring various external Input/Output. Another reason for using LabVIEW is it permits developers to understand the exact flow in the design of the program. To be specific, the developed testbed uses reconfigurable NI hardware USRP RIO as transceiver. From the Figure 1.9 we can observe two workstations connected to the USRP terminals. This set up can be considered as the practical proof for implementation of performed theoretical analysis. The hardware of USRP will internally contain low frequency daughter board for radio frequency translations,Analog to Digital Converter (ADC)/ Digital to Analog Converter (DAC) for development of the DSP chips inside the USRP.

It is worth mentioning, all the general purpose operations like digital up/down conversion, interpolation/decimation are actually implemented on the FPGA of the USRP and the LabVIEW handles the baseband operations like modulation/demodulation. In the LabVIEW software, the rectangular grid data is GFDM modulated by performing the signal processing operations. However, for accomplishing the channel estimate in

multipath channels pilots are placed in an interleaving manner in the data before modulating. This phenomenon creates a chance to detect pilots with less burden on control data. Hence, the transmission packet shall need a control information to detect the intended packet. Therefore, the transmission packet shall comprise of data and control bits. The control bits bear the information like source USRP IP, error awareness codes, and the arrangement of data in the transmission packet. In this work, we used continuous transmission scheme for about 1000 iterations which has two requirements: Firstly, a high throughput communication is required between workstation and software, which is achieved by using a NI PXIe-PCIe8371 card. Secondly, usage of costly DSP chips for fast operations like extraction and processing of 5G waveforms which are taken care by RIO devices. Though the transmission scheme is continuous, the transmitter will send one frame at a time. USRP RIO is having two channels for data communication, which facilitates the storage of information in buffers for continuous transmission. The steps for installation and software implementation are mentioned below:

- Install the software's like LabVIEW and RIO driver installer whose detailed information can be found: ni.com/info and http://www.ni.com/pdf/manuals/371976c.pdf.
- Use the PCI Express Interface Kit to connect the USRP RIO device to the computer and connect each work station with one USRP as shown in Figure 1.9
- Connect the AC/DC power supply to the USRP RIO device and switch on the work station.
- Open NI USRP Configuration utility and note the Local Device IP assigned by the Work station.
- The hardware parameters of the transmitter USRP are shown in Figure 1.10 where the device IP address is recognized as RIO 0 (Transmitter) by the workstation. We have chosen the transmission mode as continuous where in a data packets are transmitted continuously for 1000 iterations. The remaining parameters can be seen from real time parameters of the corresponding chapter.
- The VI used for assigning the hardware parameters is shown in the Figure 1.11. Here NI USRP open Tx session. Vi simply opens a session. Later, the NI USRP

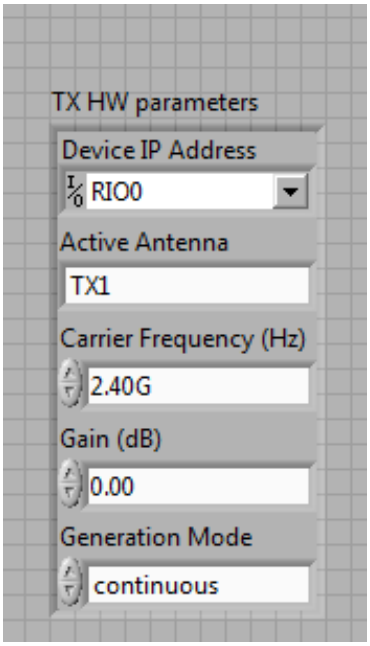

Figure 1.10: Hardware parameters of the transmitter USRP

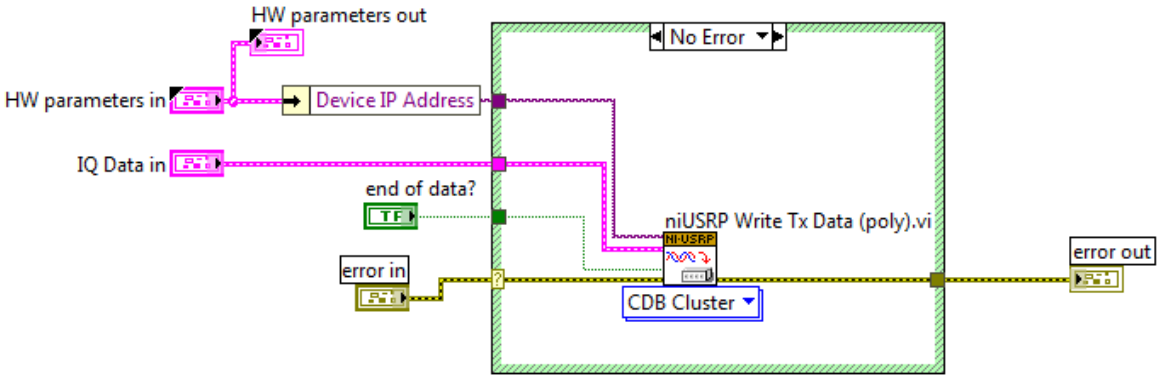

Figure 1.11: VI for assigning the hardware settings

Configure signal coheres the modulation parameters and is transmitted into air in IQ data form if no error signal is present in the generation of GFDM signal as shown in Figure 1.12

- In the receiver, the USRP RIO can receiver its data in two channels hence the Enable channels is considered as 0. If one desires to send a large amount of data then both channels can be selected as 0 and 1. Since the setup is Single Input Single Output (SISO) in nature there is no need to use an octoclock for synchronizing the USRP with internal clock as reference. We used internal clock as a reference and the VI can be seen in Figure. 1.13. For making the BER measurement of real time

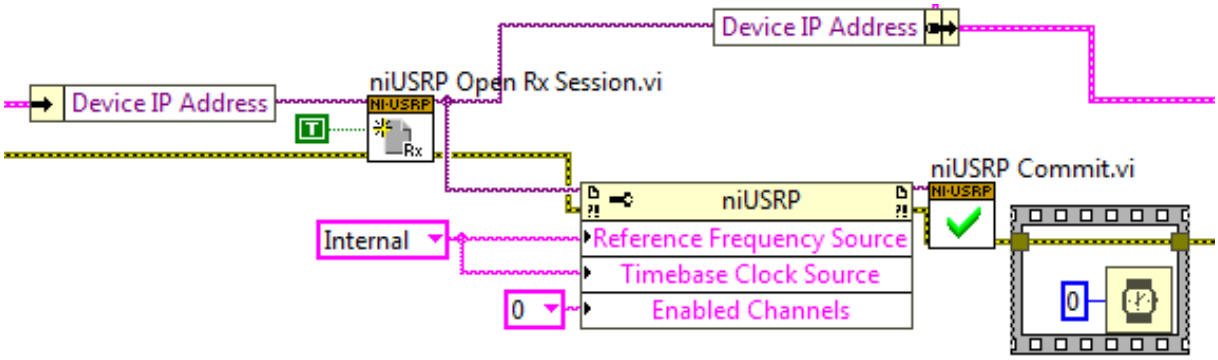

Figure 1.12: Transmitting data from USRP

analysis both the channels are selected.

- The reverse operations done in accordance to the transmitter are performed in the receiver. The detailed descriptions can be found in Figure 1.14 and Figure 1.15.

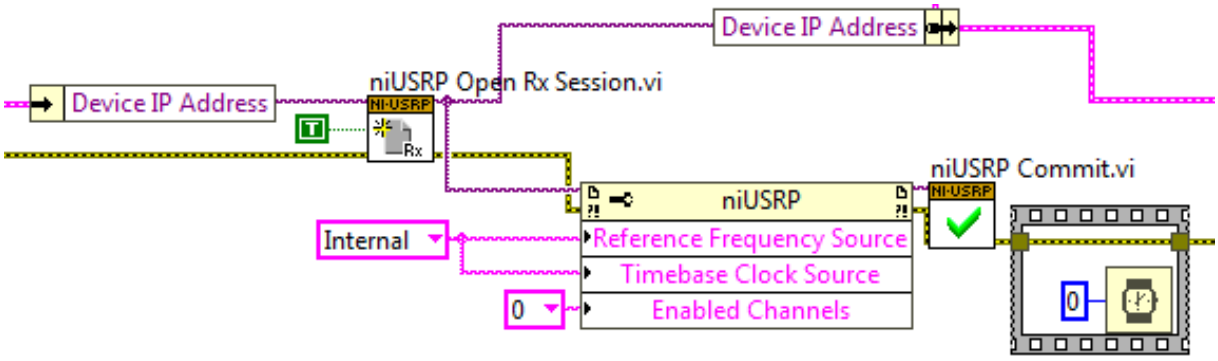

Figure 1.13: Receiving data from USRP

USRP contains antennas named TX1/RX1, RX2, TX1/RX1, and RX2. Two antennas act as receiver (RX2, RX2) and the other two can operate as transceiver (TX1/RX1, TX1/RX1). The internal hardware of USRP contain low frequency daughter board for radio frequency translations, ADC/DAC for development of the DSP chips inside the USRP. USRP is having ability to operate in a wide frequency range of 1.2-6 GHz which covers all the mobile communication. The basic set-up used for the implemented GFDM demonstrator is shown in the Figure 1.9. We can observe two workstations connected to the transmitter USRP (TX USRP) and receiver USRP (RX USRP) in the whole thesis. Since the ADC of the USRP is capable of sampling at 200M/s practically, the practical limit for bandwidth of transmission is 100Mhz. However, this bandwidth suits most practical systems. To increase the speed and the accuracy, the transmitter USRP uses two

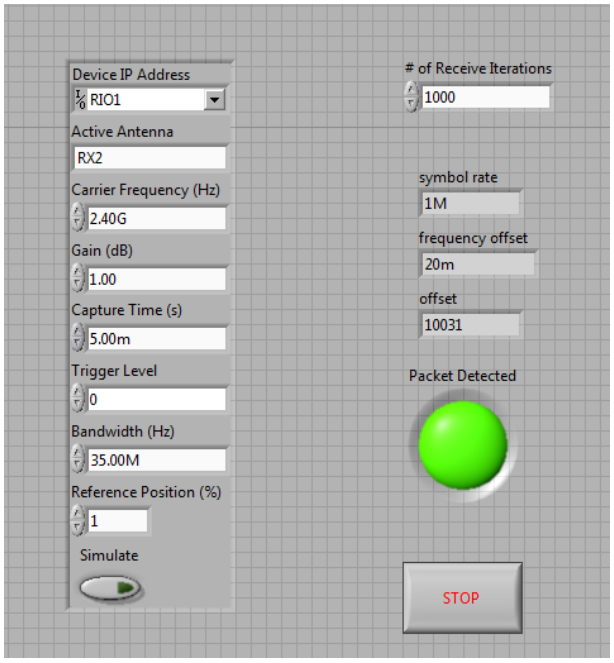

Figure 1.14: Hardware parameters of the receiver USRP

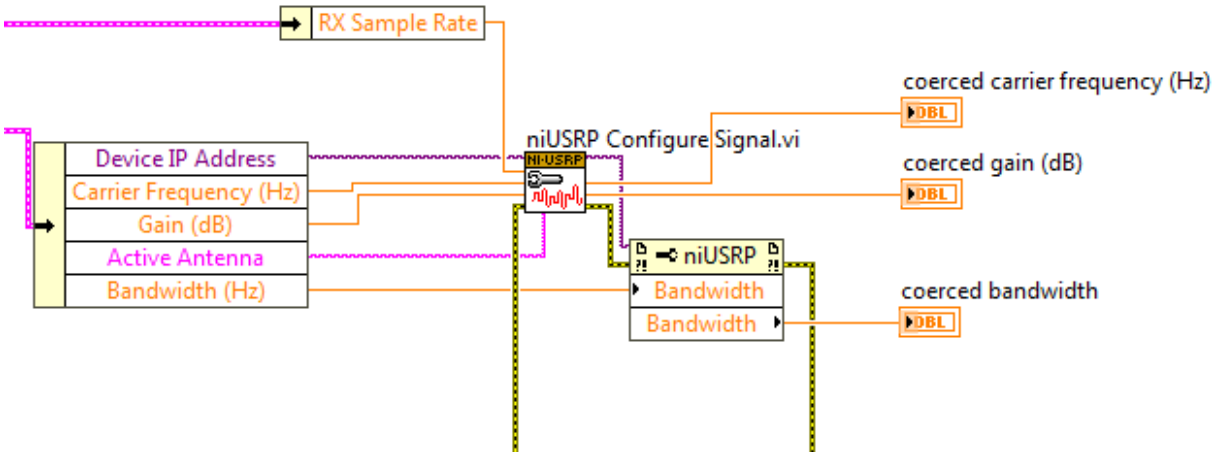

Figure 1.15: VI for assigning the hardware settings in receiver USRP

ADC for obtaining digitalized Intermediate Frequency (IF) signal, which will be implemented on FPGA and transmitted into air after RF up conversion. The primary duty of main board is receiver USRP to perform rate conversion and using a anti-aliasing filter. The proposed estimation algorithms in the receiver can be performed only after identification of exact data packet. Practically, the USRP iterates over packet length and notes the presence of significant presence of the energy. The carrier power of the USRP signal is very high when compared to the actual payroll data and hence it is difficult for the receiver to identify the packet with the transmitter USRP device ID. Hence, SNR is

computed at the receiver when its higher than threshold, the packet is identified and the STO and CFO estimations are done as presented in the subsequent chapters.

Chapter 2

Synchronization of GFDM and its variants

Due to the non orthogonal nature of GFDM signal, it is prone to severe ICI and ISI which results in STO and CFO. This makes synchronization the hardest problem in real channel environments [39]. In general, all the mentioned synchronization techniques use rectangle pulse shaping filter for pilot preamble which create non negligible OOB radiations. Further, employing rectangular filtering for standard IEEE 802.11 preamble with multiple identical data leads to spikes and slow decaying of side lobes which in turn leads to destruction of the advantage of GFDM. These traditional data aided methods of synchronization avoid the effect of egress noise in pilot preamble destroying its spectral advantage. To safeguard this advantage, preamble needs to be pulse shaped. The main contribution of this work is the derivation of generalized ML estimation of frequency and time offsets for receiver synchronization in GFDM systems, using the modified preamble by the application of matrix inversion lemma. The dependency of the choice of the filter on CRLB of frequency offset estimation is also emphasized. The performance of the system is analysed over Additive White Gaussian Noise (AWGN) and multipath channel environments. After analysing the ML estimate of the traditional GFDM system this chapter also focusses on a blind STO estimate for UW-GFDM system. To detail, the primary motive behind introduction of UW is to exploit the correlations in frequency domain which results in coding gain. However, perfect STO compensation is a prerequisite and is the first task to be done. This chapter presents a blind metric for the estimation of STO using the structure of UW-GFDM system without requirement of pilot symbols present in UW positions. The developed algorithm can blindly estimate the block du-

ration, symbol duration, number of redundant subcarriers and number of subcarriers. The obtained simulation results verify the feasibility of the proposed algorithm in various channel conditions.

2.1 Introduction

Let us use $d_k(m)$ for representing the QAM symbol to be carried by k^{th} subcarrier at m^{th} time slot. Hence, $\mathbf{d_k} = [d_k(0) \cdots d_k(M-1)]$ will show all the time slots a subcarrier k and while $\mathbf{d} = [\mathbf{d_1}\ \mathbf{d_2}\ \cdots\ \mathbf{d_k}]$ is the complete data vector which is to be GFDM modulated. Notationally, we can interchangeable use $\mathbf{d}$ and $\mathbf{d_k}$ as,

$$\mathbf{d_k}(n) = \mathbf{d}(kM + n) \tag{2.1}$$

The process of generation of GFDM modulation is shown in steps below:

- The first step in GFDM modulation is to upsample the data on every subcarrier by the number of subcarrier K.

$$p_k(n) = \sum_{m=0}^{M-1} d_k(m)\delta(n - mK) \tag{2.2}$$

(2.2) can be alternatively represented as,

$$p_k(n) = \begin{cases} d_k(m) & n = Km \\ 0 & \text{otherwise} \end{cases} \tag{2.3}$$

where $m = 0 \cdots M-1$.

- The obtained upsampled data of the every subcarrier is circularly convolved with a prototyping filter $g(n)$ of length MK. The circularly convolved data is then upconverted to the corresponding frequency. In the final step, the upconverted data on subcarrier is amalgamated to obtain GFDM signal as,

$$\begin{aligned} x(n) &= \sum_{k=0}^{K-1} (p_k(n) \odot g(n)) e^{j\frac{2\pi kn}{K}} \\ &= \sum_{k=0}^{K-1} \sum_{m=0}^{M-1} d_k(m) g\left\{(n - mK) \text{mod} MK\right\} e^{j\frac{2\pi kn}{K}} \end{aligned} \tag{2.4}$$

where $\odot$ represents the circular convolution utilized to obtain the GFDM signal $x(n)$.

The choice of the prototyping filter $g(n)$ effect the various performance metrics of the system. Generally, Root Raised Cosine (RRC) filters are often used for circular prototyping. These filters are characterised by the Meyer auxiliary function which can be represented in its simplified form as [28],

$$G(f) = \sqrt{\frac{1}{2}\left[1 - \cos\left(\pi f I(\beta)\right)\right]}. \tag{2.5}$$

Here, the auxiliary function $I(\beta)$ is dependent on the $\beta = k/(\text{alpha} \times K)$ which defined the roll off region by changing the value of alpha in frequency domain. In other words, alpha is representing the measure of the overlap between subcarriers which are centred around normalised frequency k/K. The truncated Meyer auxiliary function is,

$$I\left(\beta\right) = \beta^4\left(35 - 84\beta + 70\beta^2 - 20\beta^3\right). \tag{2.6}$$

The matrix representation for the GFDM signal is,

$$\mathbf{x} = \mathbf{A}\mathbf{d}. \tag{2.7}$$

The $\mathbf{A}$ matrix represents all the signal processing operations like upsampling, circular convolution frequency translation etc. The data vector $\mathbf{d}$ embrace all the complex QAM modulated data symbols. Here, T in superscript represents the transpose of a matrix. The $\mathbf{A}$ matrix can be expanded as,

$$\mathbf{A} = [\mathbf{G} \quad \boldsymbol{\epsilon_1}\mathbf{G} \quad \cdots \quad \boldsymbol{\epsilon_{N-1}}\mathbf{G}] \tag{2.8}$$

where $\mathbf{G}$ is an $MK \times M$ matrix with its first column containing all the samples of the prototyping filter $g(n)$. All the other columns can be obtained by circularly shifting its immediately previous column by K. $\boldsymbol{\epsilon_1} = \text{diag}\{[\mathbf{e_i}^T, \cdots \quad \mathbf{e_i}^T]^T\}$ is an $MK \times MK$ diagonal matrix which consists of M concatenation of the vector $\mathbf{e_i} = [1, e^{\frac{2\pi i}{N}}, \cdots e^{\frac{2\pi(N-1)}{N}}]$. An extra CP is affixed at start of each GFDM symbol, which is transmitted over a multipath channel defined as $\mathbf{h} = [h(0) \cdots h(J-1)]$. In, the receiver, like OFDM, after CP removal, the GFDM signal can be represented as,

$$\mathbf{y} = \mathbf{H}\mathbf{x} + \mathbf{w} \tag{2.9}$$

where $\mathbf{H}$ is channel circulant matrix with its first column consisting of channel coefficients $[h(0) \cdots h(J-1)\ 0 \cdots 0]^T$, which are appended with $N - J$ zeros and $\mathbf{w}$ is the additive

white Gaussian noise (AWGN). The channel will be estimated by using pilots is used for performing signal detection by the process of zero forcing equalization. The signal detected assuming the perfect channel estimation and synchronization $\hat{\mathbf{y}}$ is

$$\hat{\mathbf{y}} = \mathbf{W_N^H \Lambda^{-1} W_N y} = \mathbf{x} + \mathbf{W_N^H \Lambda^{-1} W_N w} \tag{2.10}$$

where $\mathbf{W_N}^H$ and $\mathbf{W_N}$ represent N point IFFT and FFT matrices, $\mathbf{\Lambda}$ contains eigenvalues which are found by performing DFT of first column of channel matrix $\mathbf{H}$. Here $\mathbf{W_N^H \Lambda^{-1} W_N}$ in (2.10) indicates inverse channel response decomposed by using circulant matrix property. As a result, we can rewrite the detected signal as

$$\hat{\mathbf{y}} = \mathbf{x} + \mathbf{H^{-1} w} \tag{2.11}$$

The original data symbols after channel equalization can be obtained by multiplying with receiver matrix $\mathbf{A_r}$. We consider matched filter in this work as receiver filter in order to maximize the SNR. Finally, the estimated data $\hat{\mathbf{d}}$ is,

$$\hat{\mathbf{d}} = \mathbf{A_r} \hat{\mathbf{y}} \tag{2.12}$$

Since $\mathbf{A_r}$ is obtained by using matched filter operation, $\mathbf{A_r} = \mathbf{A^H}$ where H is hermitian of a matrix. The matched filter produces an output in such a way that it maximizes the ratio of output peak power to mean noise power in its frequency response. This is having low complex structure when compared with traditional MMSE receivers and works well for indoor channel environments. In this work, the data aided synchronization is performed after limiting the pilot preamble with an arbitrary pulse shape. The main contribution of this work is deriving an ML estimation algorithm for time and frequency offset estimation for any number of sets of identical data for the preamble after employing pulse shaping. To avoid repitition, the system model of the traditional GFDM is not mentioned, which can be seen from 1.6.4 of introduction. The CRLB for CFO is derived and the influence of choice of filters on it is discussed. We conclude that the usage of pulses like Tukey will improve the crucial spectral response with a little increment in estimation error. Another vital contribution is, prototyping GFDM system model for real time environment employing USRP as transmitting hardware which is driven by LABVIEW software. Widely accepted IEEE 802.11 short preamble is utilized for adjusting the misalignments which occur due to indoor channel variations. It will be proved in real time results that the suggested procedure provides smooth transitions in the received spectral response.

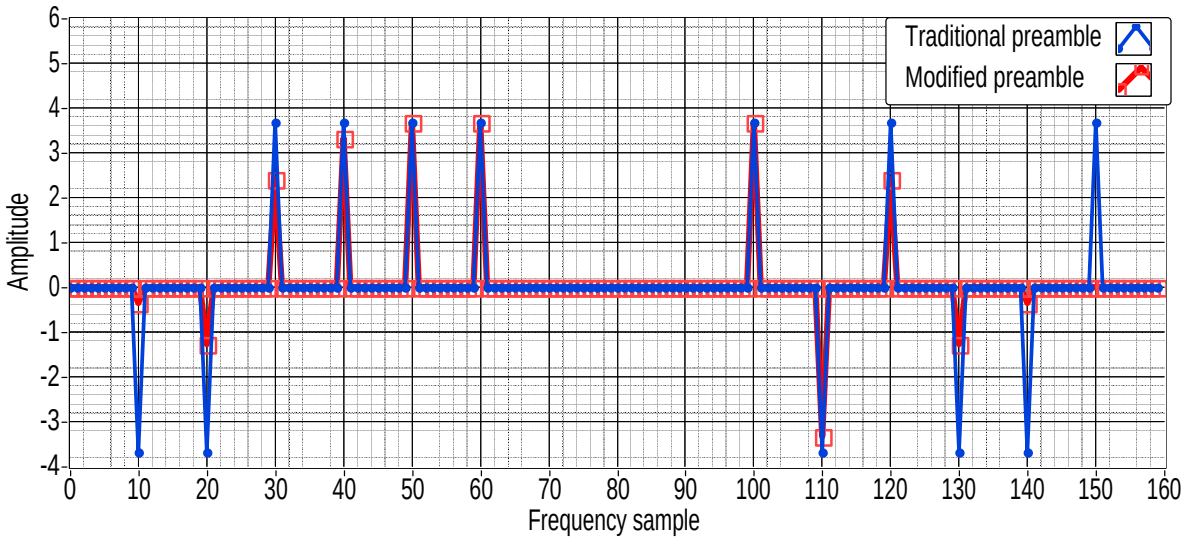

Figure 2.1: Comparisons of traditional and proposed preamble

The standard IEEE 802.11 preamble will consist of ten identical symbols which are of short length of 16 and two long symbols. The short symbols are utilized for symbol synchronization and long symbols are used for channel estimation. The frequency domain representation of traditional and the Tukey pulse shaped preamble with ten short symbols are shown in the Figure 2.1. We can clearly observe that, the proposed preamble in frequency domain is having a less amplitude at its start and end. This is the primary reason of reduction of OOB emission in the spectral response of the GFDM system which will be discussed in result section. In this section, ML algorithm is derived assuming a non-dispersive channel with AWGN nature for simplicity. An extension for dispersive channels can be done by replacing the **A** with **HA** in the process of obtaining GFDM signal **x** where **H** represents the block circulant matrix [55]. The signal model with perfect channel estimation can be given as,

$$r(n) = e^{j2\pi\epsilon n/N} x(n-\theta) + w(n) \tag{2.13}$$

The received signal $r(n)$ from air would have a STO of θ and frequency shift factor ϵ along with complex additive white Gaussian noise (AWGN) $w(n)$ were j in the exponential term is representing $sqrt(-1)$. The pilot preamble inserted is at the start of the data packet will be utilized to perform ML estimation. The preamble of the received signal $r(n)$ is anticipated to have the pilot preamble which consists of contiguous samples with N_p sets of identical data of size L. Let the index sets $I^i = \{\theta + iL \cdots \theta + (i+1)L\}$

symbolize all sets of identical data in the pilot preamble which can be indexed with $I^i, i = 0, 1, \cdots N_p - 1$. To safeguard the spectral advantage, all these sets of data are pulse shaped before transmission. An important note is that even after pulse shaping the samples in N_p sets i.e., $r(k), k \in \cup_{i=0}^{N_p-1} I^i$ are pairwise correlated. This is because we have used the same pulse shape filter for all identical parts of the preamble. Then these pulse shaped samples are assembled into a $L \times 1$ vector $\mathbf{r}$, defined as $\mathbf{r} = [r(1)\ r(2) \cdots r(L)]^T$. Hence for $m, n \in [0, N_p - 1]$ and $m \geq n$ we obtain

$$\forall k \in I^0 : \mathbf{E}[r(k+nL)r^*(k+mL)] = \begin{cases} \sigma_s^2\sigma_g^2 + \sigma_n^2, & m = n \\ \sigma_s^2\sigma_g^2 e^{-j(m-n)\epsilon^{'}}, & m - n = 1, 2, \cdots N_p - 1 \\ 0, & \text{otherwise} \end{cases} \quad (2.14)$$

In (2.14), $\mathbf{E}[.]$ represents the expectation operator. So, $\sigma_s^2 = \mathbf{E}[x^2(k)]$ and $\sigma_n^2 = \mathbf{E}[w^2(k)]$ denotes the signal and noise power respectively. σ_g^2 represents the energy of pulse shaping filter and $\epsilon^{'} = 2\pi L\epsilon/N$ is the CFO corresponding to the set I^0. The log likelihood function $\Lambda(\theta, \epsilon)$ is expressed as logarithm of the probability density function (PDF) $f(\mathbf{r}|\theta, \epsilon)$ with conditioned variables θ and ϵ, since they have to be estimated. The PDF of L observed samples of $\mathbf{r}$ with above conditions can be represented as,

$$\begin{aligned} \Lambda(\theta, \epsilon) &= \ln \Bigg\{ \prod_{k \in I^0} f(r(k), r(k+L), \cdots, r(k+(N_p-1)L) \\ &\qquad \times \prod_{k \notin \cup_{p=0}^{N_p-1} I^p} f(r(k)) \Bigg\}) \\ &= \ln \Bigg\{ \prod_{k \in I^0} \frac{f(r(k), r(k+L), \cdots, r(k+(N_p-1)L))}{f(r(k) f(r(k+L) \cdots f(r(k+(N_p-1)L))} \\ &\qquad \times \prod_{k=1}^{N_p \times L} f(r(k)) \Bigg\}. \end{aligned} \quad (2.15)$$

Here the conditioned variables θ and ϵ are dropped for simplicity. For every k we assume $f(r(k))$ is one dimensional Gaussian with zero mean, its PDF will be of the form,

$$f(r(k)) = \frac{1}{\pi\left(\sigma_g^2\sigma_s^2 + \sigma_n^2\right)} \exp\left[\frac{-|r(k)|^2}{(\sigma_g^2\sigma_s^2 + \sigma_n^2)}\right]. \quad (2.16)$$

In (2.15), the denominator is multiplication of N_p complex Gaussian PDF which will be simplified into,

$$\begin{aligned}\prod_{m=0}^{N_p-1} f(r(k+mL)) &= \left(\frac{1}{\pi(\sigma_g^2\sigma_s^2+\sigma_n^2)}\right)^{N_p} \\ &\quad\times \exp\left(\frac{-\sum_{m=0}^{N_p-1}|r(k+mL)|^2}{(\sigma_g^2\sigma_s^2+\sigma_n^2)}\right) \\ &= \left(\frac{1}{\pi(\sigma_g^2\sigma_s^2+\sigma_n^2)}\right)^{N_p} \times \exp\left(\frac{-\mathbf{z}^H(k)\mathbf{z}(k)}{(\sigma_g^2\sigma_s^2+\sigma_n^2)}\right),\end{aligned}$$

where $\mathbf{z}(k) = [r(k)\ r(k+L)\cdots\ r(k+(N_p-1)L)]^T$. The numerator in (2.15) can be expressed as a joint PDF of $f(\mathbf{z}(k))$ given by

$$f(\mathbf{z}(k)) = \frac{1}{\pi^{N_p}\det(\mathbf{R})}\exp\left(-\mathbf{z}^H(k)R^{-1}\mathbf{z}(k)\right) \tag{2.17}$$

where $\mathbf{R}$ denotes the correlation matrix. Then the expectation of $\mathbf{z}$ using (2.14) will be resulted into,

$$\begin{aligned}R =& \mathbf{E}\left[\mathbf{z}(k)\mathbf{z}^H(k)\right] \\ =& \begin{bmatrix} \sigma_s^2\sigma_g^2+\sigma_n^2 & \sigma_s^2\sigma_g^2e^{-j\epsilon'} & \cdots & \sigma_s^2\sigma_g^2e^{-j(N_p-1)\epsilon'} \\ \sigma_s^2\sigma_g^2e^{j\epsilon'} & \sigma_s^2\sigma_g^2+\sigma_n^2 & \cdots & \sigma_s^2\sigma_g^2e^{-j(N_p-2)\epsilon'} \\ \vdots & \vdots & \ddots & \vdots \\ \sigma_s^2\sigma_g^2e^{j(N_p-1)\epsilon'} & \sigma_s^2\sigma_g^2e^{j(N_p-2)\epsilon'} & \cdots & \sigma_s^2\sigma_g^2+\sigma_n^2 \end{bmatrix} \\ =& \sigma_g^2(\eta I + \sigma_s^2\mathbf{q}\mathbf{q}^H),\end{aligned} \tag{2.18}$$

where I and $\eta = \sigma_n^2/\sigma_g^2$ in (2.18) represents the identity matrix and the ratio of noise power to energy of the pulse shaping filter respectively. The value of normalized σ_g^2 is unity for rectangular filter but in the case of other filters its value deteriorates. So, the ratio η is the measure of increase in noise power because of pulse shaping. The vector $\mathbf{q} = [1, e^{j\epsilon'}, \cdots e^{(N_p-1)\epsilon'}]$ separates the effect of ϵ' for the defined set. The determinant of the matrix $\det(\mathbf{R})$ can be obtained as $(\sigma_g^2)^{N_p}\left(\eta^{N_p} + N_p\eta^{N_p-1}\sigma_s^2\right)$. Then inverse of the matrix obtained after utilization of lemma proposed in [66] is given by

$$\mathbf{R}^{-1} = \frac{I}{\eta\sigma_g^4}(\sigma_g^2 - \frac{\sigma_s^2\mathbf{q}\mathbf{q}^H}{(\eta+N_p\sigma_s^2)}) \tag{2.19}$$

Then joint PDF after substituting (2.19) into (2.17) results into

$$f(\mathbf{z}(k)) = \frac{1}{\pi^{N_p}(\sigma_g^2)^{N_p}\left(\eta^{N_p} + N_p\eta^{N_p-1}\sigma_s^2\right)} \times \exp^{-\frac{I}{\sigma_n^2}\mathbf{z}^H(k)\mathbf{z}(k) + \frac{\sigma_s^2\mathbf{z}^H(k)\mathbf{q}\mathbf{q}^H\mathbf{z}(k)}{\eta\sigma_g^4(\eta+N_p\sigma_s^2)}} \tag{2.20}$$

By simple manipulation we can solve

$$\mathbf{z}^H(k)\mathbf{q}\mathbf{q}^H\mathbf{z}(k) = \mathbf{z}^H(k)\mathbf{z}(k) + 2\sum_{m=1}^{N_p-1}\mathrm{Re}\left\{\gamma_m(k)\mathrm{exp}^{\mathrm{jm}\epsilon^1}\right\} \tag{2.21}$$

where γ is the correlation coefficient given by $\gamma_m(k) = \sum_{p=m}^{N_p-1} r(k+(p-m)L)r^*(k+pL)$. Here superscript $*$ denotes complex conjugate operation and Re is the real part of the complex number. By substituting (2.21), the log likelihood function becomes,

$$\begin{aligned}\Lambda(\theta,\epsilon) = \sum_{k=\theta}^{\theta+L-1} & -\ln(\pi^{N_p}(\sigma_g^2)^{N_p}\left(\eta^{N_p} + N_p\eta^{N_p-1}\sigma_s^2\right) \\ & -\frac{I}{\sigma_n^2}\mathbf{z}^H(k)\mathbf{z}(k) + \frac{\sigma_s^2\mathbf{z}^H(k)\mathbf{q}\mathbf{q}^H\mathbf{z}(k)}{\eta\sigma_g^4(\eta+N_p\sigma_s^2)} \\ & + N_p\ln\pi(\sigma_g^2\sigma_s^2+\sigma_n^2) + \frac{\mathbf{z}^H(k)\mathbf{z}(k)}{(\sigma_g^2\sigma_s^2+\sigma_n^2)} \\ & + \sum_{k=1}^{N_p\times L}\ln f(r(k))\end{aligned} \tag{2.22}$$

By simple manipulations the $\Lambda(\theta,\epsilon)$ value can be simplified as below,

$$\begin{aligned}\Lambda(\theta,\epsilon) = \sum_{k=\theta}^{\theta+L-1}\Bigg\{ & \ln c_1 + 2c_2\sum_{m=1}^{N_p-1}\mathrm{Re}\left\{\gamma_m(k)\mathrm{exp}^{\mathrm{jm}\epsilon'}\right\} \\ & -c_3\mathbf{z}^H(k)\mathbf{z}(k)\Big\} + \sum_{k=1}^{N_p\times L}\ln f(r(k))\end{aligned} \tag{2.23}$$

where $c_1 = \frac{(\eta+\sigma_s^2)^{N_p}}{\eta^{N_p-1}(\eta+N_p\sigma_s^2)}$, $c_2 = \frac{\sigma_s^2}{\sigma_g^2\eta(\eta+N_p\sigma_s^2)}$ and $c_3 = \frac{(N_p-1)\sigma_s^4}{\eta\sigma_g^2(\eta+N_p\sigma_s^2)(\eta+\sigma_s^2)}$. The first term and last term are not considered for estimation since they are independent of θ and ϵ. Then ML estimate results into

$$\hat{\theta},\hat{\epsilon} = \arg\max_{\theta,\epsilon}\sum_{k=\theta}^{\theta+L-1}\left[\sum_{m=1}^{N_p-1}\mathrm{Re}\left\{\gamma_m(k)\mathrm{exp}^{\mathrm{jm}\epsilon'}\right\} - \frac{N_p-1}{2}\rho\mathbf{z}^H(k)\mathbf{z}(k)\right] \tag{2.24}$$

The above equation (2.24) is obtained after neglecting the positive multiplication constants and $\rho = \sigma_s^2/(\sigma_s^2 + \eta)$. However, we can observe from (2.24) that, the estimation is done using ML will require $N_p^2 L^3$ multiplication. In the first step the STO is estimated as,

$$\hat{\theta} = \arg\max_{\theta} \sum_{m=1}^{N_p-1} \left[\sum_{k=\theta}^{\theta+L-1} |\gamma_m(k)| \; - \frac{N_p - 1}{2} \rho \mathbf{z}^H(k)\mathbf{z}(k) \right] \tag{2.25}$$

Here, the obtained STO $\hat{\theta}$ can be used to estimate the CFO ϵ. The proposed ML algorithm presumes that the CFO estimate makes $\angle \left[\sum_{k=\hat{\theta}}^{\hat{\theta}+L-1} \gamma_m(k)\right] + m\epsilon^{'} = 0$ for $m = 1, \cdots N_p - 1$ where $\angle$ represents the angle. Therefore, we can alternatively find the estimate of CFO for a index m as,

$$\epsilon^{'} = -\frac{1}{m} \angle \sum_{k=\hat{\theta}}^{\hat{\theta}+L-1} \gamma_m(k) \tag{2.26}$$

All the $N_p - 1$ estimates obtained by varying $m = 1, \cdots N_p - 1$ we can find the final estimated CFO can be obtained as,

$$\epsilon_{ML}^{'} = \frac{-N}{2\pi L(N_p - 1)} \sum_{m=1}^{N_p-1} \frac{1}{m} \angle \sum_{k=\hat{\theta}}^{\hat{\theta}+L-1} \gamma_m(k) \tag{2.27}$$

If the CFO is computed using (2.27), then it may require $N_p^2 L^2$ multiplication and thus will result in low complexity.

2.2 Cramer Rao lower bound on CFO estimation

In this section CRLB for unbiased CFO estimation is derived considering STO as a priori. CRLB is defined as sharpness of estimating the unknown parameter. To quantify mathematically we have to determine the peak of the negative second derivative of likelihood function. So, CRLB is

$$\mathbf{E}[(\hat{\epsilon}(r) - \epsilon)^2] \geq \left\{ -\mathbf{E} \left[\frac{\partial^2 \ln f(r|\theta, \epsilon)}{\partial \epsilon^2} \right] \right\}^{-1} \tag{2.28}$$

By performing second derivative we obtain

$$\frac{\partial^2 \ln f(r|\theta,\epsilon)}{\partial \epsilon^2} = -2c_2 \left(\frac{2\pi L}{N}\right)^2 \sum_{k=\theta}^{\theta+L-1} \sum_{m=1}^{N_p-1} \sum_{p=m}^{N_p-1} m^2 \mathrm{Re}\left\{ \sum_{p=m}^{N_p-1} r(k+(p-m)L) r^*(k+pL) \exp^{\mathrm{jm}\epsilon'} \right\} \tag{2.29}$$

Substituting the constant c_2 as we computed in the previous section into (2.29) yields

$$\frac{\partial^2 \ln f(r|\theta,\epsilon)}{\partial \epsilon^2} = -\frac{8\pi^2 L^3 \sigma_s^2}{N^2 \eta(\eta + N_p \sigma_s^2)} \sum_{m=1}^{N_p-1} m^2 (N_p - m) \tag{2.30}$$

By expansion of the summation in (2.30) the second derivative will be simplified into

$$\frac{\partial^2 \ln f(r|\theta,\epsilon)}{\partial \epsilon^2} = \frac{2\pi^2 L^3 N_p^2 ((N_p^2-1)\sigma_s^4)}{3N^2 \eta(\eta + N_p \sigma_s^2)} \tag{2.31}$$

Finally, the CRLB can be given by

$$\mathbf{E}[(\hat{\epsilon}(r) - \epsilon)^2] \geq \frac{3N^2 \eta(\eta + N_p \sigma_s^2)}{2\pi^2 L^3 N_p^2 ((N_p^2-1)\sigma_s^4)} \tag{2.32}$$

The following conclusions can be made after observing the bound:

- As the energy of the pulse shape filter in the symbol interval decrease we observe raise in η value, which in turn increase the bound value. It indirectly inference an increase in the error floor.
- When data samples in each set or number of sets used i.e., when L, N_p increase the bound is going to decrease. It is to be remembered that, the increase of number of sets will require a trade off in data efficiency.
- Presence of multiple sets in the preamble will offer an advantage of increase in range of CFO estimation at the cost of BER.

2.3 Results

This paper validates real time implementation of the GFDM system in indoor room environment using IEEE 802.11 short preamble by employing pulse shaping. For demon-

Figure 2.2: Experimental set-up used for testing algorithm in real time environment

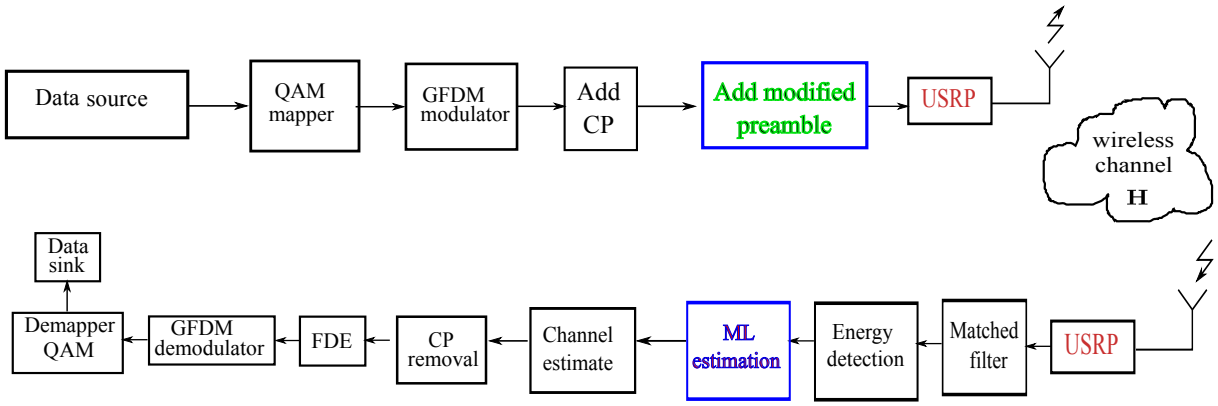

Figure 2.3: Block diagram of the real time implementation of GFDM system with National instruments USRP's

stration, the hardware platform used is NI USRP 2953R which is interfaced with LABVIEW software of NI. USRP is capable of operating in frequency range of 1.2 to 6 GHz with a bandwidth of 120 MHz. These configurations enable us to test all waveforms used in today's mobile communication. PC shown in the Figure 2.2 is connected to USRP using a NI PXIe-PCIe8371 which is having a high throughput of 832 MB/sec. The real time demonstrator is having two USRP terminals, one acting as transmitter and other as receiver. Both USRP's are connected to workstations for base-band processing. Parameters used for demonstration are tabulated in Table 2.1. The transmitter USRP acquires digital IQ samples via PCI-Express card which performs digital to analog conversion and transmits over air. In receiver USRP, IQ samples captured by USRP are passed to the host PC using another PCI-Express connection for performing baseband operations. Since

USRP performs principal operations like decimation, up and down frequency conversion etc in hardware it exhibits real time communication scenario. It is to be noted that, after performing all signal processing operations on GFDM symbol, a zero padding sequence of length 8 is added at the start and at the end to a complete packet. This is done in order to differentiate the received signals in time. After performing all the required baseband operations, RF up-conversion is done and transmitted over the air using the transmit antenna. Initially, based on the simulation parameters which are tabulated in Table 2.1, the mean square error (MSE) vs SNR analysis for CFO and STO over AWGN as well as dispersive channel conditions for various pulse shaping filters are presented. The chosen dispersive channel is Rayleigh with 8 taps linearly varying from 0dB to −8dB. The typical distance between both USPR is around 5 m and hence testing in Rayleigh channel is mandatory for demonstrating the multipath channels

Table 2.1: Parameters for Simulated and real time GFDM system

Parameter	**Value**
Number of subcarriers	64
Number of subsymbols	5
CP length	8
Prototyping filter	Root raised cosine
Filter roll off factor	0.9
Transmitter oversampling factor	2
Reciever oversampling factor	2
Capture time	4 ms
Transmitter sampling rate	4M
Zero pad length	8
Preamble pulse shaping	Tukey,rect
Receiver sampling rate	4M
Transmitter gain	0dB
Receiver gain	1dB
Carrier frequency	2.4GHz

Figure 2.4, illustrates the MSE vs SNR of CFO over AWGN and dispersive channel.

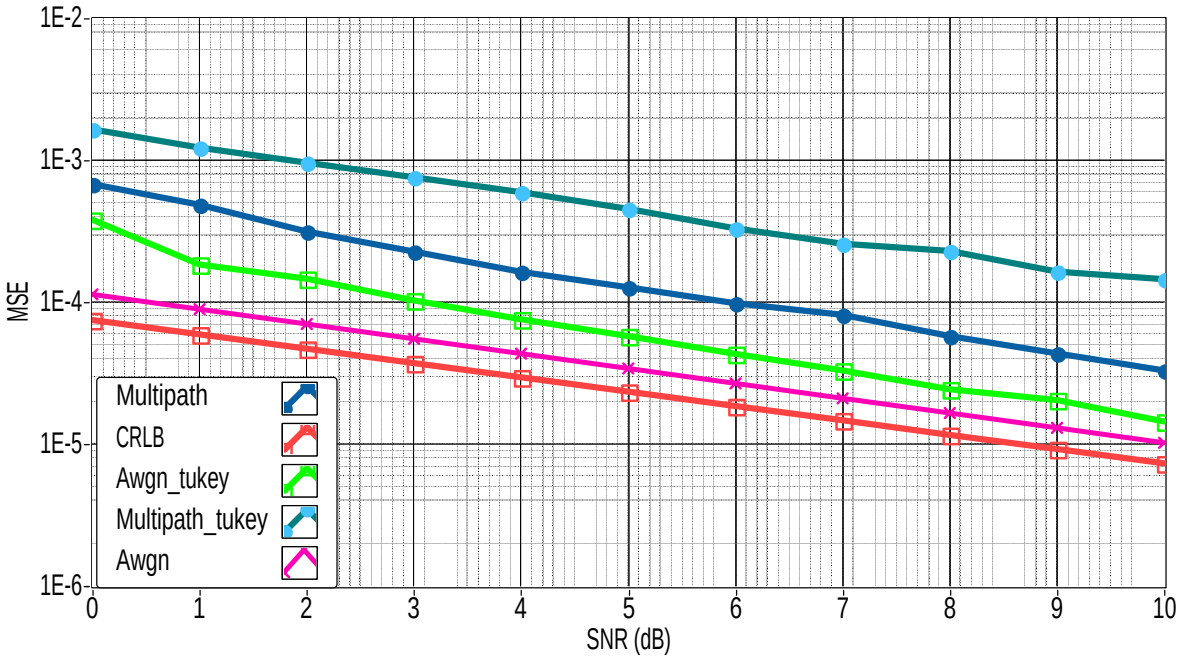

Figure 2.4: MSE of the CFO estimate for various SNRs

For pulse shaping, two types of filters are employed namely Rectangular and Tukey. From the figure it is evident that as the SNR increases, a better MSE is attained for all the cases. The theoretical analysis carried out in Section IV for CRLB is plotted against SNR. It can be viewed that at an SNR of 10 dB, the observed error floor is 1.7×10^{-5}. Without loss of generality, the bound is plotted by considering the rectangular pulse shape filter. It is obvious that, both pulse shaping filters yield good performance over AWGN channel. There is a slight degradation in performance over dispersive channel conditions.Over AWGN channel, at an SNR of 10 dB, Rectangular filter attains an MSE of 2.61×10^{-5} while Tukey filter has MSE of 5.87×10^{-5}. In case of dispersive channel environment, the performance deteriorates for Tukey pulse shaping filter when compared with Rectangular pulse shaping filter. This is clearly observed because at an SNR of 10 dB, Tukey attains an error of 1.28×10^{-4} while Rectangular achieves 3.2×10^{-5}. The reason behind the accuracy of the result is that among received preamble set, it is easy to prove that the product $r(k + (p - m)L)r^*(k + pL)$ in (2.29) results into continuous summation of constant multiplying random variables which follow chi-square distribution with two degrees of freedom and three zero mean Gaussian random variables. So, with the increase in number of preamble data, the real and imaginary part of $\gamma_m(k)$ by statistical properties converge to $\sin(2\pi m\epsilon')$ and $\cos(2\pi m\epsilon')$ respectively. Therefore, at a consistent

time offset estimation, variance of each term converges to zero indicating the best possible accuracy for CFO estimation for the proposed scheme

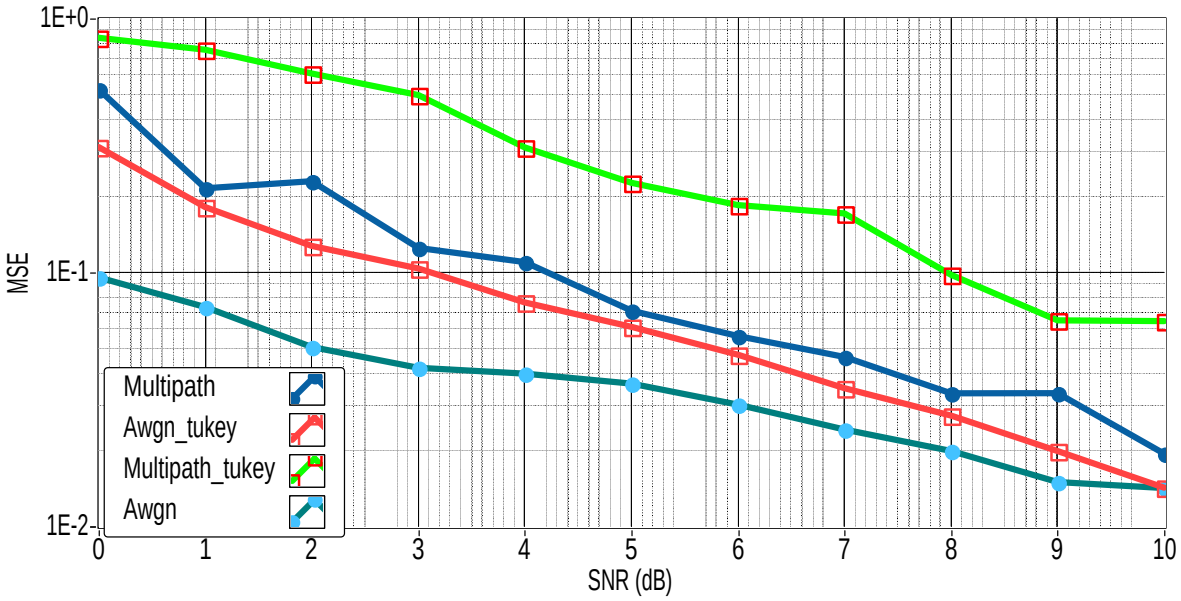

Figure 2.5: MSE of the STO estimate for various SNR in dB

The MSE for STO vs SNR for both pulse shaping filters namely Rectangular and Tukey over AWGN as well as dispersive channel is depicted in Figure 2.5. Here, it can be observed that a huge amount of error is obtained when Tukey pulse shaping is employed over dispersive channel environment. At an SNR of 5 dB the observed error is 0.22546 while the error decreases progressively as the SNR increases. At an SNR of 10 dB the error attained for Rectangular and Tukey filer is 0.0193286 and 0.0634 respectively over dispersive channel. However, the performance is improved over AWGN channel for both pulse shaping filters. The peak of likelihood function is broadened by the channel dispersion for multipath environments. This results in high error floor of STO estimation at low SNR.

The usage of Tukey filter resulted in higher MSE than the traditional rectangular filter because of increase in the value of η as evidenced from Figure 2.4, 2.5. The exact advantage of using this filter can be depicted in the spectral response of real time results. The IEEE 802.11a standard preamble consists of ten short symbols and two long symbols which are identical with each other. For demonstration simplicity, we have used 10 repeated short symbols for time and frequency estimation. The data is transmitted in IQ representation, but the Quadrature phase data is only shown since it provides enough

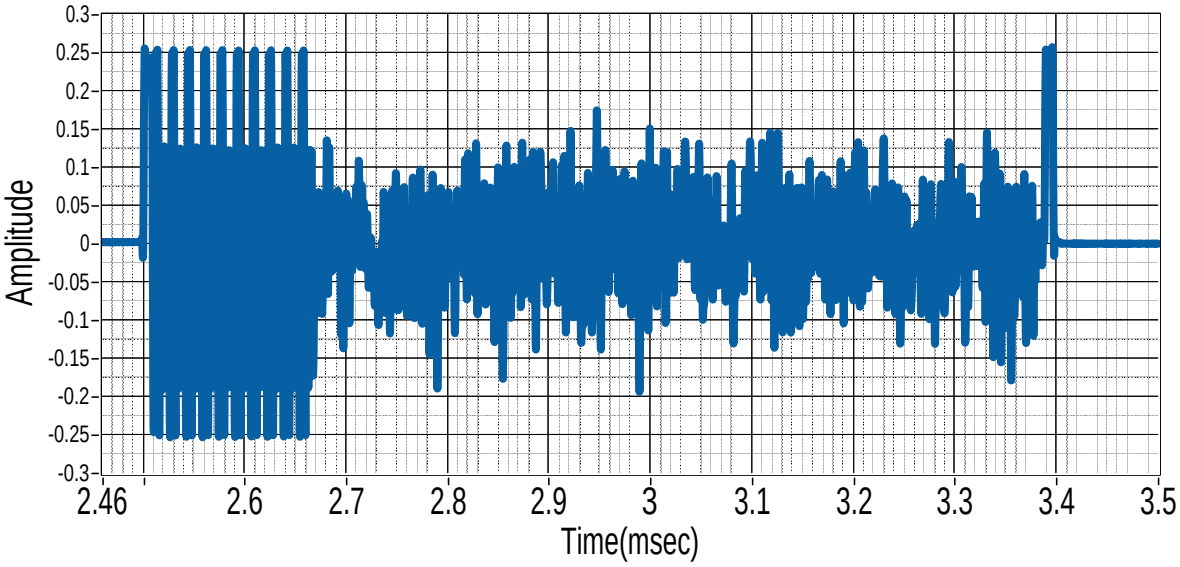

Figure 2.6: Received Quadrature data after STO estimation at SNR=10dB

interpretation. Each short symbol in the preamble extends to a duration of 4 micro seconds and hence consists of 16 samples. High amplitude in the data packet occurs because of this preamble as depicted in Figure 2.6. For the proposed preamble, each 16 length short sequence is windowed by generating a tukey filter with ramp up and down of 2 bits. The repetition in preamble enables us to enhance the CFO estimation range later in the receiver. The discontinuities in the amplitude of the Quadrature signal in Figure 2.6 occurs because of circular prototyping. The advantage of this representation lies in reduction of the energy spending required by the USRP terminal.

The received spectrum is depicted in Figure 2.7 where a minimum OOB radiation of -46 dB has been observed. This is achieved because of localization of time and frequency using a prototype filter. So, at every subcarrier we could get reduction in egress noise which was the major concern in OFDM systems. Since we are presenting real time results a more realistic spectrum is shown in Figure 2.7. This spectrum is obtained after adding rectangular pulse shaped preamble of length 160 to the GFDM symbol. The zigzag nature of spectrum occurs because of addition of noise. We also observe spikes in the spectrum due to the rectangular filtering of preamble, decreasing its reliability in scrambled spectrum applications. In this figure, half of the subcarriers are disabled intentionally to illustrate the difference in OOB emissions between the conventional and proposed preamble. Figure 2.8, clearly shows the advantage of enforcing the Tukey pulse

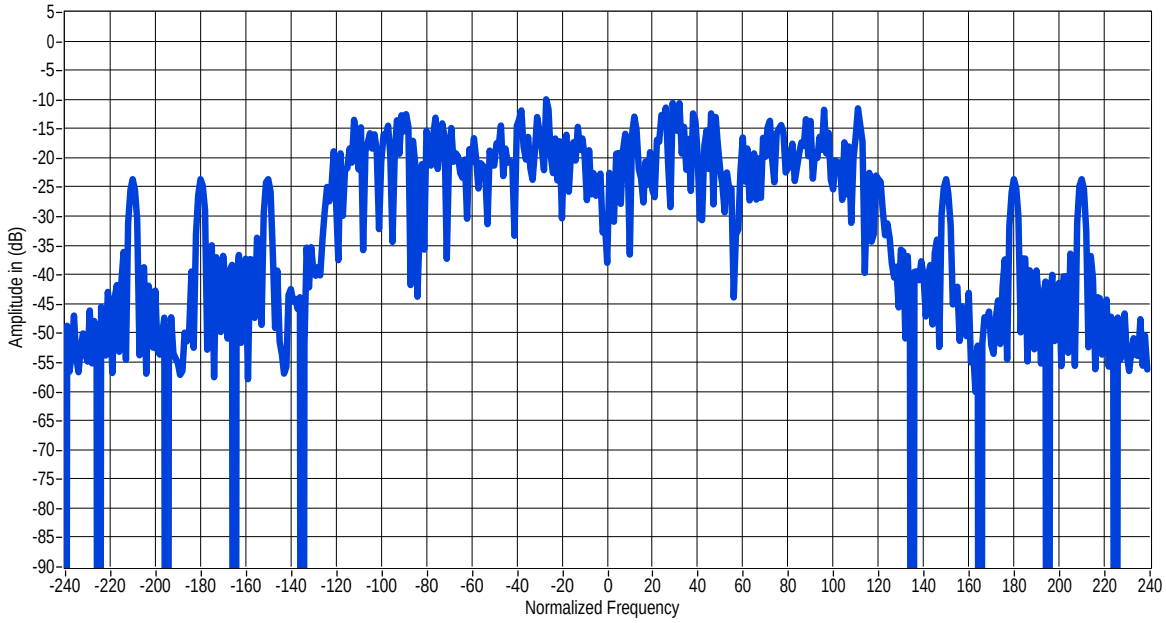

Figure 2.7: Received GFDM spectrum with IEEE 802.11 preamble without pulse shaping

shaping in GFDM system. Though there are little spikes but the maximum amplitude of spikes is decreased from -26 dB to -35 dB. A relatively sharp decay in side lobes is observed due to incorporation of pulse shaping in preamble which in turn leads to reduction of OOB emission. Hence, the advantage of GFDM is maintained.

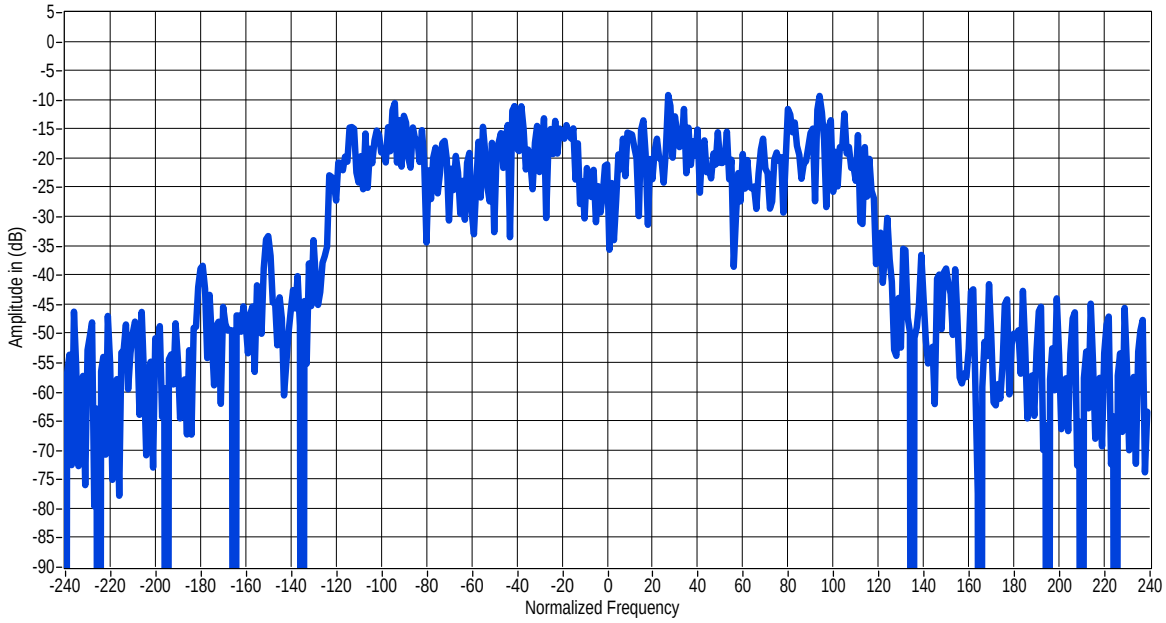

Figure 2.8: Received GFDM spectrum with IEEE 802.11 preamble after pulse shaping

The observed experimental values in indoor environments are tabulated in Table 2.2. Energy detection method incorporated in the receiver not only estimates the data

Table 2.2: Observed experimental values in indoor environments for various pulses

Parameter	Spike	MSE at SNR=5dB	MSE at SNR=10dB
Tukey	-40.757 dB	0.00010171	2.64E-05
Xia	-37.28 dB	5.76E-05	1.44E-05
Rectangular	-31.8457 dB	3.69E-05	1.17E-05
CRLB	-	2.34E-05	7.31E-06

packet along with misalignments which arises due to channel delay but also includes the time lag introduced by pulse shaping and matched filtering. Figure 2.6 shows the received IQ signal and its corresponding spectrum is shown in Figure 2.8 where both are diminished in amplitude, distorted in time and frequency. These impairments occur due to indoor channel environments. The spectrum after enforcing synchronization algorithms which suggest that the system performance is not destroyed by adding pulse shape to the preamble. GFDM combats the real time environments similar to OFDM despite of its non orthogonal nature. An important point to be observed is that there is a lag in the captured IQ signal by USRP. Indirectly it is a measure of transfer capability, so one wants it to be as minimum as possible. In this regard, we are able to capture the GFDM signal along with the pulse shaped preamble at a value of 3.5 ms as shown in Figure 2.6. Lag in the IQ received signal is not only because of transmission wait but also real time processing delay of USRP hardware.

2.4 UW-GFDM Synchronization

Recently the variant of GFDM named as UW-GFDM is proposed [28]. The authors have suggested a two step process for its generation. The first step involves in introduction of correlations in the frequency domain by replacing the data part of time domain signal with block of zeros at UW positions. The purpose of introducing correlations in frequency domain is to obtain coding gain. In the second step, application desired UW can be inserted in the position of zeros to satisfy requirements like synchronization, channel estimation which leads to improvement in system BER. In short, UW is a deterministic sequence obtained by replacing the zeros in time domain for a UW-GFDM signal which

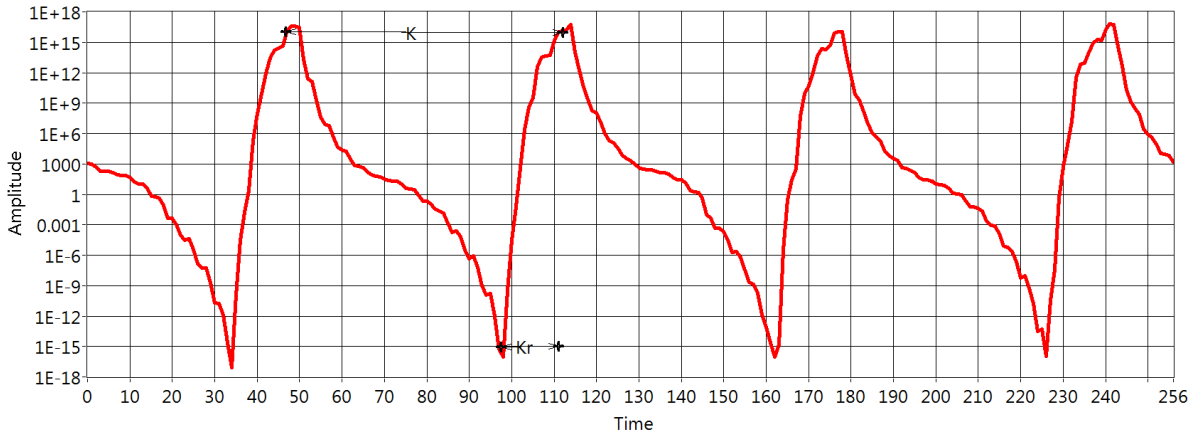

Figure 2.9: Behaviour of the proposed timing metric for the AWGN channel conditions

sacrifices certain subcarriers named as redundant subcarriers in every subsymbol inorder to obtain coding gain [67].

It is important to note that, even for the case of null UW sequence, a systematic code is present within the sequence of subcarriers of every subsymbol. The coding gain in the UW-GFDM is achieved at the cost of strict synchronization. If the received data is not in the range of designed GFDM window due to improper time offset, it will destroy the system performance. In literature we find many methods employing preamble aided synchronization [42]. But they rely on the fact that the probability of false alarm or probability of not receiving the preamble is minimum. Instead, in this work, we propose a metric by avoiding the step 2 in generation of UW-GFDM system. The proposed scheme uses the fact that the energy in the locations of UW is minimum. The suggested scenario would result in low power consumption along with STO estimation. In this work, the structure of UW-GFDM is used for performing STO estimation for the first time. The proposed estimation algorithm involves with the usage of zeros which occur due to presence of redundant subcarriers in every subsymbol. However, the existent literature uses either CP or pilots for doing the same. so we present MSE comparison that involves varying the number of redundant subcarriers which is more appropriate than prior methods of comparison.

The final UW-GFDM after step 1 will be of the form,

$$\mathbf{x} = [\mathbf{x_{1d}}\ \mathbf{0}\ \mathbf{x_{2d}}\ \mathbf{0} \cdots \mathbf{x_{(M-1)d}}\ \mathbf{0}] \tag{2.33}$$

Every $\mathbf{0}$ in (2.33) is of length K_r and are present at a equidistant by amount of K. In

the step 2, an application driven UW is inserted in the place of 0 in the vector **x**. We avoid step 2 of the generation of UW-GFDM symbol and propose a metric using already available zeros in the next section. The signal model for complex received samples $r(n)$ effected with an integer STO of θ in AWGN channel of w(n) can be given as,

$$r(n) = x(n-\theta) + w(n) \tag{2.34}$$

2.5 Proposed algorithm

The primary idea of the proposed metric lies in utilizing the fact that the energy in the locations of UW is minimum. This scenario not only performs blind STO estimation but also achieves low power consumption. The presence of GFDM signal can be detected i.e., STO estimation can be performed upon the receipt of only one subsymbol. The important system parameters like redundant subcarriers, subsymbol start time can be found with the aid of zeros corresponding to the other symbols. The metric proposed for the estimation of above mentioned parameters is,

$$M(\theta) = \frac{\sum_{n=0}^{K_r-1} |r(n+\theta)|^2}{\sum_{m=1}^{M}\sum_{n=0}^{K_r-1} |r(n+mK-K_r+\theta)|^2} \tag{2.35}$$

The denominator in (2.35) is the summation of squares of the received vectors of length K_r which are present at a distance of K. The maximization of the proposed metric happens when the denominator is minimum, i.e., when the estimated index coincides with locations of the zeros in the original UW-GFDM structure. This idea leads to a large difference between the peak value and the troughs. Another essential point in the design of the metric is to circumvent the divide by zero error. This will automatically occur in multipath channels due to presence of signal fading. In the same way, in the presence of AWGN the noise would have a finite variance and to increase the probability of avoidance of the error, when M summations are performed. The numerator in (2.35) is indicating the signal power, which is mandatory to balance the channel in multipath environments. This operation may also be regarded as a part of automatic gain control. The timing metric for the AWGN channel for an UW-GFDM signal with 64 subcarriers, 4 subsymbols and an UW of length 16 is shown in the Figure.2.9. We considered the AWGN

channel at a SNR of 10 dB, where the SNR represents the total signal (all subcarriers in every subsymbol) to noise power ratio. We can clearly observe repetition of peak and trough in regular intervals in the proposed metric. This fancy structure of the proposed metric is highly useful for timing estimation, empowering it to achieve a more accurate estimation. The required system parameters can be found in the following way,

2.5.1 Number of subsymbols

This is the first and foremost step in the synchronization algorithm. From the Figure.2.9, it can be clearly depicted that the number of peaks which occur is equal to number of subsymbols M present in the UW-GFDM, which lead to its straightforward estimation. There won't be any uncertainty in the estimation of the peaks because the typical values of peak for AWGN environments are at a very high value of 10^{16}.

2.5.2 Number of subcarriers

After finding all the peaks, we can observe that all of them occurs at equidistance. This occurs due to the presence of equidistant zeros in the structure of UW-GFDM system. Incidentally this would lead to estimation of number of subcarriers K, by finding the difference in the time indices between the consecutive peaks in the proposed metric.

2.5.3 Symbol time offset estimation

Frame detection can be performed by identifying the maximum among the peaks present the proposed metric,

$$\theta = \left(K - \arg\max_{n} M(\theta) \text{mod } K\right) \tag{2.36}$$

Typically the values of all the peaks will be the same in AWGN channels. Here, an important observation for finding the time offset estimation is, utilization of mod operator. This is introduced considering multipath channel environments since all subsymbols present in the system may not experience the same signal fading. However, in relative comparison, a single peak occur for every subsymbol. However, it is not mandatory that the peak always

occur at the first subsymbol. So utilization of mod will lead to a legitimate expected value for time offset.

2.5.4 Number of redundant subcarriers

We have used peaks for finding all the above mentioned system parameters. One can utilize trough for finding the same. However, inorder to determine the number of redundant subcarriers which is crucial parameter for demodulation we require both peaks and troughs. From the Figure.2.9, it is evident that, the we can determine the number of redundant subcarriers with the aid of difference in between the time indexes of the peak and trough present in the metric. This may lead to a confusion in multipath channels because the peak and crest of different subsymbols may be selected. This will be automatically avoided by the proposed expression where the value K from the section 2.5.2 is used for determining the value of K_r,

$$K_r = \left(K - \arg\min_n M(\theta) \text{mod } K\right) \tag{2.37}$$

- We can observe that the peak occurs at equidistance. This occurs due to the presence of insertion of equidistant zeros in the structure of UW-GFDM system. Incidentally this would lead to estimate the number of subcarriers K.

  $$K = \arg\max_n M[\theta] \tag{2.38}$$

  Channel conditions may not experienced in the same way for all the subsymbols present in the system. It is not mandatory that the peak always occur at the K^{th} time instant. However, the highest peak among all the subsymbols will be selected

- As the maximum occurs at the K_r index of the subsymbol we can determine the number of redundant subcarriers with the aid of difference in between the time indexes of the peak and trough present in the metric.

- The number of peaks which occur are the number is equal to number of subsymbols M present in the UW-GFDM.

The behaviour of the metric in multipath environments results into relatively broader peak. This is due to the fading environment created by these channels. It is remembered

that by allocating sufficient redundant carriers, even for the case of multipath channel environments metric provides good performance which will evidenced later in the result section.

2.6 Results and discussion

The structure of UW-GFDM is used for performing STO estimation for the first time. The offset is estimated by proposing an algorithm that involves in the usage of zeros which are existent in every subsymbol created in the process of generation of redundant subcarriers. However, the existent literature uses either CP or pilots for doing the same. It is also observed that MSE comparison that involves varying the number of redundant subcarriers is more appropriate than prior methods of comparison. In this section, performance of the proposed time synchronization scheme is evaluated by MSE for a UW-GFDM system with simulation parameters shown in Table 2.3. From (2.35), the algorithm is only dependent on the energy in the interval of K_r, whose value has to be properly chosen if low MSE is desired. This is because, the proposed metric doesn't use the traditional approach of utilizing auto correlation or cross correlation which are highly dependent on SNR. However, an increment in K_r may require compromise in throughput efficiency.

Table 2.3: Simulation parameters

Parameter	**UW-GFDM**
Mapping	16-QAM
Number of Sub Carriers(K)	64
Number of Sub Symbols(M)	4
Number of redundant subcarriers(K_r)	16
Cyclic prefix	8
prototyping filter	RRC
Roll off factor	0.2

Figure 2.10 shows the MSE versus SNR for the proposed blind STO estimation for UW-GFDM system. Here, for the purpose of interpretation we have considered different

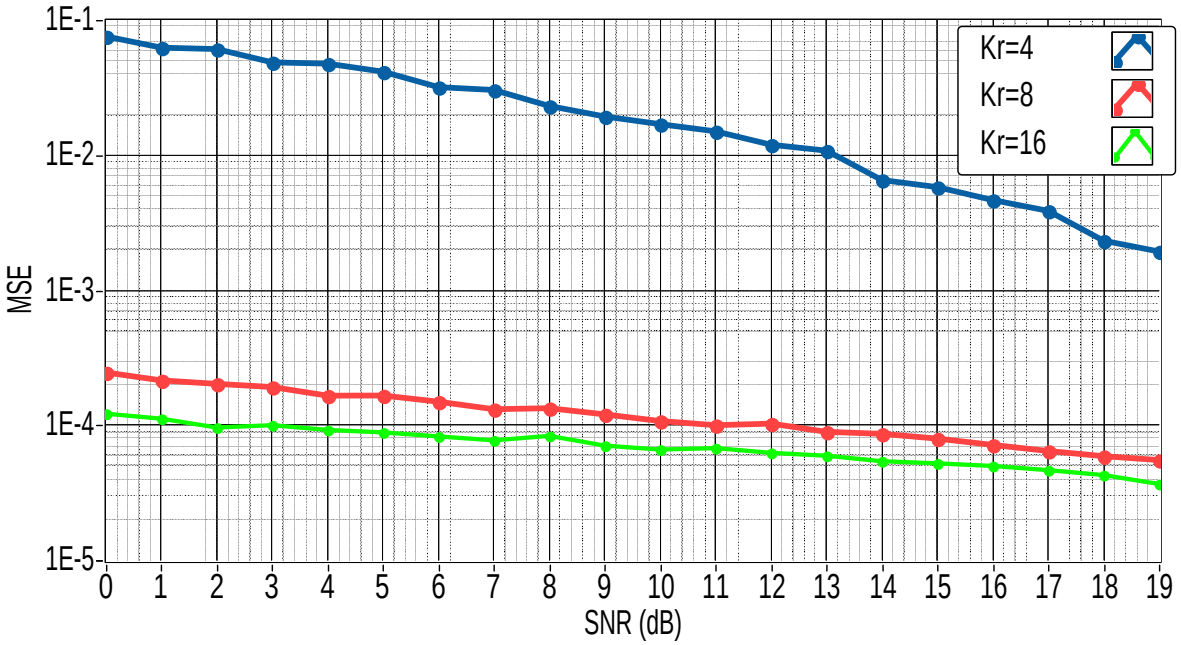

Figure 2.10: MSE of STO estimation for AWGN channel

values of redundant carriers and the type of channel considered is AWGN channel. It can be observed that, the MSE for the proposed method is not much dependent on the value of SNR and decreases with increase in K_r. However, in simulations there a slight improvement in MSE with increase in SNR for every case. As an example for $N_r = 16$ the MSE are 0.0169545 and 0.0019335 at SNR of 9 dB and 19 dB respectively.

Even for multipath channel environment, we observed an improvement in MSE with increase in value of K_r. Due to the effect of fading, numerical value of error is high in these channels when compared with AWGN. Similar to the AWGN channels, MSE is not highly dependent on SNR and only depends main on the value of K_r as shown in Figure 2.11. We can conclude from Figure 2.10 and Figure 2.11 that MSE is highly dependent on chosen K_r of the system.

We observed a specific code in frequency domain in the system which is the primary reason for high coding gain. Another important metric which is to be considered is, variations of PAPR with increase in the coding gain. The well accepted complementary CDF, which represents the probability that PAPR of a UW-GFDM block exceeds a given threshold (PAPR0) is used for measurement of PAPR,

$$CCDF(PAPR_0) = P_r(PAPR > PAPR_0) \tag{2.39}$$

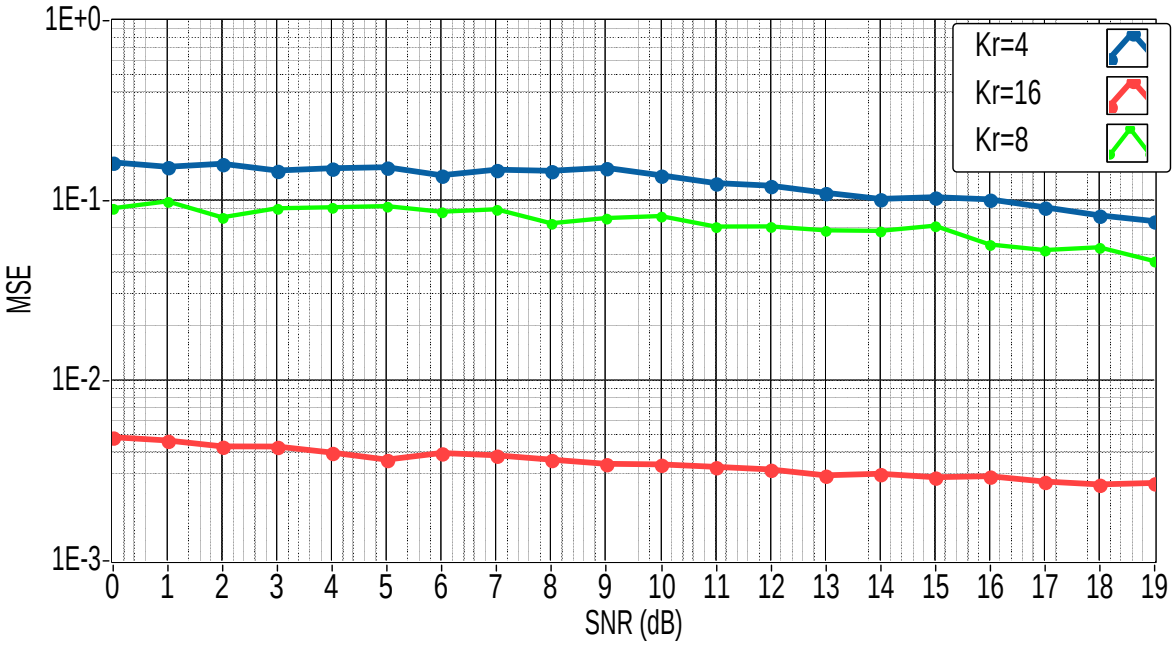

Figure 2.11: MSE of STO estimation for multipath channel

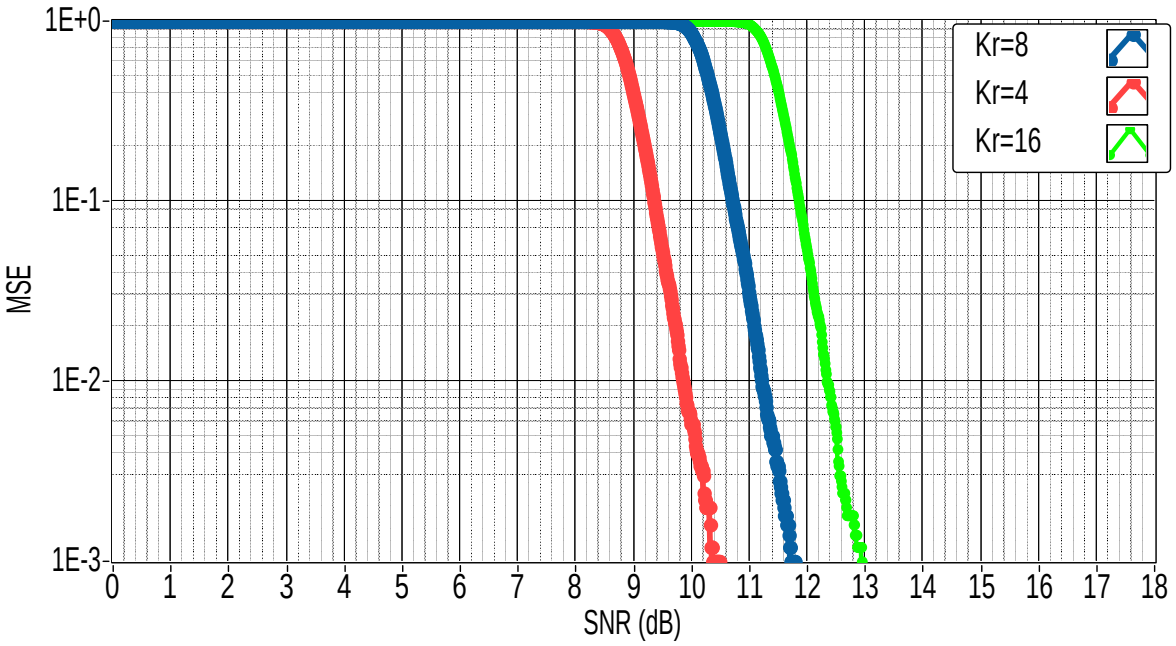

Figure 2.12: PAPR plot for different values of K_r

The conducted simulation results indicate that as the K_r value increases from 4 to 16, PAPR performance becomes worse. Hence for a high coding gain, a sizeable superimposition happens in frequency domain which requires compromise on PAPR as evidenced from the Figure. 2.12.

2.7 Conclusion

The synchronization of UW-GFDM and GFDM are addressed in this chapter. The ML estimation algorithm using pulse shaped multiple sets of identical data for correcting the time and frequency misalignments for GFDM systems is derived. This is done to preserve the spectral advantage of the system. The CRLB for the frequency offset for an arbitrary pulse shape is also obtained. The main advantage of this modified preamble occur in the real time results by reduction of slope and unwanted spikes in the spectrum characteristics. The proposed method of time synchronization for UW-GFDM system is doesn't depend on SNR and mainly depends on the value of number of redundant subcarriers. We observed by increasing the number of redundant subcarriers we achieve effective synchronization and coding gain at the cost of PAPR and data efficiency.

Chapter 3

Blind CFO estimation and jitter noise reduction using oversampling

3.1 Introduction and Motivation

The usage of discrete prolate spheroidal sequences as prototype filters in MGFDM was found to improve the orthogonality of the system. In this chapter, the first part will deal with the real time transmission of MGFDM is carried using USRP by implementing various channel estimation and synchronization algorithms. We employed all the correction algorithms using a windowed preamble to satisfy low OOB requirements. However, the high speed performance of MGFDM system is heavily effected by jitter noise, since it results in improper sampling instances. jitter noise is one of the more complex limitation in GFDM systems which demands high data rates [68]. The timing jitter in GFDM radios which feature high frequency bandpass sampling nature will allow a little tolerance for error free transmission since the system is designed assuming uniform sampling intervals. Low pass timing jitter which occurs due to Phase Lock Loops (PLL) is considered in this chapter. In specific, we discuss the effect of oversampling on jitter noise in an oversampled GFDM system. It will be proved that the jitter noise is not a function of subcarrier or subsymbol indexes and oversampling will reduce noise equally across all subcarriers. Furthermore, we observe a linear reduction in degradation caused by timing jitter upon increasing oversampling. The proposed theory is validated using USRP 2953R hardware interfaced with LabVIEW software. Conventional training sequence based methods allevi-

ate the effect of time and frequency misalignments by using the concept of data repetition in the pilot preamble, which recedes data efficacy. This chapter enlightens various aspects in real time implementation of blind GFDM signal transceiver using oversampling for CFO correction in indoor environments. Moreover, the numerical value of CFO is independent of subcarrier and subsymbol indices i.e., the effect of change in frequency is same for all subcarriers and doesn't depend on the subsymbol location in the GFDM block. In this chapter, we exploit the constant phase obtained from difference of phase shift between neighbouring samples in twice oversampled signal for CFO estimation. The CRLB for the oversampling based GFDM signal model is derived. Also, we prove through simulation that, the proposed algorithm results in a little error floor. More importantly, the proposed method is data efficient because of the fact that, it utilizes only one GFDM symbol using reliable ML estimation in the presence of noise and multipath channels. In simulation, synchronization and channel estimation can be performed without any order in their implementation. The channel equalization on unsynchronized data would lead to improper selection of MGFDM block which cause erroneous effects. After examining the importance of this phenomenon, we implemented various synchronization algorithms before channel estimation. The results for spectrum and time domain waveforms in the received USRP show a satisfactory performance of system. This work also discuss the effect of oversampling on jitter noise in an oversampled GFDM system. Moreover, the constellation diagrams received in USRP validate the result by showing a good agreement with simulations.

3.2 MGFDM System Model

MGFDM system consists of K subcarriers and M sub symbols in a block of N elements, in a way single carrier is bearer of M overlapping sub symbols in time. Data symbols are obtained by QAM or PSK modulation and $d_k(m)$ is used for representing a data symbol on k^{th} subcarrier at m^{th} time slot, so $\mathbf{d_k} = [d_k(0) \cdots d_k(M-1)]^T$ shows to

be data on the k^{th} subcarrier. Here T stands for transpose operation.

$$\begin{aligned} x(n) &= \sum_{k=0}^{K-1} (p_k(n) \odot g(n)) e^{j\frac{2\pi kn}{K}} \\ &= \sum_{k=0}^{K-1} \sum_{m=0}^{M-1} d_k(m) g\left\{(n - mK) \text{mod} MK\right\} e^{j\frac{2\pi kn}{K}} \end{aligned} \tag{3.1}$$

where $p_k(n) = \sum_{m=0}^{M-1} d_k(m)\delta(n - mK)$ is subcarrier processing and $\odot$ represents the circular convolution utilized to obtain the MGFDM signal $\mathbf{x} = [x_0\ x_1 \cdots x_{N-1}]$. Here $g(n)$ is the prototyping filter used to nullify OOB radiations which is chosen a Multitaper filter in this work. It is interesting to note that the same MGFDM system would act as Multitaper windowed OFDM when $M = 1$. The summation in matrix representation can be formulated as [24],

$$\mathbf{x} = \mathbf{A}\mathbf{d} \tag{3.2}$$

Matrix $\mathbf{A}$ is a $N \times N$ matrix which incorporates all the necessary signal processing steps like upsampling, frequency translation along with subcarrier filtering. While $\mathbf{d} = [\mathbf{d_0}^T\ \mathbf{d_1}^T \cdots \mathbf{d_{K-1}}^T]^T$ represents the vector containing the data symbols. CP is appended at the start of every MGFDM symbol, which is analysed over multipath channel with coefficients $\mathbf{h} = [h(0) \cdots h(J-1)]$. The received signal after cyclic prefix removal can be expressed as

$$\mathbf{y} = \mathbf{H}\mathbf{x} + \mathbf{n} \tag{3.3}$$

where $\mathbf{H}$ is matrix of dimension $N \times N$ with its first column as $[h(0) \cdots h(J-1)\ 0 \cdots 0]^T$, which is obtained after appending $N - J$ zeros and $\mathbf{n}$ represents the additive white Gaussian noise (AWGN). The signal detection at receiver is performed by zero forcing equalization of the channel in frequency domain. The detected signal under perfect channel estimation and synchronization $\hat{\mathbf{y}}$ is

$$\hat{\mathbf{y}} = \mathbf{W_N^H \Lambda^{-1} W_N y} = \mathbf{x} + \mathbf{W_N^H \Lambda^{-1} W_N n} \tag{3.4}$$

where $\mathbf{W_N}^H$ and $\mathbf{W_N}$ represent N point IFFT and FFT matrices, $\mathbf{\Lambda}$ contains eigenvalues which are found by performing DFT of first column of channel matrix $\mathbf{H}$. Here $\mathbf{W_N^H \Lambda^{-1} W_N}$ in (3.4) indicates inverse channel response decomposed by using circulant matrix property. As a result, we can rewrite the detected signal as

$$\hat{\mathbf{y}} = \mathbf{x} + \mathbf{H^{-1}n} \tag{3.5}$$

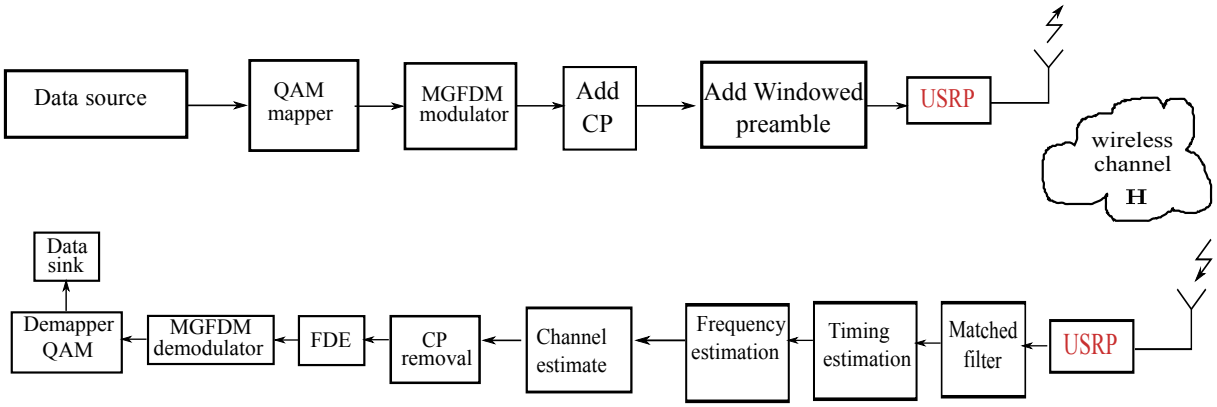

Figure 3.1: Block diagram of the real time MGFDM transmission system

The original data symbols after channel equalization can be obtained by multiplying with receiver matrix $\mathbf{A_r}$. We consider matched filter in this work as receiver filter in order to maximize the SNR. Finally, the estimated data $\hat{\mathbf{d}}$ is,

$$\hat{\mathbf{d}} = \mathbf{A_r}\hat{\mathbf{y}} \tag{3.6}$$

Since $\mathbf{A_r}$ is obtained by using matched filter operation, $\mathbf{A_r} = \mathbf{A^H}$ where H is hermitian of a matrix. In real time transmission GFDM signal is sensitive to presence of STO, CFO. Despite of the fact of applying enough cyclic prefix, GFDM is prone to give errors [23]. For that reason simple equalization performed in (3.4) is not achievable. To compensate these impairments a windowed preamble is added at the start of every data packet. We will use same preamble for correction of all misalignments that occur due to indoor channel. This practice is traditionally followed in IEEE 802.11 wireless standard. Therefore, the received signal with all effects can be represented as

$$y(n) = e^{j\frac{2\pi\epsilon n}{N}} \sum_{j=0}^{J-1} \sum_{n=0}^{N-1} h_n x_{j-n-\theta} + W(n) \tag{3.7}$$

The signal from air would have a STO of θ and frequency shift factor ϵ along with AWGN $W(n)$. Presence of a constant θ is easily correctable by the receiver but the time jitter of τ_n cause deviation from the actual sampling rate resulting in system performance degradation.

3.3 Synchronization and channel estimation

In this section different steps in the implementation of MGFDM system are presented. The transmitted signal is received only at certain times, so STO estimation involves MGFDM frame detection, while CFO estimation involves in estimating the frequency distortion created due to the channel. The exact order in the implementation of the MGFDM system is shown in Figure 3.1.

3.3.1 Frame detection

Frame detection assumes that among the samples the windowed preamble is present [41]. The received signal r and its preamble r_p are of length N and N_p correspondingly. we use autocorrelation property for MGFDM frame detection.

$$\rho(n) = \left| \sum_{k=0}^{N_p-1} r_p(k)^* r(k+n) \right|^2 \tag{3.8}$$

where $*$ represents the hermitian operation which is used for performing STO estimation. Firstly, we collect the values of $\rho(n)$ for $n = 0 \cdots N_p - 1$. Transmission in indoor environment would have it's first channel tap as dominant. This factor contribute to accurate frame detection independent of channel behaviour.

$$\theta = \arg\max_n \rho[n] \tag{3.9}$$

By solving for θ, correlation peak occur only at preamble, so exact MGFDM frame can be identified.

3.3.2 CFO estimation

CFO estimate is done by using self referenced method which relies on periodic nature of training sequence instead of its correlation properties. To elaborate, the CFO is estimated using repeated nature of the preamble by finding the least squares (LS) estimate between two equal half's of length $N_p/2$ present in the preamble.

$$\bar{\epsilon} = \frac{\text{phase}\left(\sum_{k=J}^{\frac{N_p}{2}-1} r^*(k) r(k+\frac{N_p}{2}) \right)}{\pi N_p} \tag{3.10}$$

The above equation (3.10) will give good results, if the chosen training symbol is capable of estimating the range of CFO. It is worth mentioning that incorrect offset estimate would rotate the signal and complicates the channel equalization.

3.3.3 Channel estimation

The preamble which is CFO compensated is utilized for channel estimation. LS estimate of channel is found by minimizing mean squared error between sent and received preamble

$$\bar{\mathbf{H}} = (\mathbf{r_p^* r_p})^{-\mathbf{1}} \mathbf{r_p^* x_p} \tag{3.11}$$

where $\mathbf{r_p}$ and $\mathbf{x_p}$ represents the received and sent preambles.

3.4 Effect of oversampling

To illustrate the effect of oversampling on timing jitter, we assume perfect STO, CFO, channel estimation. This is achieved by using the windowed preamble as shown in (3.9), (3.10) and (3.11). A matrix model for received MGFDM signal by focussing on effect of time jitter with channel matrix $\mathbf{H}$ is,

$$\mathbf{r} = \mathbf{WHAd} \tag{3.12}$$

where $\mathbf{W}$ is the effect of time jitter in matrix of dimension $N \times N$ [69]. Amalgamating all the notations, effect of oversampling on the detected data in matrix notation is given by

$$\hat{\mathbf{d}} = \mathbf{A_r H^{-1} r} = \mathbf{R^L UWVd} = \mathbf{Sd} \tag{3.13}$$

Oversampling matrix $\mathbf{R^L}$ is defined as $LN \times N$ matrix with one's present in its column having index as integer multiples of L at Lnth position. Here the column index n extends from 0 to $N-1$. The introduced matrices are defined as $\mathbf{U} = \mathbf{A_r H^{-1}}$ and $\mathbf{V} = \mathbf{HA}$ are of dimension $N \times N$ with its corresponding values $u_{l,0}u_{l,1}\cdots u_{l,N-1}$ and $v_{m,0}^T v_{m,1}^T \cdots v_{m,N-1}^T$, where $u_{l,i}$ is ith column vector of the matrix $\mathbf{U}$ and $v_{m,i}$ denotes ith row vector of the

matrix $\mathbf{V}$. Then the $\mathbf{S}$ matrix can be represented as,

$$\mathbf{S} = \mathbf{R^L}[u_{l,0}u_{l,1}\cdots u_{l,N-1}]\mathbf{W}\begin{bmatrix} v^T_{m,0} \\ v^T_{m,1} \\ \vdots \\ \\ v^T_{m,N-1} \end{bmatrix} \tag{3.14}$$

Let us consider oversampling factor L to be a integer, Then the elements of the matrix $\mathbf{S}$ can be represented in simplified form as,

$$\mathbf{S} = \begin{cases} e^{j\left(\frac{2\pi\tau_i\frac{i}{L}}{T}\right)}u_{l,\frac{i}{L}}v^T_{m,\frac{i}{L}} & 0 \leq Li \leq (N-1)L \\ 0 & \text{otherwise} \end{cases} \tag{3.15}$$

where i varies from 0 to $N-1$, τ_i demonstrates the effect of jitter which is the deviation from the uniform time interval and T is representing the time period. In a way, the above equation (3.15) shows the representation of how zero insertion is done because of oversampling, since it may have a maximum of N non zero elements. The average power P which is $E[\mathbf{S}^2]$ can be calculated as,

$$P = \frac{1}{LN}\sum_{i=0}^{LN-1}\sum_{h=0}^{LN-1} E\left[[u_{l,i}v^T_{m,i}][u_{l,h}v^T_{m,h}]^*\right] E\left[e^{j\left(\frac{2\pi\tau_i i}{T}\right)}e^{j\left(\frac{2\pi\tau_h h}{T}\right)}\right] \tag{3.16}$$

Using the simplification $e^{j\eta} \approx 1+\eta$ in the above equation (3.16) the simplified expression for the second term is

$$e^{j\left(\frac{2\pi\tau_i i}{T}\right)} \approx (1 + j\frac{2\pi\tau_i i}{T}) \tag{3.17}$$

plugging it back into (3.16) the expectation results into

$$E\left[e^{j\left(\frac{2\pi\tau_i i}{T}\right)}e^{j\left(\frac{2\pi\tau_h h}{T}\right)}\right] = E\left[\left(1 + j\frac{2\pi\tau_i i}{T}\right)\left(1 + j\frac{2\pi\tau_h h}{T}\right)\right] \tag{3.18}$$

$$E\left[e^{j\left(\frac{2\pi\tau_i i}{T}\right)}e^{j\left(\frac{2\pi\tau_h h}{T}\right)}\right] \approx \left(\frac{2\pi i}{T}\right)^2 E[\tau_i^2] + E\left[j\left(\frac{2\pi\tau_h i}{T}\right)\right] + E\left[j\left(\frac{2\pi\tau_h h}{T}\right)\right] \tag{3.19}$$

Avoiding the positive coefficient results and assuming τ_i and τ_h as uncorrelated and are white in their nature i.e., $E[\tau_i] = 0$ and $E[\tau_h] = 0$, (3.18) can be simplified. By substituting equation (3.19) into (3.16) we obtain

$$P = \frac{1}{LN}\sum_{i=0}^{N-1}\sum_{j=0}^{N-1} E\left[[u_{l,Li}v^T_{m,Li}][u_{l,Lj}v^T_{m,Lj}]^*\right]\left(\frac{2\pi i}{T}\right)^2 E[\tau_i^2] \tag{3.20}$$

In (3.20) the index is changed from i to Li of (3.16) since N elements can be non zero. MGFDM block with baseband bandwidth of $MK/2T$ require the receiver analogue to digital converter (ADC) to sample at minimum Nyquist rate of T/MK. The above derivation is performed assuming all the carriers are active. Instead, if the no of active carriers range from K_l to K_u the bandwidth required would reduce to $N_a = M(K_u - K_l)/2T$. Hence the equation (3.20) for active carrier case will be modified as

$$P = \frac{1}{LN_a} \sum_{i=0}^{N_a-1} \sum_{j=0}^{N_a-1} E\left[[u_{l,Li} v_{m,Li}^T][u_{l,Lj} v_{m,Lj}^T]^*\right] \left(\frac{2\pi i}{T}\right)^2 E[\tau_i^2] \tag{3.21}$$

From (3.21) it is clear that power of the timing jitter is decreased by a factor of L, so by increasing the value of integer oversampling a reduction in the noise power is noticed. Assuming symbol period is unchanged, reducing number of subcarriers participate in transmission, will reduce the overall data rate. This in turn reduces transmit power and the required bandwidth.

3.5 Results and Discussions

This work presents various aspects in real time implementation of MGFDM system using a windowed preamble as depicted in Figure 3.2. The transmitted and received signals are plotted using the Labview software which is interfaced with National instruments hardware USRP-RIO. Secondly, the effect of oversampling on reduction of jitter noise power in MGFDM system is presented. We observed by increasing the integer oversampling a clear reduction in noise power. The real time constellation diagrams validated the analysis showing very good agreement. The parameters used for simulations and real time implementation are shown in Table 3.1.

Transmitter data packet is obtained by performing MGFDM modulation on QAM symbols which are arranged on active subcarriers. Further, all necessary constituents like CP and preamble are added to every symbol and data packet respectively in the order specified in Figure 3.1. The obatined signal is sent from host PC to USRP in 16 bit resolution. This work uses Barker sequence with rectangular filtering as windowed preamble in order to maintain OOB advantage. The spectrum shows there is large difference of 40dB between the in band radiation and OOB. This is because of the deeper side lobes

Table 3.1: Parameters for Simulated and real time MGFDM system

Parameter	**Value**
Number of subcarriers	64
Number of sub symbols	4
CP length	8
Prototyping filter	Multitaper filter
Filter roll off factor	0.9
Preamble shaping filter	Rectanular
Transmitter oversampling factor	4
Reciever oversampling factor	4
Preamble	44 length barker sequence
Transmitter sampling rate	4M
Zero pad length	8
Receiver sampling rate	4M
Transmitter gain	0db
Receiver gain	1db
Carrier frequency	2.4GHz

present in multitaper filters. This characteristic of multitaper filters makes it as a suitable prototype filter for scrambled spectrum applications. After these base band operations, RF up-conversion is done and transmitted over the air using the transmitter USRP.

The received signal is then brought to the receiver sampling rate using USRP daughterboard by down conversion and re directed to host PC for compensation of indoor channel effect. The frame detection algorithm is implemented using correlation between same two halves in the preamble [41]. The metric yields much better performance by not only using correlation in numerator but also removing channel dependency by using energy in the denominator. This advantageous metric has plateau effect as weakness due to presence of CP. In ISI channels, relatively a shorter plateau is created because the CP will be utilized to compensate channel ambiguity.

In simulations to illustrate the effect of jitter, a variance of $\frac{0.6T}{N}^2$ is manually applied. Notice that, the jitter variance is not changed when the oversampling parameter L is

Figure 3.2: Set up for real time transmission of MGFDM system

varied. The Figure 3.3 evidences a significant decrement in the bit error rate (BER) due to the noise created by time jitter by increasing oversampling. Better BER performance occurs solely due to linear degradation of the noise power with increase of oversampling factor. An interesting point is, since the jitter function is not a function of subcarrier index, the noise reduction is done equally across all carriers.

Figure 3.4 shows the effect of oversampling high speed GFDM system effected by jitter noise after performing demodulation. Time jitter results in rotational effects and ICI as suggested in [69]. Incrementing the integral oversampling shows an improvement in the shape of constellation, as clearly depicted in the Figure 3.4.

3.6 CFO estimation using oversampling

Generally, oversampling in multicarrier techniques is done to facilitate perfect reconstruction at the receiver. In this work, we consider a twice oversampled signal and observe a peculiar property which can be used for CFO estimation and signal detection. We consider $T_s = T/N$ as sample interval where T is the symbol duration. The twice oversampled signal is arranged alternatively into two groups with each group corresponding to odd and even indexes. The sampling instances for $x(n)$ occur at every $t = t_s + nT_s + \theta$, where θ is STO and t_s is the starting time of the GFDM symbol. Assuming perfect STO, for $n = 0, 1, \cdots N-1$ we represent two sets of data as $x_1(n)$ and $x_2(n)$. All even samples

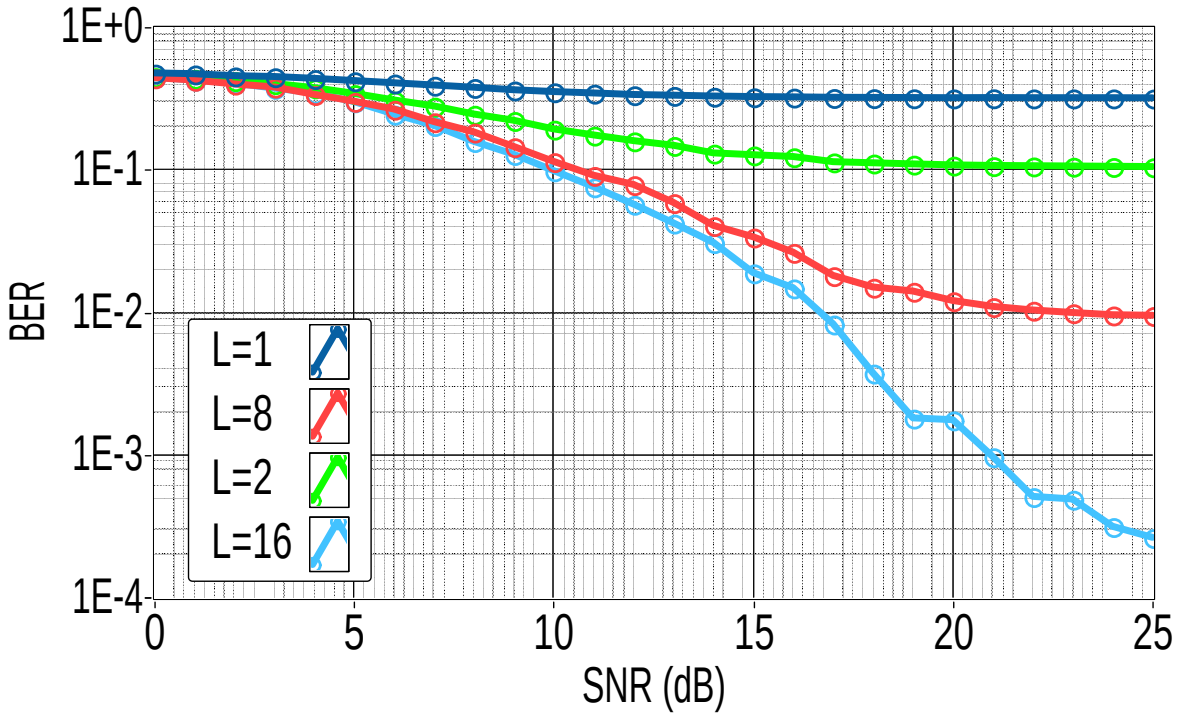

Figure 3.3: BER reduction due to oversampling in GFDM with Time jitter

are collected for $t_s = 0$ reducing itself to the usual GFDM model,

$$x_1(n) = \sum_{k=0}^{K-1} \sum_{m=0}^{M-1} d_k(m) g \left\{ (n - mK) \mathrm{mod} N \right\} e^{j \frac{2\pi kn}{K}}. \tag{3.22}$$

In the other case of $t_s = T_s/2$, the discrete model is given by,

$$x_2(n) = \sum_{k=0}^{K-1} \sum_{m=0}^{M-1} d_k(m) g \left\{ (n + \frac{1}{2} - mK) \mathrm{mod} N \right\} e^{\frac{j2\pi k(n+\frac{1}{2})}{K}}. \tag{3.23}$$

From the above two equations (3.22) and (3.23), we can notice that, the changes in the signal model occurs in phase term and also in prototype filters used for their generation. The phase change solely arises due to the difference in their sampling time where as the prototyping filters will differ by a constant half in their time. After reorganizing the sample points alternatively into groups the matrix representation for above sets of data are,

$$\mathbf{x_1} = \mathbf{Ad}, \tag{3.24}$$

$$\mathbf{x_2} = \mathbf{PA_1 d}, \tag{3.25}$$

where $\mathbf{P} = \mathrm{diag}\ (1 \cdots\ e^{j\frac{\pi}{K}} \cdots e^{j\frac{k\pi}{K}})$ is diagonal matrix for phase difference between the subcarriers of $\mathbf{x_1}$ and $\mathbf{x_2}$. Each element in the diagonal of the matrix $\mathbf{P}$ is repeated

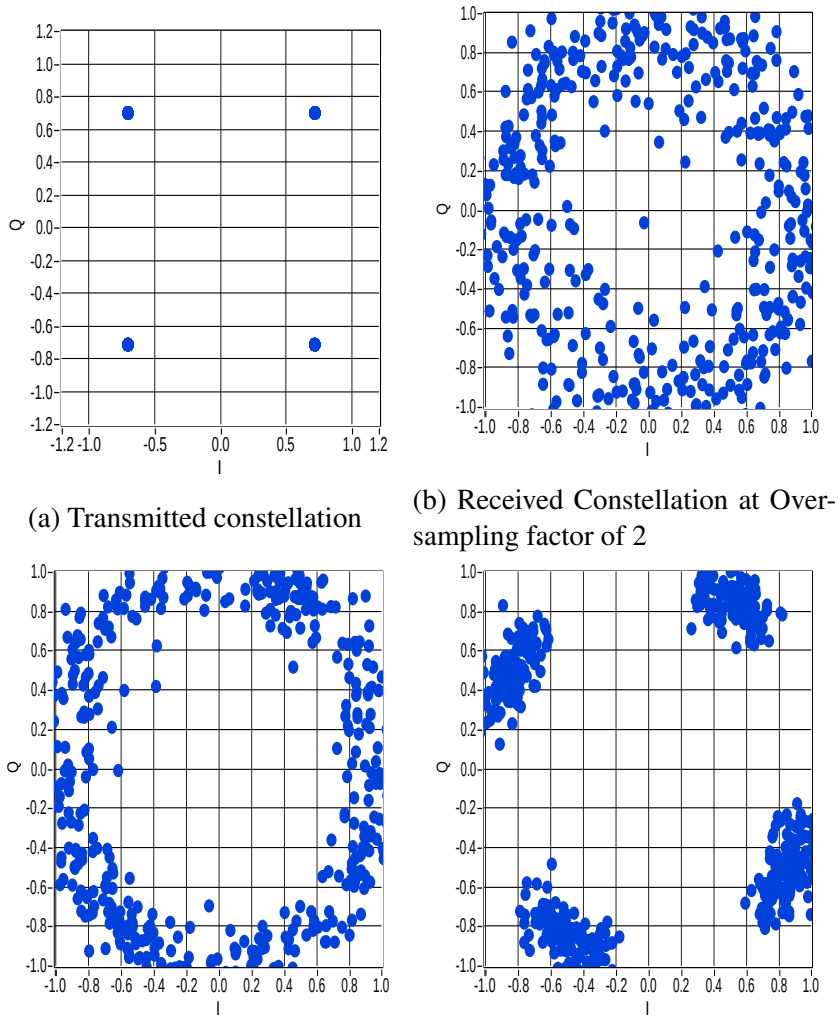

(a) Transmitted constellation

(b) Received Constellation at Oversampling factor of 2

(c) Received Constellation at Oversampling factor of 8

(d) Received Constellation at Oversampling factor of 16

Figure 3.4: Effect of Oversampling on GFDM system with Time jitter

M times since each subcarrier is bearing M subsymbols. Another interesting point is, in the presence of CFO i.e.,ϵ, both $\mathbf{x_1}$ and $\mathbf{x_2}$ will have difference in rotations of their constellations by an amount of $\mathbf{P}$. Here $\mathbf{A}$ and $\mathbf{A_1}$ represent the GFDM modulation matrices of $\mathbf{x_1}$ and $\mathbf{x_2}$ correspondingly. Despite of the fact of applying enough CP, GFDM is prone to have errors [20]. For that reason, simple equalization is not possible. In real time transmission using USRP, GFDM signal is sensitive to presence of STO and CFO.

Therefore, the received signal with all effects can be represented as,

$$y(n) = e^{j\frac{2\pi\epsilon n}{N}} \sum_{l=0}^{L-1} \sum_{n=0}^{N-1} h_n x_{l-n-\theta} + W(n). \tag{3.26}$$

Here $W(n)$ is representing the additive white Gaussian noise and ϵ is the CFO of the GFDM signal for an L length channel. The transmitted signal is sent in packets, which will be received only at certain times. Hence the estimation of θ primarily involves in symbol arrival time estimation. Blind symbol arrival can be estimated by maximizing the discrete time energy of received samples, which is calculated as,

$$J[v] = E\left[\left|r\left(nQT_s + v\right)\right|^2\right] = \frac{1}{N}\sum_{n=0}^{N-1}\left|r\left(nQT_s + v\right)\right|^2, \tag{3.27}$$

where E stands for expectation, r is the signal after matched filtering, v represents estimated time offset and Q is the oversampling factor. The resultant v after maximization of cost function $J(v)$ would give accurate result for larger Q value. An alternate approach named early-late gate algorithm is used in [23],

$$E\left|r\left(nQT_s + v\right)\right|^2 = 2\Re\left\{E\left[r(nQT_s + v)\frac{\delta}{\delta v}r^*(nQT_s + v)\right)\right]\right\}, \tag{3.28}$$

where $\Re$ represents the real part. This approach would consider discretizing the differentiated cost function assuming differentiation and expectation are exchangeable, since they are linear operators. First order difference by using the central difference method can be approximated for a small δ as,

$$\frac{d}{dv}r^*(nQT_s + v) = r^*(nQT_s + v + \delta) - r^*(nQT_s + v - \delta). \tag{3.29}$$

By substituting (3.29) into (3.28) and computing expectation of (3.28) by using sample averaging results into,

$$J[v]_\delta = \frac{1}{N}\sum_{n=0}^{N-1} 2\Re\left[r(nQT_s + v)\ \left(r^*(nQT_s + v + \delta) - r^*(nQT_s + v - \delta)\right)\right]. \tag{3.30}$$

A typical value of δ to be a multiple of T_s/Q. The estimated v is used for finding the data packet which contains GFDM symbols and its necessary constituents including CP but doesn't remove channel impairments.

3.7 ML Estimation

In this section, a blind joint CFO and data estimation is proposed using ML estimation. After signal detection, the corresponding oversampled GFDM signal at the receiver considering non dispersive conditions can be illustrated similar to the equations (3.24) and (3.25) as,

$$\mathbf{y_1} = \mathbf{CAd} + \mathbf{w_1}, \tag{3.31}$$

$$\mathbf{y_2} = \mathbf{e^{j\frac{\epsilon}{2}}CPA_1d} + \mathbf{w_2}, \tag{3.32}$$

where $\mathbf{w_1}$, $\mathbf{w_2}$ represents the uncorrelated complex additive white Gaussian noise. $\mathbf{C}$ =diag $(1\ e^{j\frac{\pi\epsilon}{N}} \cdots e^{j\frac{(N-1)\pi\epsilon}{N}})$ is the matrix representation of the effect of CFO. In presence of CFO, it is important to note that, a constant phase shift by a scalar of $e^{j\frac{\epsilon}{2}}$ occurs between $\mathbf{y_1}$ and $\mathbf{y_2}$. This factor is independent of subcarrier frequency and subsymbol location which enables us to utilize it for ML estimation. It occurs only due to the difference of sampling between odd and even samples of the oversampled signal. This method leads to heuristic but a sensible method in the absence of noise. In case of noiseless channels, a straight forward CFO estimation is possible using equations (3.31), (3.32) and knowing the fact that $\mathbf{d}$ is unknown for both vectors. To prove this fact, let us define two vectors $\mathbf{r_1}$ and $\mathbf{r_2}$ as,

$$\mathbf{r_1} = \mathbf{A^H C^H y_1}, \tag{3.33}$$

$$\mathbf{r_2} = e^{-j\frac{\epsilon}{2}}\mathbf{A_1^H P^H C^H y_2}. \tag{3.34}$$

We can simply solve (3.33), (3.34) and observe vectors $\mathbf{r_1}$, $\mathbf{r_2}$ are equal in the absence of noise,

$$\mathbf{r_1} = \mathbf{r_2} = \mathbf{d}. \tag{3.35}$$

This would give a simple estimate for ϵ. The above estimation is unlikely to happen in noise scenario. However, in presence of noise minimizing the distance between $\mathbf{r_1}$ and $\mathbf{r_2}$ would lead to ML estimate of CFO,

$$\epsilon = \min_{\epsilon} (\mathbf{r_1} - \mathbf{r_2})^{\mathbf{H}} (\mathbf{r_1} - \mathbf{r_2}). \tag{3.36}$$

This minimization reduces itself into finding roots present on unit circle for a polynomial of order $2N$. The noise vectors $\mathbf{w_1}$ and $\mathbf{w_2}$ are assumed to follow complex Gaussian with

zero mean and covariance matrix $\sigma^2 I$. Then likelihood function for joint estimation of data $\mathbf{d}$ and CFO ϵ is,

$$\lambda(\epsilon, \mathbf{d}) = \frac{1}{(\pi\sigma^2)^N} \exp\left\{ \frac{-1}{\sigma^2} \left[(\mathbf{y_1} - \mathbf{CAd})^{\mathbf{H}} (\mathbf{y_1} - \mathbf{CAd}) \right.\right. \\ \left.\left. + (\mathbf{y_2} - e^{j\frac{\epsilon}{2}} \mathbf{CPA_1 d})^{\mathbf{H}} (\mathbf{y_2} - e^{j\frac{\epsilon}{2}} \mathbf{CPA_1 d}) \right] \right\} \quad (3.37)$$

We have to maximize this function for estimating ϵ and $\mathbf{d}$

$$(\epsilon_{ML}, \mathbf{d_{ML}}) = arg \max_{\epsilon, \mathbf{d}} \lambda(\epsilon, \mathbf{d}). \quad (3.38)$$

This is equivalent to minimizing,

$$S(\epsilon, \mathbf{d}) = (\mathbf{y_1} - \mathbf{CAd})^{\mathbf{H}} (\mathbf{y_1} - \mathbf{CAd}) + (\mathbf{y_2} - e^{j\frac{\epsilon}{2}} \mathbf{CPA_1 d})^{\mathbf{H}} (\mathbf{y_2} - e^{j\frac{\epsilon}{2}} \mathbf{CPA_1 d}), \quad (3.39)$$

Taking gradient of $S(\epsilon, \mathbf{d})$ for the data vector $\mathbf{d}$ and setting its value at zero would yield,

$$\frac{\partial S(\epsilon, \mathbf{d})}{\partial \mathbf{d}} = -2\mathbf{A}^{\mathbf{H}} \mathbf{C}^{\mathbf{H}} (\mathbf{y_1} - \mathbf{CAd}) - 2e^{-j\frac{\epsilon}{2}} \mathbf{A_1^H P^H C^H} (\mathbf{y_2} - e^{j\frac{\epsilon}{2}} \mathbf{CPA_1 d}) = 0. \quad (3.40)$$

The ML estimate of the data $\mathbf{d_{ML}}$ after simplification is,

$$\mathbf{d_{ML}} = \frac{1}{2} (\mathbf{A}^{\mathbf{H}} \mathbf{C}^{\mathbf{H}} \mathbf{y_1} + e^{-j\frac{\epsilon}{2}} \mathbf{A_1^H P^H C^H y_2}). \quad (3.41)$$

The above equation (3.41) is applicable for any value of ϵ. Thus after obtaining the data vector $\mathbf{d_{ML}}$ we can plug into $S(\epsilon, \mathbf{d})$ to obtain value for ϵ,

$$\mathbf{S}(\epsilon_{\mathbf{ML}}, \mathbf{d_{ML}}) = \frac{1}{2} \left(\mathbf{r_1}(\epsilon) - \mathbf{r_2}(\epsilon) \right)^{\mathbf{H}} \left(\mathbf{r_1}(\epsilon) - \mathbf{r_2}(\epsilon) \right) \quad (3.42)$$

where $\mathbf{r_1}$ and $\mathbf{r_2}$ are defined in equations (3.33), (3.34). The motivation for the algorithm is from the closer inspection of equations (3.24) and (3.25) in which the number of observations are obtained from symbol rate sampling. Assuming all carriers are active, there are $N + 1$ observations to be estimated in total. N is for the data estimation and 1 is coming from the CFO estimation. Thus by oversampling by a factor of two the number of observations are doubled without increase in unknowns. This provides the probability of estimating the required parameters without any extra information. For the case of multipath channel environments, $\mathbf{A}$ should be replaced with $\mathbf{HA}$ and similar calculations have to be performed. The channel impulse response for each subchannel of an oversampling system is quite different. Namely, the circulant channel matrices for (3.31), (3.32) are not

be the same. So, for the case of odd samples $\mathbf{H_1 A_1}$ has to be considered. The simplified representation for (3.36) is,

$$\begin{aligned}\epsilon =& \max_{\epsilon}(\mathbf{r_1^H r_2} + \mathbf{r_2^H r_1}) \\ =& e^{j\frac{\epsilon}{2}} \left(\mathbf{y_1^H COC^H y_2} + \mathbf{y_2^H CO^H C^H y_1}\right),\end{aligned} \tag{3.43}$$

where $\mathbf{O} = \mathbf{A A_1^H P^H}$ in (3.43) is easily computable in the receiver and $\mathbf{r_1^H r_1}$, $\mathbf{r_2^H r_2}$ are neglected since they don't contribute for CFO estimation. We know $\mathbf{C}$ is a diagonal matrix, hence the computational complexity of the proposed method is $2N^2$.

CRLB

CRLB can be considered as a measure for sharpness of estimating an unknown parameter. To quantify mathematically, we need to determine Fisher Information Matrix (FIM) which requires second order derivatives of the above log likelihood functions with respect to the unknown parameters $\mathbf{d}$ and ϵ. After neglecting constant terms the log likelihood from (3.37) can be expressed as,

$$\begin{aligned}\lambda(\epsilon, \mathbf{d}) = -\frac{1}{\sigma^2}(\mathbf{y_1} - \mathbf{CAd})^{\mathbf{H}}(\mathbf{y_1} - \mathbf{CAd}) \\ - \frac{1}{\sigma^2}(\mathbf{y_2} - e^{j\frac{\epsilon}{2}}\mathbf{CPA_1 d})^{\mathbf{H}}(\mathbf{y_2} - e^{j\frac{\epsilon}{2}}\mathbf{CPA_1 d}).\end{aligned} \tag{3.44}$$

Let us divide λ into two terms where the first and second are shown with λ_1 and λ_2. The first term λ_1 in its simplified form is,

$$\lambda_1 = -\frac{1}{\sigma^2}\left(\mathbf{y_1^H y_1} - (\mathbf{CAd})^H \mathbf{y_1} - (\mathbf{CAd})\mathbf{y_1^H} + \mathbf{d^H d}\right). \tag{3.45}$$

The above equation (3.45) is simplified using matrix properties $\mathbf{A^H A} = \mathbf{I}$ and $\mathbf{C^H C} = \mathbf{I}$. For λ_1 we have,

$$\frac{\partial \lambda_1}{\partial \mathbf{d}} = \frac{1}{\sigma^2}\left((\mathbf{CA})^{\mathbf{H}}\mathbf{y_1} + (\mathbf{y_1^H CA})^{\mathbf{H}} - 2\mathbf{d}\right). \tag{3.46}$$

Extending the above equation to obtain second order derivative results into,

$$\frac{\partial^2 \lambda_1}{\partial \mathbf{d^2}} = \frac{-2}{\sigma^2} I, \tag{3.47}$$

since $\mathbf{C}$ is a function of ϵ we consider two matrices $\mathbf{U} = \text{diag}(0, 1, 2 \cdots N-1)$ and $\mathbf{V} = \text{diag}(1/2, 3/2 \cdots \frac{N-1}{2})$, which will be useful in finding gradients with respect to matrix $\mathbf{C}$

for even and odd indices respectively. The remaining derivatives for λ_1 are,

$$\begin{aligned}\frac{\partial^2\lambda_1}{\partial\mathbf{d}\partial\epsilon} &= \frac{2}{\sigma^2}j(\mathbf{UCA})^H\mathbf{y_1},\\ \frac{\partial^2\lambda_1}{\partial\epsilon\partial\mathbf{d}} &= \frac{2}{\sigma^2}j(\mathbf{UCA})^H\mathbf{y_1},\\ \frac{\partial^2\lambda_1}{\partial\epsilon^2} &= \frac{-2}{\sigma^2}(\mathbf{U^2CAd})^H\mathbf{y_1}.\end{aligned} \tag{3.48}$$

By performing similar operations on λ_2 the second derivatives can be obtained as,

$$\begin{aligned}\frac{\partial^2\lambda_2}{\partial\mathbf{d^2}} &= \frac{-2}{\sigma^2}I\\ \frac{\partial^2\lambda_2}{\partial\mathbf{d}\partial\epsilon} &= \frac{2}{\sigma^2}j(e^{j\frac{\epsilon}{2}}\mathbf{VCPA_1})^H\mathbf{y_2},\\ \frac{\partial^2\lambda_2}{\partial\epsilon\partial\mathbf{d}} &= \frac{2}{\sigma^2}j(e^{j\frac{\epsilon}{2}}\mathbf{VCPA_1})^H\mathbf{y_2},\\ \frac{\partial^2\lambda_2}{\partial\epsilon^2} &= \frac{-2}{\sigma^2}(e^{j\frac{\epsilon}{2}}\mathbf{V^2CPA_1d})^H\mathbf{y_2}.\end{aligned} \tag{3.49}$$

The final FIM matrix $\mathbf{F}$ is summation of expectations of λ_1 and λ_2, which can be written as,

$$\begin{aligned}\mathbf{F} = \frac{-2}{\sigma^2}\mathbf{E}\left\{\begin{bmatrix} I & -j(\mathbf{UCA})^H\mathbf{y_1}\\ -j(\mathbf{UCA})^H\mathbf{y_1} & (\mathbf{U^2CAd})^H\mathbf{y_1}\end{bmatrix}\right\}\\ + \frac{-2}{\sigma^2}\mathbf{E}\left\{\begin{bmatrix} I & -j(e^{j\frac{\epsilon}{2}}\mathbf{VCPA_1})^H\mathbf{y_2}\\ -j(e^{j\frac{\epsilon}{2}}\mathbf{VCPA_1})^H\mathbf{y_2} & (e^{j\frac{\epsilon}{2}}\mathbf{V^2CPA_1d})^H\mathbf{y_2}\end{bmatrix}\right\}.\end{aligned} \tag{3.50}$$

Using the equations (3.31) and (3.32), we can easily deduce $\mathbf{E}[\mathbf{y_1}] = \mathbf{CAd}$ and $\mathbf{E}[\mathbf{y_2}] = e^{j\frac{\epsilon}{2}}\mathbf{CPA_1d}$. Since the expectations in matrix $\mathbf{F}$ is applicable only for $\mathbf{y_1}$ and $\mathbf{y_2}$ we can simplify FIM matrix by substitution. As an example, the expected value at $2,1$ index can be evaluated as $\mathbf{E}[(\mathbf{UCA})^H\mathbf{y_1}] = \mathbf{A^HC^HUCAd}$ and its corresponding element in λ_2 is $\mathbf{E}[(e^{j\frac{\epsilon}{2}}\mathbf{VCPA_1})^H\mathbf{y_2}] = \mathbf{A_1^HP^HC^HVCPA_1d}$. To find the CRLB for estimation of ϵ we need to invert the FIM and find element corresponding to ϵ i.e., first row and first column which is represented with $[\mathbf{F}^{-1}]_{1,1}$. The first step in obtaining inverse is to find the determinant of the FIM matrix, which after simplification is,

$$\begin{aligned}|\mathbf{F}| = (\mathbf{CAd})^\mathbf{H}(\mathbf{UCA})(\mathbf{VCPA_1})^\mathbf{H}(\mathbf{CPA_1d})\\ + (\mathbf{CPA_1d})^\mathbf{H}(\mathbf{VCPA_1})(\mathbf{UCA})^\mathbf{H}(\mathbf{CAd})\end{aligned} \tag{3.51}$$

By expanding the individual terms the above equation will be,

$$|\mathbf{F}| = \mathbf{d^H A^H C^H U C A A_1^H P^H C^H V C P A_1 d} + \mathbf{d^H A_1^H P^H C^H V C P A_1 A^H C^H U C A d} \quad (3.52)$$

Since the matrices $\mathbf{U}$, $\mathbf{V}$ and $\mathbf{C}$ are diagonal $\mathbf{C^H U C} = \mathbf{U}$ and $\mathbf{C^H V C} = \mathbf{V}$. So the CRLB for CFO estimation using the oversampled GFDM model is,

$$\text{CRLB} = [\mathbf{F}^{-1}]_{1,1} = \sigma^2/2 \times \frac{1}{\mathbf{C_1} + \mathbf{C_2}} \quad (3.53)$$

Here the values computed by mathematical analysis are $\mathbf{C_1} = (\mathbf{Ad})^{\mathbf{H}}\mathbf{U}(\mathbf{PA_1A^H})^H\mathbf{V}(\mathbf{PA_1d})$ and the second term is $\mathbf{C_2} = (\mathbf{PA_1d})^H\mathbf{V}(\mathbf{AA_1^HP^H})^{\mathbf{H}}\mathbf{U}(\mathbf{Ad})$. The numerical CRLB for the proposed oversampled GFDM system is detailed in the result and discussion section.

3.8 GFDM Testbed Description

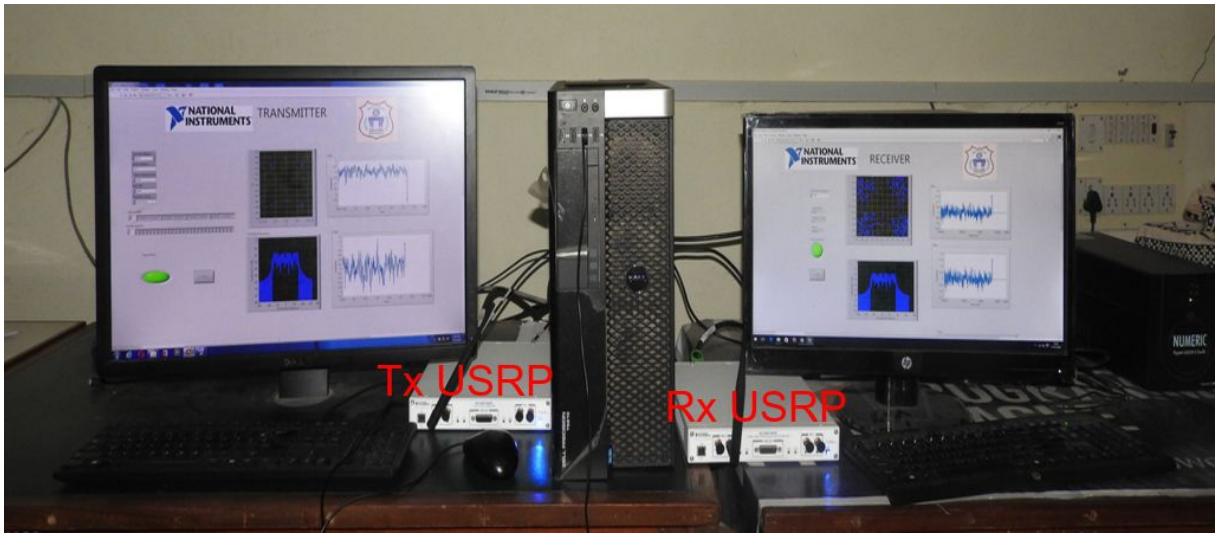

Figure 3.5: Experimental set-up used for testing algorithm in real time environment

The implementation depicted in Figure 3.5 shows a workstation PC connected to USRP via NI PXIe-PCIe8371 which can transfer data at throughput of 832 MB/sec. The two USRP stations shown act as transmitter and receiver for GFDM system. Another essential point is, work station PC will completely perform all baseband operations of the transceiver. Parameters for testing real time prototype of GFDM are tabulated in Table 3.2. In short, USRP reads the signal in IQ (Inphase Quadrature) representation

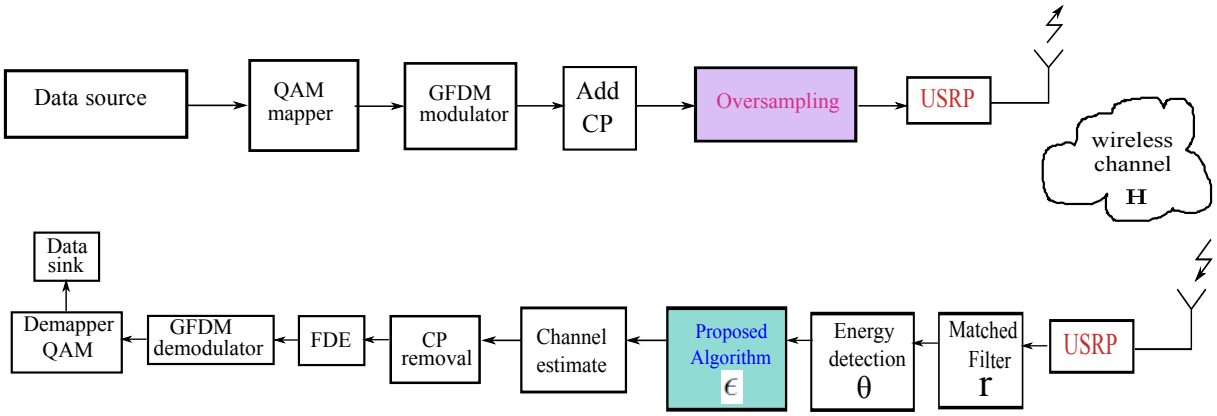

Figure 3.6: Block diagram of the implemented GFDM System

from PC and performs digital to analog conversion before sending through transmitter (TX1) antenna. The captured IQ samples from receiver antenna (RX2) of USRP are down converted and sent to PC using PCI-Express card for compensation of channel effect.

Table 3.2: Parameters for Simulated and real time GFDM system

Parameter	**Value**
Number of subcarriers	64
Number of subsymbols	5
CP length	8
Prototyping filter	Root raised cosine
Filter roll off factor	0.9
Transmitter oversampling factor	2
Reciever oversampling factor	2
Capture time	4 ms
Transmitter sampling rate	4M
Zero pad length	8
Receiver sampling rate	4M
Transmitter gain	0db
Receiver gain	1db
Carrier frequency	2.4GHz

3.9 Results and Discussions

We examine effect of CFO in two aspects for performance analysis of GFDM systems. Firstly we consider BER versus SNR curves to see its behaviour in simulations. Later, we validate blind signal transmission by showing the transmitted and received waveforms along with constellation diagram received in USRP for final reconstructed signals. Another advantage of the proposed method in practice is ease in the design of front end filter. Since the proposed method uses twice oversampling, a relatively uncomplicated analog filter can be utilized to circumvent the aliasing from high frequencies. However, it is hard to have a analog filter which doesn't allow certain frequency range but much easier to an analog filter that reject high frequencies with oversampling. Hence, by using the proposed method, an effective band limiting can be performed.

3.9.1 Simulation results

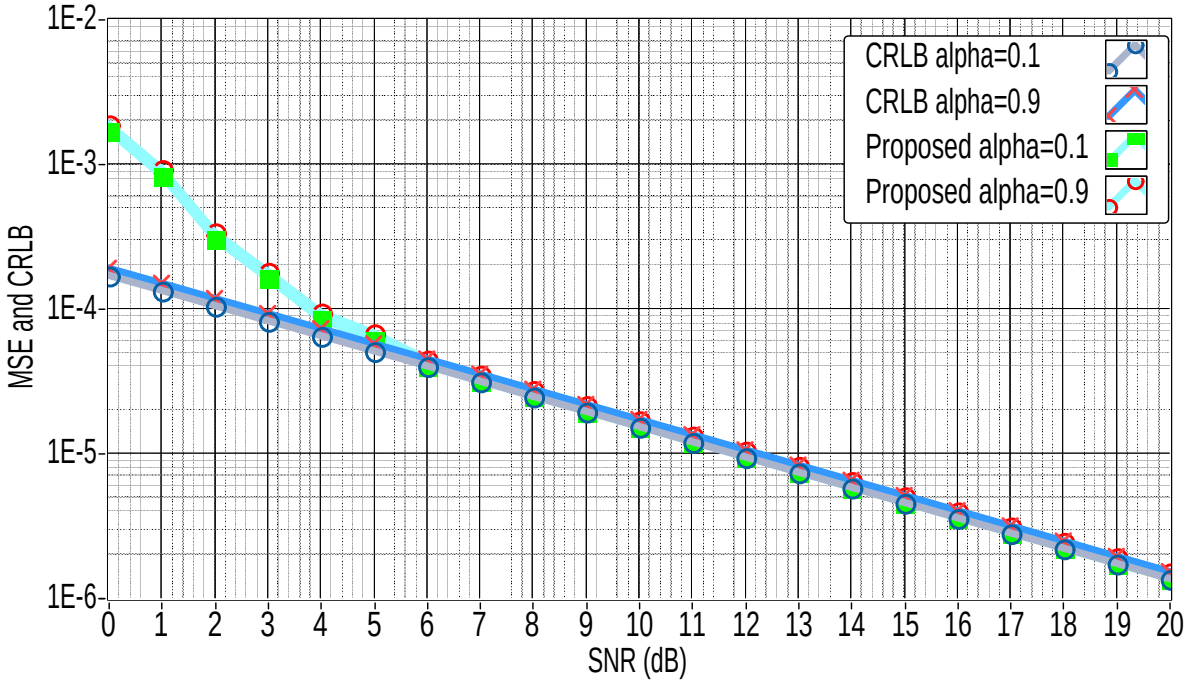

Figure 3.7: MSE of CFO estimation for AWGN channel

Figure 3.7 shows the Mean Square Error (MSE) versus SNR for the proposed blind CFO estimation for GFDM system. Here, it can be seen that, the MSE for the proposed method fully exploits the intrinsic phase shift between neighbouring data samples of

the oversampled GFDM symbols. The method operates near CRLB at usable values of SNR i.e., at a typical SNR values greater than 6. Another interesting observation from simulation results is, varying roll off factor of RRC doesn't show much effect on the MSE. In the Figure 3.8 for the purpose of comparison we have used the method proposed in

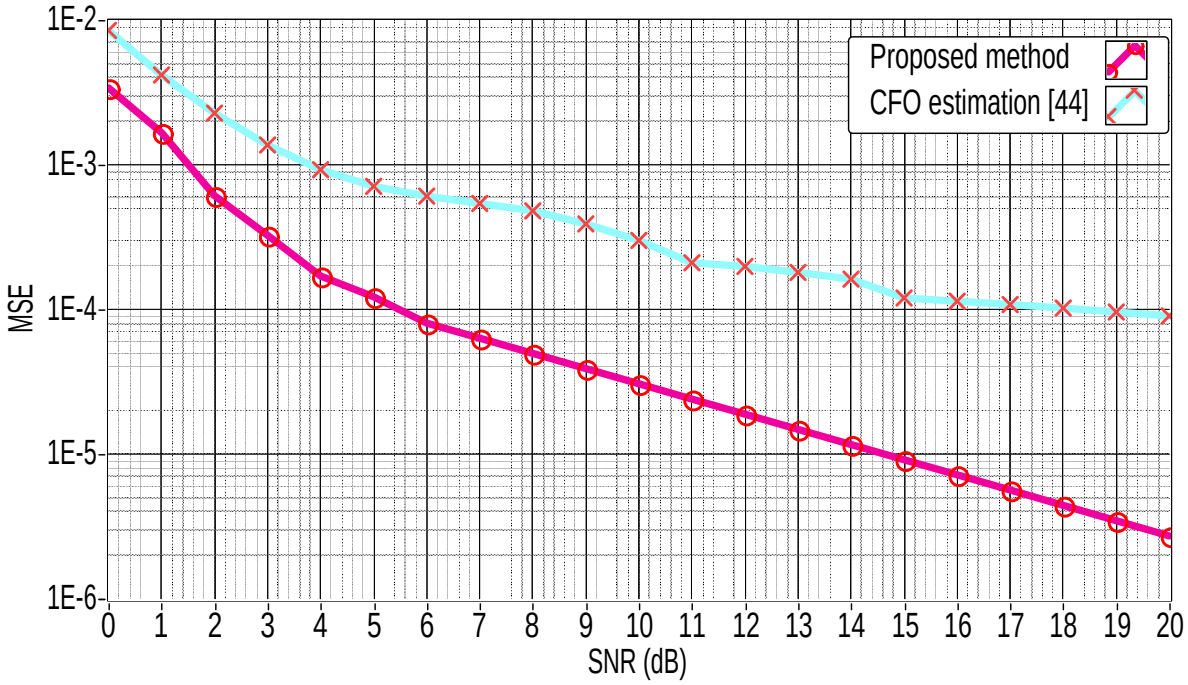

Figure 3.8: MSE of CFO estimation for channel in [44]

[44] and the considered channel is following Rayleigh fading. In the transmitter, GFDM system uses circular convolution mechanism with a flexible prototyping filter for avoiding OOB emissions. On the other hand, this enforces non orthogonal nature to the system. This non orthogonal nature adds self inter carrier interference to the system. In [44], the authors employ the idea of correlation between CP and GFDM symbol for achieving time and frequency synchronization at the receiver. The increase in self interference results in ICI and degrades the performance of the ML estimator. However, the proposed method is more reliable as in the Figure 3.8. This advantage is achieved due to reduction of self interference with oversampling for GFDM system [24]. Additionally, [44] relies on the concept of clean CP, i.e., by leaving the channel noise, the copy of the GFDM signal must be present at the end. However, in multipath channel environments, ISI from the previous GFDM symbol clearly modifies CP. Hence, the correlation between CP and original GFDM symbol is destroyed leading to erroneous detection. As a result,

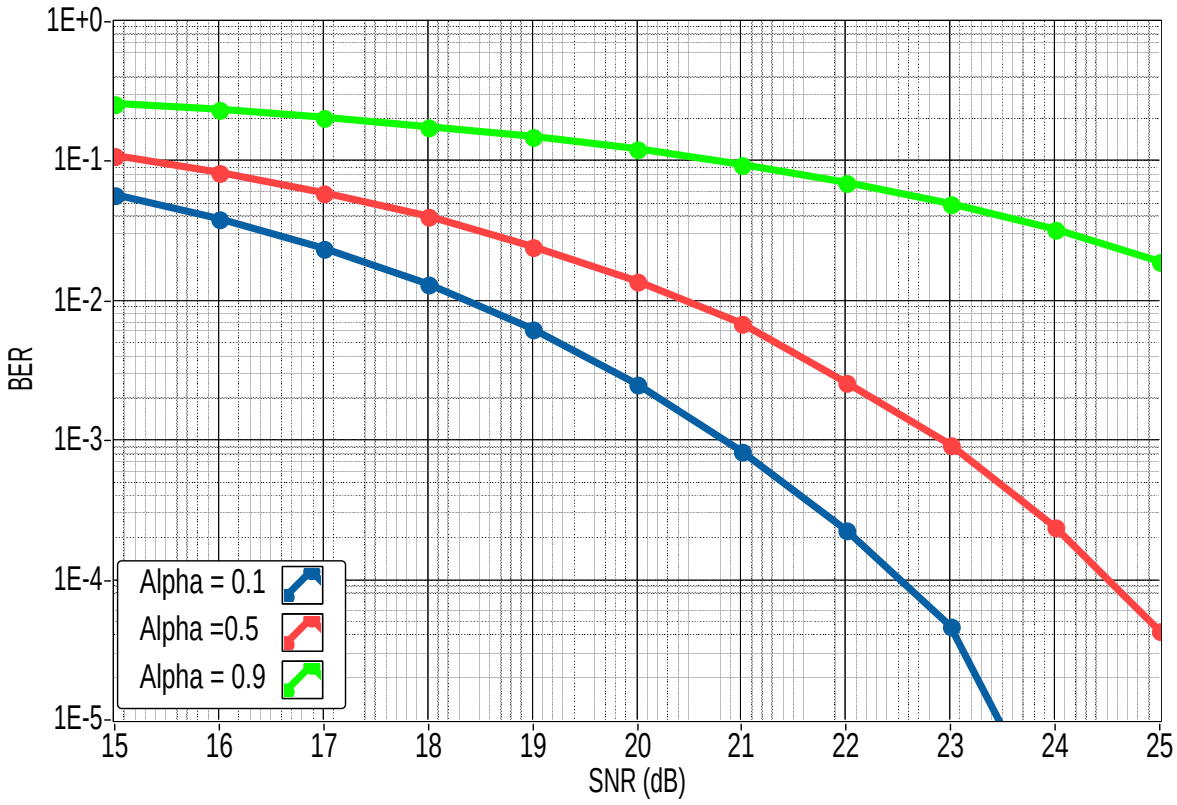

Figure 3.9: Effect of Pulse shape factor on BER of GFDM system

MSE in CFO estimation increases. We can also see that, for the entire SNR range, the proposed estimation algorithm performs better than the method proposed in [44]. Figure 3.9, illustrates the BER performance at $\epsilon = 0.5$ by taking into consideration the effect of roll-off factor α on GFDM system. It can be evidenced that, upon increasing the roll-off factor α, the BER performance deteriorates. However, this is due to the fact that, when $\alpha = 0.1$, the prototyping filter emanates as the rectangular filter with reduced side lobes. This approach follows the OFDM characteristics hence, yielding a better BER performance. When $\alpha = 0.9$ the performance is degraded due to the occurrence of more side lobes which in turn lead to out-of band radiation.

3.9.2 Real time results

We will now analyse these algorithms in real time scenarios. The GFDM signal is generated by using the parameters as mentioned in Table 4.4 is sent from host PC to USRP in 16 bit resolution. USRP separates the signal into its in-phase and quadrature

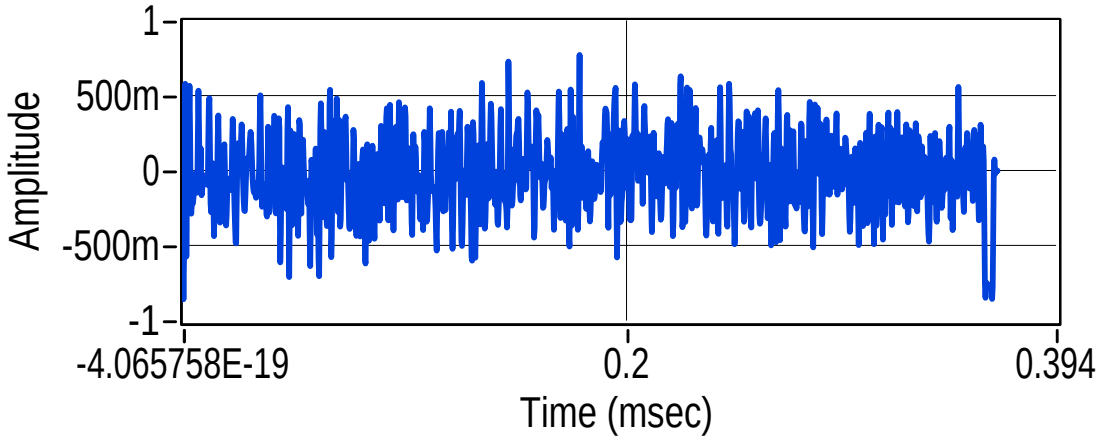

Figure 3.10: Transmitted in phase Data of GFDM signal

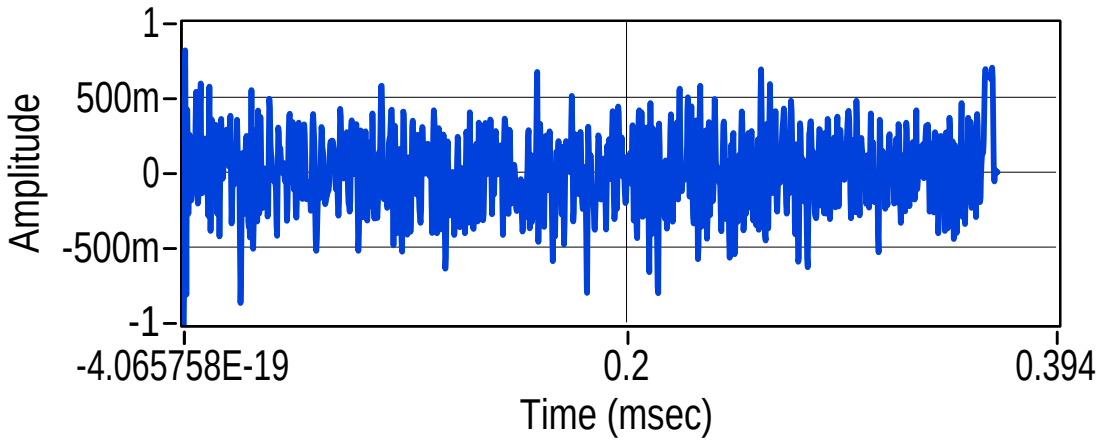

Figure 3.11: Transmitted quadrature phase Data of GFDM signal

phase (IQ) representation and up converts to specified carrier frequency of 2.4 GHz. IQ signal representation for transmitted GFDM signal is depicted in Figure 3.10, 3.11. A single data packet shown in the above figures comprises of 5 GFDM symbols of size 64 with a CP of 16 and a zero padding sequence of 4 bits at its start and end to differentiate between packets. Since the signal is twice oversampled and sent at a sampling rate of 2M each packet is of duration $3.68 * 10^{-4}$. A small delay in the start of the packet is due to the processing delay in Transmitter USRP. We can observe difference in amplitude of the signal which occurs due to circular protyping filter used in generation.This type of filtering destroys the orthogonality present in the signal but the main advantage can be seen from the spectrum of the transmitted signal which is depicted in Figure 3.14. The spectrum shown has an minimum OOB of -46dB, because of the deeper side lobes present in prototype filters. This characteristic of RRC filters makes it as a suitable

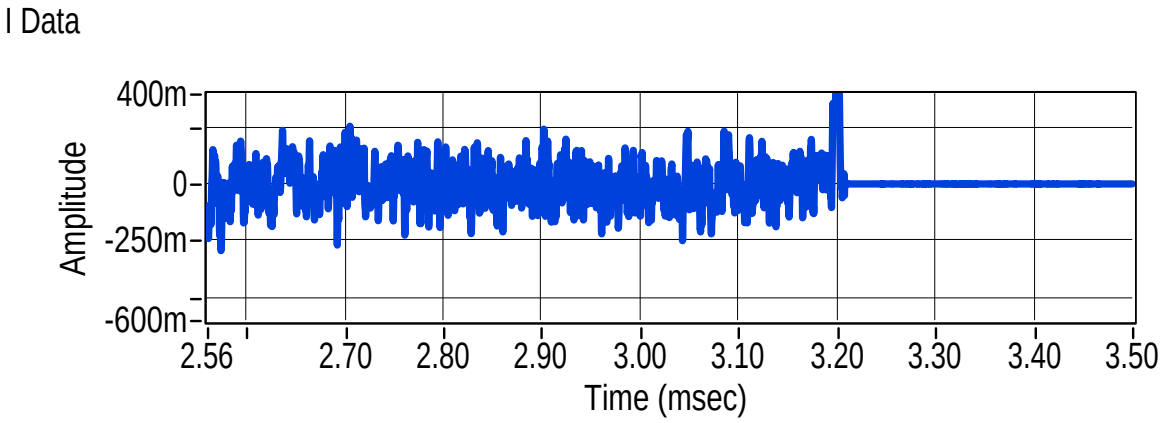

Figure 3.12: Received in phase Data of GFDM signal

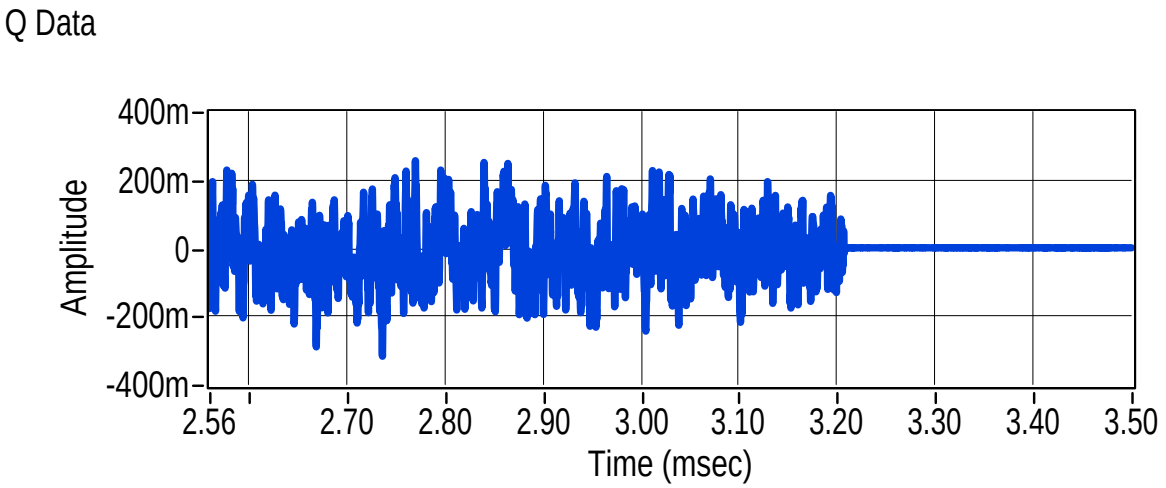

Figure 3.13: Received quadrature phase Data of GFDM signal

prototype filter for scrambled spectrum applications. After these base band operations RF up-conversion is done and transmitted over the air using the transmit antenna TX USRP. The signal is distorted in indoor environment and received IQ signal after STO

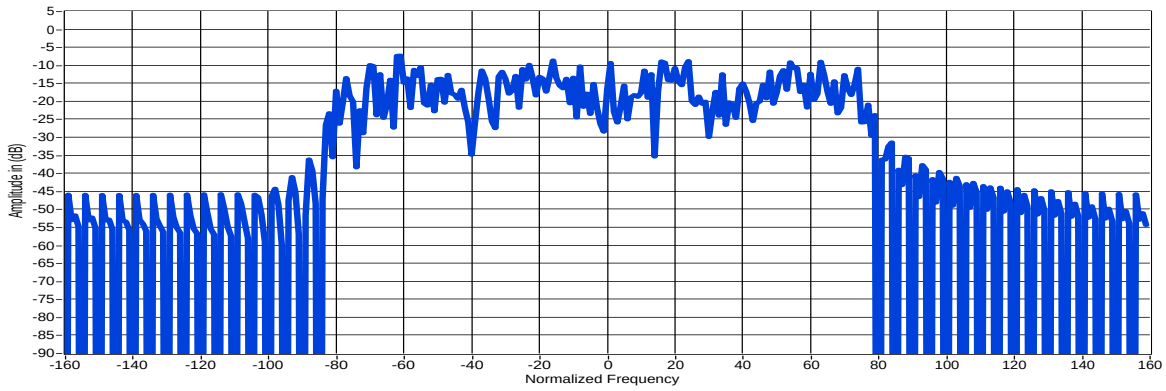

Figure 3.14: Transmitted spectrum

Table 3.3: Observed experimental values in indoor environments at alpha=0.1

Parameter	BER	Estimated SNR	Estimated CFO
AWGN at SNR=5dB	0.351768	2.40 dB	0.161358
AWGN at SNR=30dB	1.67E-06	29 dB	0.000981639
Multipath at SNR=5dB	0.367047	1.95dB	0.192362
Multipath at SNR=30dB	0.000228333	27.90dB	0.000116936

estimation is depicted in Figure 3.12,3.13. The STO estimator continuously performs the maximization of summation for received samples and identifies the packet as shown in Figure 3.6. We can clearly observe the decrement in amplitude due to channel distortion along with time delay for reception of the packet. The zero padding which is inserted

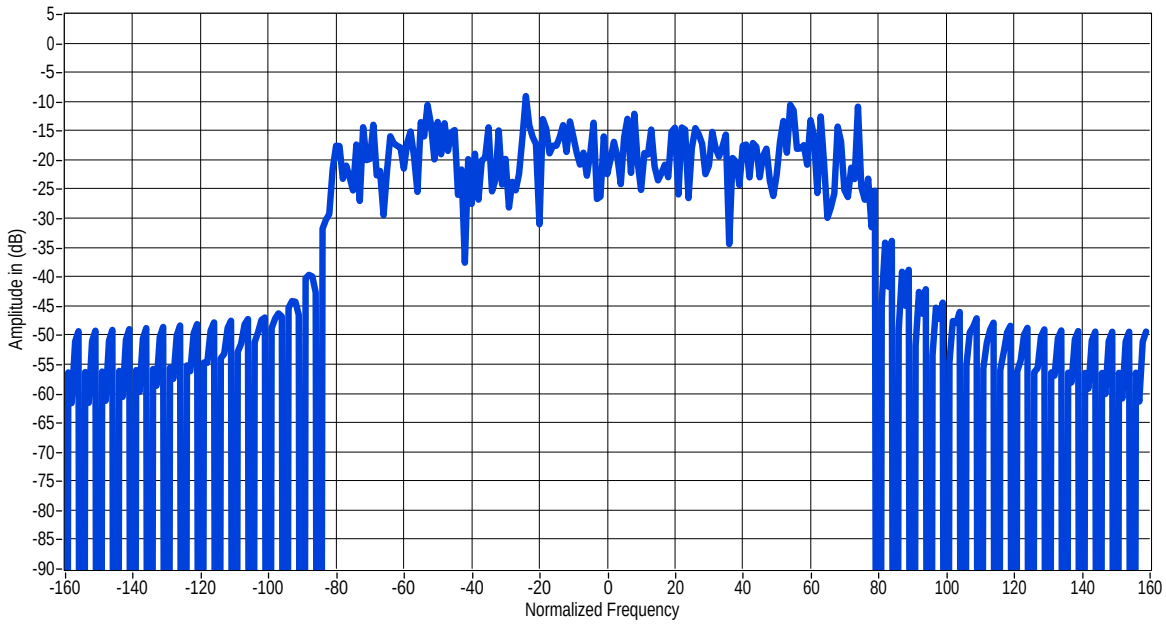

Figure 3.15: Received spectrum

to differentiate the packets after packet selection is removed and we consider packet to mitigate channel misalignments. The spectrum of the received signal is depicted in Figure 3.15. Since the spectrum is dependent on the amplitude of the IQ signal we had amplitude distortion in the received spectrum.

We considered the constellation diagrams for demonstrating the effect of CFO in GFDM signals. The Figure 3.16, illustrates the transmitted constellation for GFDM system employing 4-QAM modulation scheme. Figure 3.18, illustrates the effect of CFO on

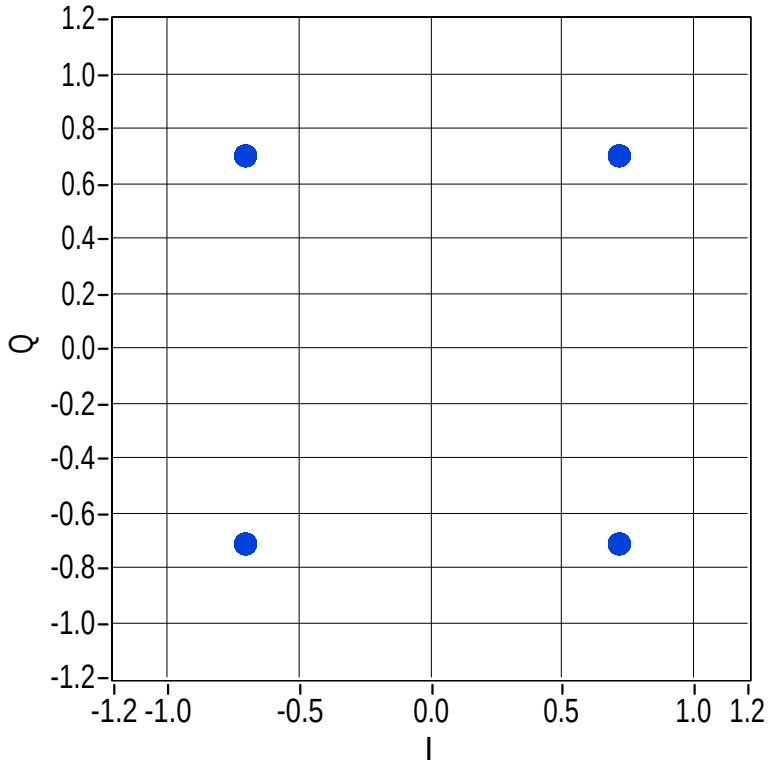

Figure 3.16: Transmitted constellation

Table 3.4: Observed experimental values in indoor environments at alpha=0.9

Parameter	BER	Estimated SNR	Estimated CFO
AWGN at SNR=5dB	0.3909	2.36 dB	0.16908
AWGN at SNR=30dB	9.7E-05	28.90 dB	0.00101639
Multipath at SNR=5dB	0.3770	1.92dB	0.20602
Multipath at SNR=30dB	0.00064863	27.10dB	0.00015660

the transmitted constellation. It is evident from the figure, that the received constellation has a circular shape. So, it is mandatory to enforce CFO estimation algorithm which is proposed. Received constellation in Figure 3.17 reveals that the transmitted constellation is seriously distorted.

This is due to the fact that, the obtained constellation is seriously affected with all sorts of channel distortions namely amplitude and phase ambiguities. Hence, it necessitates to impose the above mentioned algorithm to combat both channel effect as wells as to ensure perfect estimation of CFO. Figure 3.19, shows the received signal constellation after enforcing the blind CFO estimation algorithm which uses oversampling. It can be

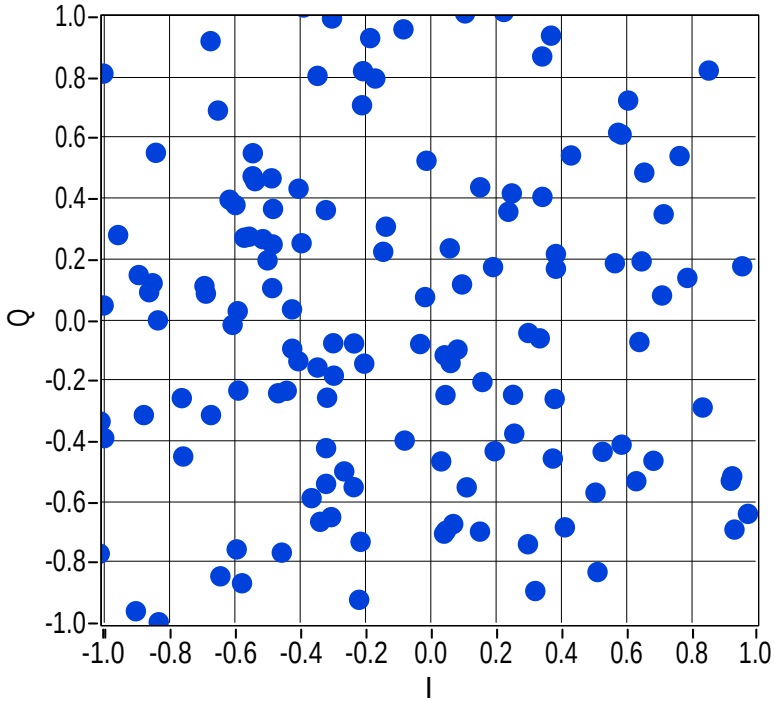

Figure 3.17: Received constellation

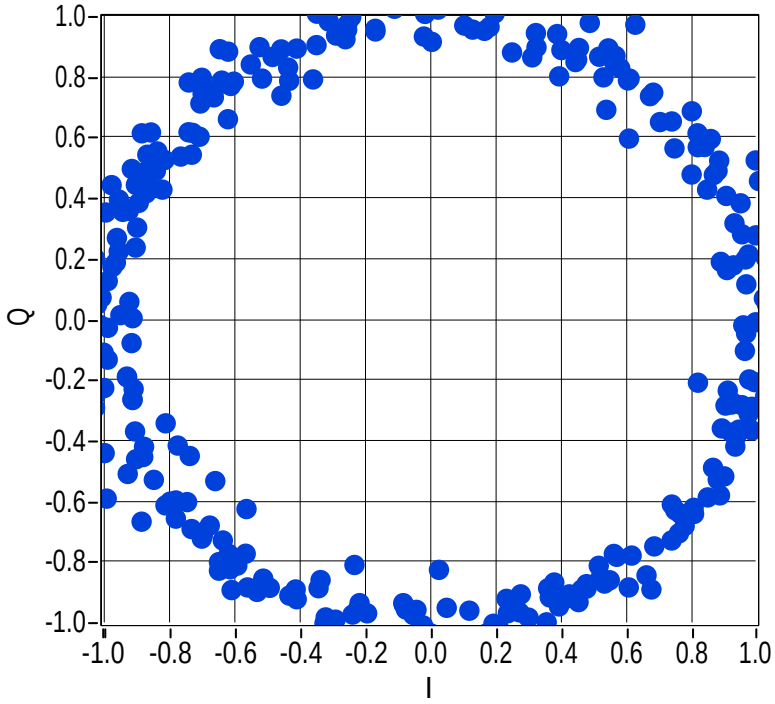

Figure 3.18: Effect of CFO constellation

viewed that, the effects of both channel and CFO are nullified. Hence, the received constellation closely matches with the transmitted constellation. The observed experimental values in indoor environments are tabulated below in Table 3.3 and 3.4. The real time re-

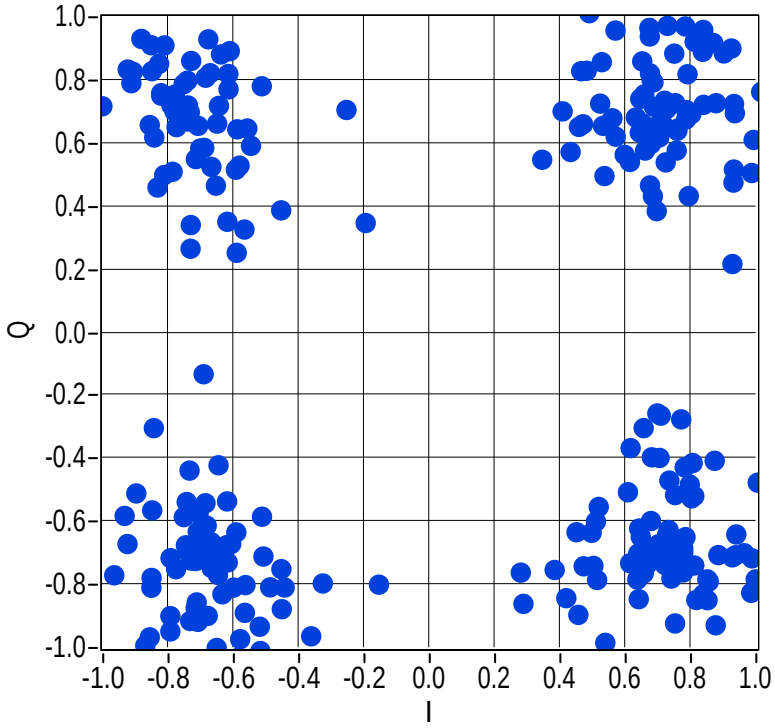

Figure 3.19: Received constellation after correction

sults clearly ensures perfect estimation of CFO even in multipath channel environments. Another important observation is, when $\alpha = 0.1$, the RRC filter emanates to rectangular filter, which improves the orthogonal characteristics and hence, yielding a better BER performance. Hence, the roll off factor creates a trade-off between achievable PAPR and BER performance. The perfection in the received spectrum validates the proposed blind CFO estimation algorithm, which uses oversampling and doesn't require any pilot symbols.

3.10 Conclusion

In this work real time prototyping of the MGFDM system using windowed preamble is performed and the spectrum characteristics of multitaper filters are investigated. Additionally, we discuss an insight into impact of oversampling on jitter noise behaviour. We observed significant improvement in the performance due to mitigation of jitter noise power effect by oversampling in simulations and mathematical analysis. The second part of the work presents various aspects in real time implementation of GFDM system by us-

ing blind estimation of channel impairments. The intrinsic phase shift which has occurred between neighbouring samples of the oversampled GFDM symbol is exploited for offset estimation and correction. In noise less case we observed a straight forward reception whereas it leads to ML estimate of CFO in the presence of Gaussian noise. The real time results primarily focus on the time and spectral response using USRP hardware for indoor channel environment. The comparison of BER analysis between GFDM with RRC pulse shaping filter by varying the roll off factor is provided for the proposed method. We concluded that, with usage of RRC filters with low roll off factor has high reduction in BER. Eventually the proposed algorithm in this work combats both channel induced distortions effects as well as effectively estimates the CFO. This kind of algorithm finds its flexibility to be incorporated in modern 5G communication system.

Chapter 4

Reduction of complexity in GFDM-SLM system

OFDM is an efficient modulation technique in terms of implementation and is the predominant physical layer technique for all the wireless and wired standards in the present 4G technology. It used an unique idea of chunking the information into multiple smaller sets and has revolutionised the idea of multi carrier transmission. One of the main advantages of this technique is simple implementation. This is achieved by using DSP chips for implementing the FFT algorithms. This procedure immensely reduced the cost and size of the transmitter. The deployment of smart phones with data-hungry applications will demand not only high speed but also low power since the battery life is limited. Another way of seeing this problem is, 5G applications like IoT cannot afford the luxury of high power amplifier. It is worth mentioning that, even for the traditional 4G mobile communication using OFDM, PAPR is a potential barrier for uplink communication. This forced the mobile user to perform frequent charging of their mobile phones. More importantly, all the multicarrier techniques including GFDM are having multiple symbols in time and hence is suffering from high PAPR. Though the PAPR of GFDM is much less than OFDM, it is necessary to further reduce the PAPR in order to make the system efficient for practical applications. Additionally, the flexible time-frequency grid structure of GFDM requires highly adaptive complex procedures for modulation/demodulation as a primary drawback for its implementation. We observe later in this chapter that, the reduction in PAPR by using the non distorting schemes may increase the computational complexity and bandwidth inefficiency. Hence, by applying the traditional PAPR techniques to GFDM system further increases the complexity. This motivated the authors to

reduce the complexity without much compromising on the BER and PAPR performance as will be discussed in this chapter.

4.1 Introduction

The GFDM system consists of K subcarriers, with each corresponding to M time-slots, amounting to $N = K \times M$ elements in a complete block. The independent and identical complex QAM modulated data which is to be GFDM modulated, is represented with $d_m(k)$ where $m = 0 \cdots M-1$ and $k = 0 \cdots K-1$. Here $\mathbf{d} = [\mathbf{d_0^T}\ \mathbf{d_1^T} \cdots \mathbf{d_{M-1}^T}]^T$ represents the grid of data symbols, where $\mathbf{d_m} = [d_m(0)\ d_m(1) \cdots d_m(K-1)]$ corresponds to data on every subsymbol and T in the superscript represents the transpose operation. To enable data detection in multipath environments, some data symbols are to be replaced by pilots in each subsymbol of the GFDM block. After arranging N_p pilots in the required positions, a prototype filter $g(n)$ which extends for a long length of MK can be selected to perform circular convolution for avoiding OOB emissions. Transmitted GFDM signal with the subsymbol processing methodology can be given by,

$$\begin{aligned} x(n) &= \sum_{m=0}^{M-1} g\langle n - mK \rangle_N \underbrace{\sum_{k=0}^{K-1} d_m(k) e^{j\frac{2\pi kn}{K}}}_{M\ copies\ of\ IDFT\ data} \\ &= \sum_{k=0}^{K-1} \sum_{m=0}^{M-1} d_m(k) g\left\langle n - mK \right\rangle_N e^{j\frac{2\pi kn}{K}}, \end{aligned} \tag{4.1}$$

where $\langle . \rangle$ represent the modulo operation utilized to obtain the GFDM signal $\mathbf{x} = [x_0 \cdots x_{MK-1}]$ and $n = 0, 1, \cdots N-1$. The matrix representation of the GFDM signal $\mathbf{x}$ from our previous chapters can be given as,

$$\mathbf{x} = \mathbf{A}\mathbf{d}, \tag{4.2}$$

The transmitter vector $\mathbf{x_{cp}}$ is obtained as $\mathbf{x_{cp}} = [\mathbf{x}(MK - N_{cp} + 1 : MK); \mathbf{x}]$ after attaching N_{cp} at the start of the packet. The PAPR of the transmitted GFDM signal can be calculated as,

$$\text{PAPR}\left\{\mathbf{x_{cp}}\right\} = \frac{\max\left\{|\mathbf{x}|^2\right\}}{\text{E}\{|\mathbf{x}|^2\}}, \tag{4.3}$$

where $\mathrm{E}\{.\}$ represents the expectation, $|.|$ involves in computing the magnitude of a complex number and max represents the maximum of value. It is quite important to observe that the usage of CP has no increment in PAPR since it is the part of the original signal [58]. The PAPR reduction schemes can be broadly into three categories namely distortion, coding and probabilistic which are detailed below:

- Distortion schemes distort the signal amplitude and achieve low PAPR. Clipping, companding, active constellation extension are examples for these schemes. These schemes are not practical since they effect the BER of the system.
- Coding schemes reduce the peak power by mapping the original sequence into a longer length sequences and therefore will require look up tables at the receivers. These are ideal for systems which are having few subcarriers and will result in high computational complexity for rectangular grid structures like GFDM.
- Probabilistic methods like SLM and PTS are most befitting for PAPR reduction of block structured systems like GFDM. We considered SLM technique in this work, since it requires reduced computational complexity over PTS scheme to achieve similar performance in terms of important performance metrics like ACLR and BER.

4.1.1 SLM technique

The basic principle of SLM technique is to create a number of different GFDM signal representations using data block and as name understandably suggests the sequence which yields the minimum possible PAPR will be selected for transmission [59]. The steps involved in SLM technique at the transmitter section are:

- The data block $\mathbf{d}$ will be multiplied with U non similar phase sequence vectors. we denote the u^{th} phase vector as $\phi^{(u)}$, where $u = 1, 2, ...U$. The u^{th} candidate GFDM vector can be obtained by multiplication of data block with the phase vector $\phi^{(u)}$ is denoted as $\mathbf{x}^{(u)}$.
- Let the phase vector sequence $\boldsymbol{\phi^u(n)} = \exp(j\boldsymbol{\alpha^u}(n))$ for $n = 0 \cdots N-1$ is multiplied with $\mathbf{d}$ as shown in Figure. 4.1

- . The value of $\boldsymbol{\phi^u(n)}$ is optimized iteratively in steps inorder to obtain lowest possible PAPR for the GFDM signal.

All the computed U candidate signals indirectly show the same GFDM symbol but are asymptotically independent of each other. The value of $\boldsymbol{\alpha^u}(n)$ represents the phase sequence values varies from 0 to π. Let $\bar{\boldsymbol{\phi}}\mathbf{(n)}$ be the vector, which possess the lowest PAPR and its GFDM signal is denoted with $\bar{\mathbf{x}}$. Hence, the optimized vector can be shown as $\bar{x} = \arg\min \text{PAPR}(x^{(u)})$. We know $\bar{x}$ is also a GFDM signal, hence we can represent it as,

$$\bar{\mathbf{x}} = \mathbf{A}\bar{\mathbf{d}}, \tag{4.4}$$

where $\bar{\mathbf{d}}(\mathbf{n}) = \bar{\boldsymbol{\phi}}\boldsymbol{(n)}\mathbf{d}(\mathbf{n})$ is the data vector modified in the process of SLM technique.

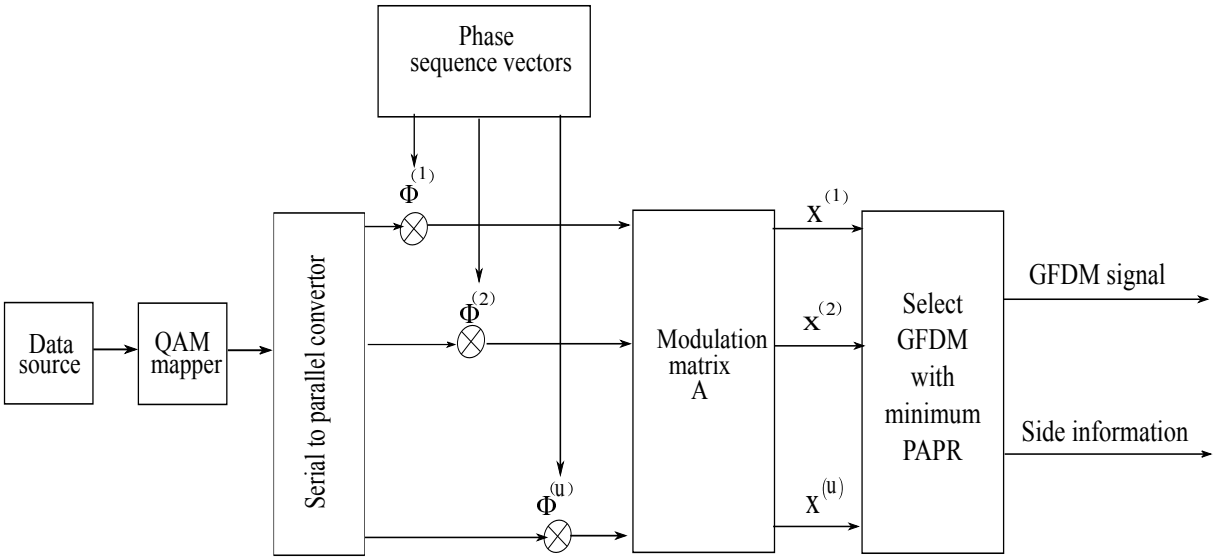

Figure 4.1: Block diagram for traditional SLM scheme

From (4.4) it can be understood that, the data detection can be possible by knowing $\bar{\boldsymbol{\phi}}$ exactly in the receiver. Hence, the phase vector $\bar{\phi}$ which yielded the lowest PAPR is transported and is named as SI [62]. The main demerit of this technique is, it will need an extra payload of $\log_2 U$ bits in the payroll data for SI transmission since it is not tractable at both transmitter and receiver [70]. Additionally, in practical communication, complex channel coding algorithms will be imposed in SI which further degrades the data efficiency. The reason behind this operation is, wrong detection of SI information may force the entire GFDM block into error.

In SLM approach, one GFDM signal with lowest PAPR is selected from a set of different candidate signals generated in the transmitter [59]. For generation of every alternative signal, the data vector which is to be GFDM modulated, is modified by multiplying with a different phase sequence vector [60]. Later, the candidate signal is generated by multiplying modulation matrix with its corresponding modified data sequence. As the name suggests, the signal which has the lowest PAPR among all generated GFDM signals is selected for transmission. The GFDM-SLM modulator suffers from two main problems which are addressed in this thesis. The main issues are

- The first issue with SLM technique is, it requires a bank of modulation matrices to generate the required set of candidate GFDM signals leading to high computational complexity. Therefore, reduction in complexity can be achieved by minimizing the number of alternative symbols. However, this scenario may decrease the PAPR reduction gain. One can utilize few number of different sequence vectors $U \leq N$ in order to reduce the complexity. But by decreasing U, SLM transmitter generates less alternate forms of GFDM signals which may require sacrifice on PAPR reduction gain. This scenario creates a trade-off between the achievable PAPR reduction and computational complexity employing SLM technique. To address this issue, we propose three methods to alleviate high complexity associated with GFDM-SLM system in this chapter.

- In the conventional SLM technique, a combination of phase rotation vectors are generated to obtain modified form of GFDM signals. Among them, the signal corresponding to minimum PAPR is selected for transmission. As a result, the phase sequence vector which is leading to low PAPR must be transmitted to the receiver. This customary SI is necessary for detection of the exact payroll data and it's necessity in conventional methodologies reduces the throughput efficiency and make the system unattractive for real time applications. Another idea to reduce computational complexity is to restrict phase sequence vectors to a small number i.e., $U \leq N$ and hence we can have the ability to check the SI by different algorithms in the receiver but this process may compromise in PAPR reduction gain. In the next chapter, a modified SLM architecture by using the advantage of non orthogonal nature of GFDM system is proposed. The PAPR reduction is achieved by using the

equispaced multiple pilots in every subsymbol which are associated with channel estimation, whose implementation is quite different from the traditional SLM.

To overcome the high complexity of the GFDM-SLM modulator, three methods are proposed in the following sections. The first method uses two GFDM signals and principle of linearity to obtain different alternative representations. This method can effectively generate alternative signals, but all the generated alternative signals are correlated with each other. To combat this problem, the proposed method 2 uses a simple conversion matrices for removing the correlations in proposed method 1. Ultimately, the proposed method 3 inherits the advantages of the afore mentioned methods and uses an extra shifting matrix to achieve trade off between PAPR gain and computational complexity. The simulation results indicate that, when compared to conventional SLM scheme, the first proposed approach has inferior PAPR reduction performance, where as second and third proposed methods almost reach performance of conventional SLM scheme. In this thesis, all the three modified SLM schemes for achieving lower computational complexity than the traditional SLM scheme without considerable mitigation in PAPR reduction gain. Each method is clearly described in the following subsections with corresponding block diagrams.

4.1.2 Method 1

The proposed method 1 uses two GFDM signals and the concept of linearity to obtain different phase sequence vectors. More importantly, the idea is to utilize available phase sequence vectors for generation of many alternative GFDM signals. To illustrate, let us consider $\mathbf{x^{(a)}}$ and $\mathbf{x^{(b)}}$ as two already known representations of the original GFDM signal generated using conventional SLM scheme. Using the linearity property let us define $\mathbf{x^{(ab)}}$ as,

$$\begin{aligned}\mathbf{x^{(ab)}} &= c_a\mathbf{x^{(a)}} + c_b\mathbf{x^{(b)}} \\ &= c_a\mathbf{A}\times\boldsymbol{\phi_a}\circ\,\mathbf{d} + c_b\mathbf{A}\times\boldsymbol{\phi_b}\circ\,\mathbf{d} \\ &= \mathbf{A}\times(c_a\boldsymbol{\phi_a} + c_b\boldsymbol{\phi_b})\circ\,\mathbf{d}, \end{aligned} \tag{4.5}$$

where c_a and c_b are the complex numerical constants which are selected in the proposed method to obtain alternative GFDM symbol representation. It is a traditional practice to utilize binary or quaternary complex numbers $\{1, -1, j, -j\}$ as elements in phase sequence vectors [59]. Hence, it is compulsory for each element of the linear summation vector $(c_a\boldsymbol{\phi_a} + c_b\boldsymbol{\phi_b})$ to have unit magnitude since $(c_a\boldsymbol{\phi_a} + c_b\boldsymbol{\phi_b})$ has to represent another valid phase sequence vector. This scenario provides us an opportunity to use $\mathbf{x^{(ab)}}$ as another alternative GFDM signal. Hence, if we have $\mathbf{x^{(a)}}$ and $\mathbf{x^{(b)}}$, another GFDM signal $\mathbf{x^{(ab)}}$ can be generated without performing actual multiplication with the modulation matrix $\mathbf{A}$. With a careful inspection, we can observe the following conditions are to satisfied in order to obtain a unit magnitude in phase sequence vector :

- Each element of $\boldsymbol{\phi_a}$ and $\boldsymbol{\phi_b}$ should take values as {1,-1}
- The numerical constants $c_a = \pm\frac{1}{\sqrt{2}}$ and $c_b = \pm\frac{j}{\sqrt{2}}$

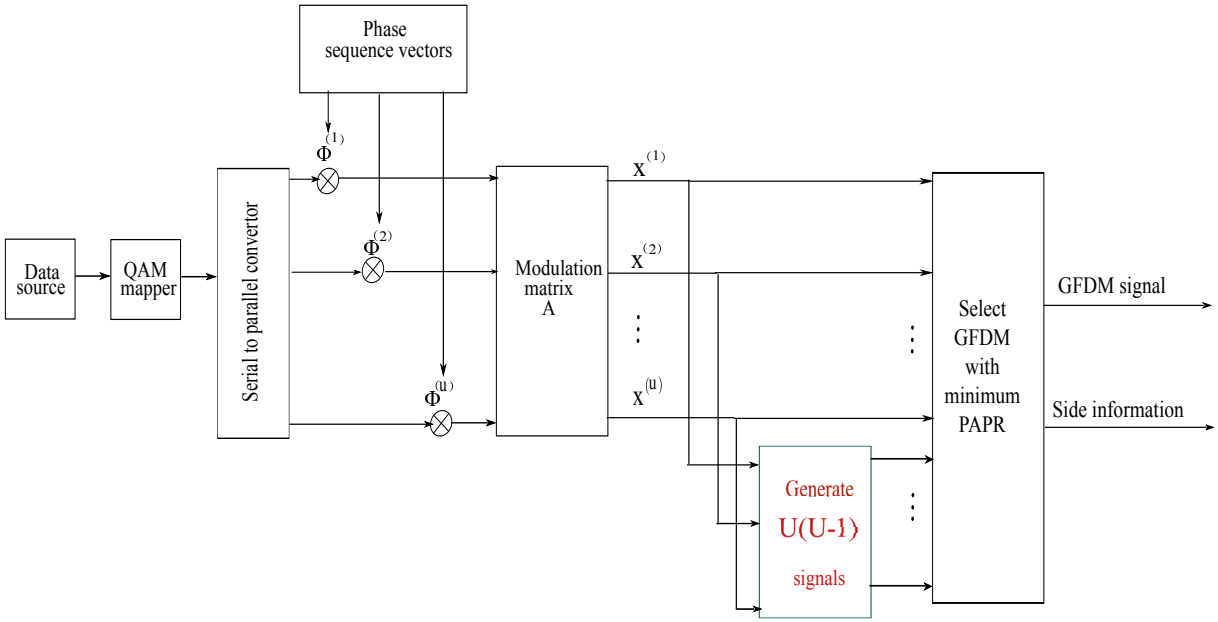

Figure 4.2: Block diagram of modified SLM scheme for proposed method 1

Since the two alternate GFDM symbols using phase sequence vectors $(\pm c_a\boldsymbol{\phi_a} + c_b\boldsymbol{\phi_b})$ will have the same numerical value of PAPR, we have to ignore this combination. In order to obtain unit magnitude for each element of the phase sequence vector, when $\boldsymbol{\phi_a}$ and $\boldsymbol{\phi_b}$ are selected from $\{1, -1\}$, we are restricted to consider constants as $c_a = \pm\frac{1}{\sqrt{2}}$ and $c_b = \pm\frac{j}{\sqrt{2}}$. The average power of the newly generated signal $\mathbf{x^{(ab)}}$ is equal to one half of

sum of average power of $\mathbf{x^{(a)}}$ and $\mathbf{x^{(b)}}$ because $|c_a^2|$ and $|c_b^2|$ is equal to half. Hence, we are not increasing average power to accomplish PAPR mitigation. Considering a generalized notation, from U independent binary phase sequences we can choose any two sequences, so there are $2\times \binom{U}{2}$ additional phase sequences in total. Hence a total of U^2 sequences can be generated as shown in Figure 4.2. For example,

- When $U = 3$, let us assume the known binary sequences are $\{\boldsymbol{\phi_1}, \boldsymbol{\phi_2}, \boldsymbol{\phi_3}\}$. Then, all the nine possible phase sequence vectors can be summarized as, $\{\boldsymbol{\phi_1}, \boldsymbol{\phi_2}, \boldsymbol{\phi_3}, \boldsymbol{\phi_1} \pm \boldsymbol{j\phi_2}, \boldsymbol{\phi_1} \pm \boldsymbol{j\phi_3}, \boldsymbol{\phi_2} \pm \boldsymbol{j\phi_3}\}$.

For a generalised representation, all the generated U^2 alternative GFDM signals in set S can be represented as,

$$\begin{aligned} S =& \{\mathbf{x^{(u)}} | 1 \leq u \leq U^2\} \\ =& \{\mathbf{x^{(u)}}\} \cup \left\{ \frac{1}{\sqrt{2}} \left(\mathbf{x^{(a)}} + j\mathbf{x^{(b)}} \right) \right\} \cup \left\{ \frac{1}{\sqrt{2}} \left(\mathbf{x^{(a)}} - j\mathbf{x^{(b)}} \right) \right\} 1 \leq a \leq u \leq b \leq U. \end{aligned} \tag{4.6}$$

The GFDM signal with minimum PAPR among all generated alternatives from the set $\mathbf{S}$ is transmitted along with its corresponding phase sequence vector denoted with $\bar{\boldsymbol{\phi}}$. However, it is important to note that, the newly generated phase sequence vector $c_a\boldsymbol{\phi_a} + c_b\boldsymbol{\phi_b}$ is statistically correlated with $\boldsymbol{\phi_a}$ and $\boldsymbol{\phi_b}$. Therefore, the PAPR reduction gain of the proposed scheme declined with increase in value of U, when compared with conventional SLM scheme. Another important point is, when M-ary signalling is used, an extra $\log_M U$ symbols must be allocated for transmitting the SI.

4.1.3 Method 2

The low complexity in SLM generation is achieved in proposed method 2 by deriving a conversion matrix for generation of alternate signals. To illustrate this relationship, let us consider $\mathbf{x}$ as original GFDM and $\mathbf{x^{(u)}}$ as u^{th} alternative signal. Then from SLM approach we can deduce the following equations,

$$\mathbf{x} = \mathbf{Ad}, \tag{4.7}$$

$$\mathbf{x^{(u)}} = \mathbf{AR_u d}. \tag{4.8}$$

We can observe (4.8) is matrix representation for u^{th} alternative GFDM signal where $\mathbf{R_u}$ is phase rotation matrix for a phase rotation vector $\boldsymbol{\phi_u}$ represented in diagonal form as,

$$\begin{bmatrix} \phi_u(0) & 0 & \cdots & 0 \\ 0 & \phi_u(1) & \cdots & 0 \\ 0 & 0 & \cdots & \phi_u(N-1) \end{bmatrix}. \tag{4.9}$$

So from (4.7) we can deduce,

$$\mathbf{d} = \mathbf{A}^{-1}\mathbf{x}, \tag{4.10}$$

where $\mathbf{A}^{-1}$ is the equivalent demodulation matrix for GFDM signal. Then we can simply obtain the relationship between the alternatives and the original GFDM signals as,

$$\mathbf{x^{(u)}} = \mathbf{A}\mathbf{R_u}\mathbf{A}^{-1}\mathbf{x}. \tag{4.11}$$

An interesting observation from (4.11) is that, the presence of $\mathbf{R_u}$ matrix differentiates the alternatives of GFDM. In other words, another GFDM matrix can be obtained by using a different phase rotation matrix. In this method, we define a conversion matrix $\mathbf{T_u} = \mathbf{ARA}^{-1}$ with a phase rotation matrix $\mathbf{R}$ and utilize it for generating additional alternatives. Since already generated GFDM signal $\mathbf{x}$ is utilized for calculating alternative signals, the proposed idea will obtain high reduction in computational complexity. In [71], authors proved $\mathbf{A}$ is block circulant in nature hence we can consider $\mathbf{T_u}$ is also block circulant. Therefore, we can represent $\mathbf{T_u}$ in the following manner,

$$\mathbf{T_u} = \begin{bmatrix} \mathbf{t_u}^{(0)} & \mathbf{t_u}^{(M-1)} & \cdots & \mathbf{t_u}^{(1)} \\ \mathbf{t_u}^{(1)} & \mathbf{t_u}^{(0)} & \cdots & \mathbf{t_u}^{(2)} \\ \vdots & \vdots & \ddots & \vdots \\ \mathbf{t_u}^{(M-1)} & \mathbf{t_u}^{(M-2)} & \cdots & \mathbf{t_u}^{(0)} \end{bmatrix}, \tag{4.12}$$

Here every $\mathbf{t_u}^{(m)}$ is a $K \times K$ matrix. It is important to note that, the first K columns of $\mathbf{T_u}$ can be obtained by multiplication of modulation matrix $\mathbf{A}$ with $\boldsymbol{\phi_u}$ [71]. By using the block circulant matrix properties the full matrix can be constructed after obtaining first K elements. This is a mandatory condition since we intend to achieve low complexity without disturbing the system design. For example,

- Let us consider a simple conversion matrix obtained by using a repeated phase sequence vector $\boldsymbol{\phi_u}$ of the form $[1\ j\ 1\ j \cdots 1\ j\ 1\ j]$. The $\boldsymbol{\phi_u}$ is repeated with

a period of 2 to satisfy matrix multiplication conditions. The $\mathbf{R}$ matrix can be constructed corresponding to repeated phase sequence vector $\boldsymbol{\phi_u}$ for generation of alternate signals. The proposed matrix will work perfectly without disturbing the flexible properties of GFDM.

- For a GFDM system with $N = 8$, if we consider $M = 2$ and $K = 4$ the conversion matrix $\mathbf{T_u}$ will be of the below form,

$$\begin{bmatrix} 1-j & 0 & 1+j & 0 & 0 & 0 & 0 & 0 \\ 0 & 1-j & 0 & 0 & 0 & 0 & 0 & 1+j \\ 1+j & 0 & 1-j & 0 & 0 & 0 & 0 & 0 \\ 0 & 0 & 0 & 1-j & 0 & 1+j & 0 & 0 \\ 0 & 0 & 0 & 0 & 1-i & 0 & 1+j & 0 \\ 0 & 0 & 0 & 1+j & 0 & 1-j & 0 & 0 \\ 0 & 0 & 0 & 0 & 1+j & 0 & 1-j & 0 \\ 0 & 1+j & 0 & 0 & 0 & 0 & 0 & 1-j \end{bmatrix}, \tag{4.13}$$

- when $M = 1$ and $K = 8$ the conversion matrix $\mathbf{T_u}$ will simulate the behaviour of OFDM as shown below,

$$\begin{bmatrix} 1-j & 0 & 0 & 0 & 1+j & 0 & 0 & 0 \\ 0 & 1-j & 0 & 0 & 0 & 1+j & 0 & 0 \\ 0 & 0 & 1-j & 0 & 0 & 0 & 1+j & 0 \\ 0 & 0 & 0 & 1-j & 0 & 0 & 0 & 1+j \\ 1+j & 0 & 0 & 0 & 1-i & 0 & 0 & 0 \\ 0 & 1+j & 0 & 0 & 0 & 1-j & 0 & 0 \\ 0 & 0 & 1+j & 0 & 0 & 0 & 1-j & 0 \\ 0 & 0 & 0 & 1+j & 0 & 0 & 0 & 1-j \end{bmatrix}. \tag{4.14}$$

We can observe from (4.13) and (4.14) and make the following conclusions

- The block circulant nature of $\mathbf{T_u}$ matrix is undisturbed with multiplication of periodic phase sequence vector
- Number of non zero elements in every row is equal to 2 for any number of subsymbols

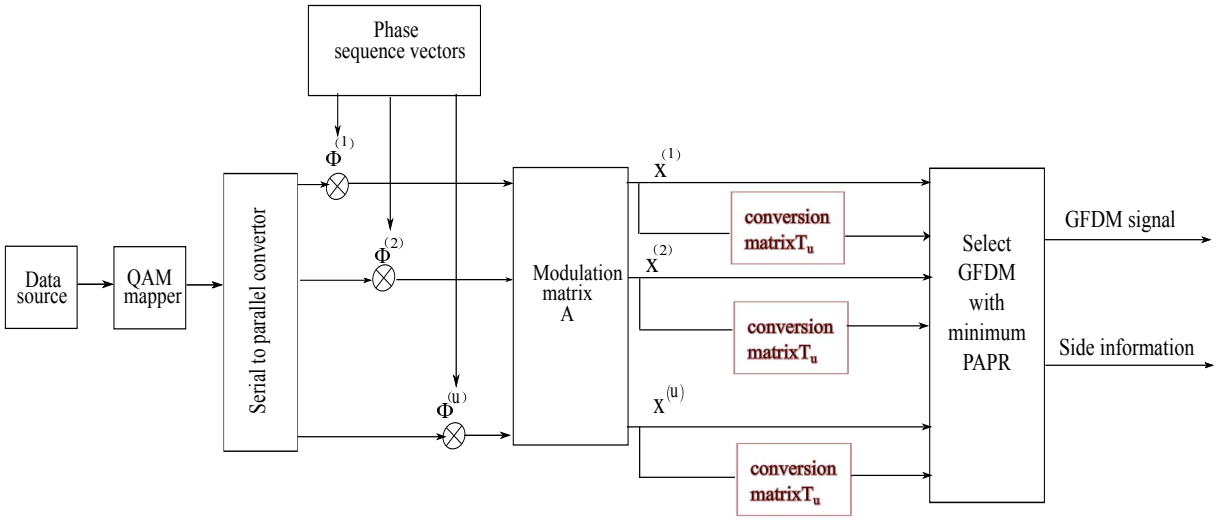

Figure 4.3: Block diagram of modified SLM scheme for proposed method 2

Hence by multiplication with $\mathbf{T_u}$ we can obtain another GFDM signal with less complexity. The Figure 4.3 represents the modified SLM transmitter with double the number of GFDM candidate signals. We can simply remove half modulation matrices and use the conversion matrix to generate candidate GFDM signals. The proposed method is clearly depicted in Figure 4.3, where we can observe U GFDM symbol representations generated using the traditional SLM method are used for obtaining another U symbols. For example, let $\mathbf{x^{(a)}}$ be an alternative generated using traditional SLM scheme with a initial phase of $\mathbf{R_a}$. The phase sequence vector of its corresponding alternative symbol is $\mathbf{RR_ax}$, where $\mathbf{R}$ is the proposed phase rotation matrix. Thus, the complexity of GFDM signal generation can be reduced to half with same number of different candidate signals in conventional SLM method. Hence by employing proposed method 2 much reduction in complexity can be achieved. Now coming to the design of the phase sequence vector, we can try different combinations from the set $\{\pm 1 \pm j\}$ for the phase sequence vector with period 2 with compulsion of one real and imaginary component. The list the other 8 other possible values periodic phase sequence vector are $\{\{1, j\}, \{1, -j\}, \{-1, j\}, \{-1, -j\}, \{j, 1\}, \{j, -1\}, \{-j, -1\}, \{-j, +1\}\}$. We considered using phase sequence vector of period 2 in this work, if increase in period of the phase sequence $\boldsymbol{\phi_u}$ is desired then sophisticated designs are to be considered for the design of conversion matrix to make it compatible for flexible block structures systems like GFDM.

4.1.4 Method 3

The concept of linearity has led to PAPR reduction in method 1, where the coefficients are selected to avoid complexity multiplications. This fundamental idea reduced the complexity of the SLM technique to a large extent. We can consider method 2 as an extension of method 1, since we borrow the idea of low complexity from linear summation and utilize GFDM block structure to further improve the PAPR reduction performance. To illustrate this idea, let us rewrite the matrix $\mathbf{T_u}$ in complex notation as,

$$\mathbf{T_u} = \Re\{\mathbf{T_u}\} + j\Im\{\mathbf{T_u}\} \tag{4.15}$$

where $\Re$ and $\Im$ represent the real and imaginary parts of the conversion matrix $\mathbf{T_u}$, which are also block circulant. By substituting (4.15) into (4.11) we obtain,

$$\mathbf{x^{(u)}} = \Re\{\mathbf{T_u}\}\mathbf{x} + j\Im\{\mathbf{T_u}\}\mathbf{x}. \tag{4.16}$$

If you compare (4.5) in method 1 with (4.16), we can clearly observe a circulant matrix

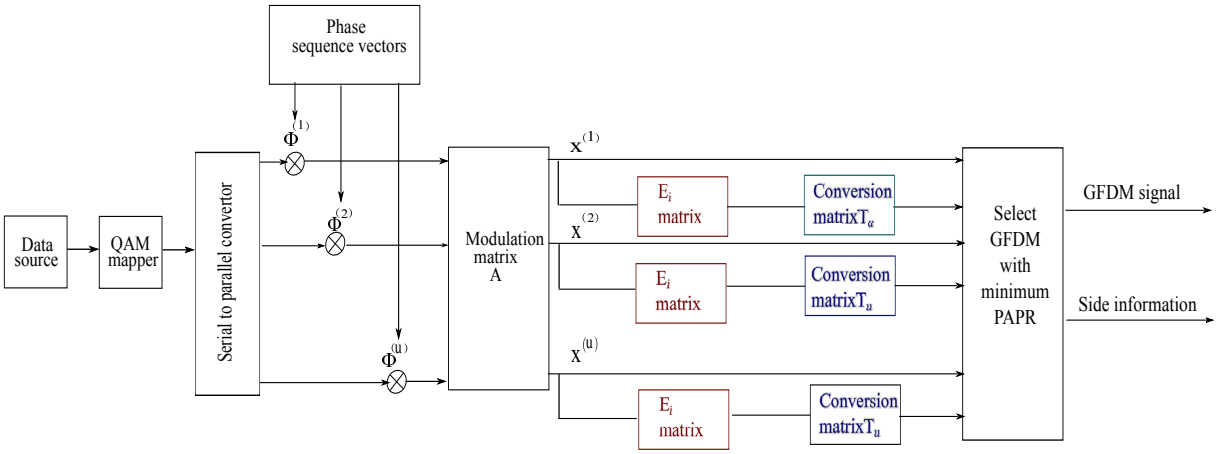

Figure 4.4: Block diagram of modified SLM scheme for proposed method 3

is placed in method 2 in the place of numerical constants of method 1. This lead to decrement in correlations and in turn yields improvement in PAPR performance. Another important observation is, a single GFDM signal is used for the generation of alternative symbols in method 2 where as method 1 selects two symbols from U candidate signals. In short, the main advantage of method 1 is generation of alternatives but there may be correlation between them. The second method cannot generate many alternatives but can provide signals which are uncorrelated. The method 3 uses the advantages of the former

methods and utilize the block matrix properties of $\mathbf{A}$ in [71] for improving the method 2. The primary idea of the method 3 is, shifting the conversion matrix $\mathbf{T_u}$ in regular intervals and using it for the generation of additional alternative signals. It is important to note that, the only condition in shifting is, the resultant matrix should not disturb the block circulant structure. The obtained matrices from their shifted versions wouldn't have much correlation between them and hence PAPR performance of the method 3 will be better than method 1. For detail description of the method 3, let us define $\mathbf{x^{(ui)}}$ as,

$$\mathbf{x^{(ui)}} = \mathbf{E_i} \times (\Re\{\mathbf{T_u}\}\mathbf{x} + j \times \Im\{\mathbf{T_u}\}\mathbf{x}) \,. \tag{4.17}$$

$\mathbf{E}_i$ is a shifting matrix defined as,

$$\mathbf{E}_i = \begin{bmatrix} \text{zeros}(N-i, i) & \mathbf{I}_{N-i} \\ \mathbf{I}_i & \text{zeros}(i, N-i,) \end{bmatrix}, \tag{4.18}$$

where $\mathbf{I_i}$ represents identity matrix of dimension $i \times i$ and zeros is representing a grid of rectangular zero matrix with indices representing number of rows and columns respectively. The introduced $\mathbf{E}_i$ in (4.17) will aid us to increase the number of alternative symbols. The effectiveness of the algorithm 3 lies in design of $\mathbf{E}_i$ which results shifting and provides us chance to generate many alternative symbols by varying i as integer multiples of K as $\{0\ K \cdots K(M-1)\}$. In fact, method 3 only increases the number of alternative representations of method 2 by using the block circulant properties. In method 2, we used the conversion matrix $\mathbf{R}$ to obtain alternative signals with different values of PAPR with less correlation. It is important to note that, the $\mathbf{E}_i$ matrix is a circulant matrix and hence by multiplying $\mathbf{E}_i$ with $\mathbf{R}$ will not disturb the block circulant nature of the newly generated signal. Finally, for generalised representation, we can obtain M alternative symbols with phases represented as $\mathbf{E_i} \times \mathbf{RR_u}$ when i varies as $\{0\ K \cdots K(M-1)\}$. The block diagram is shown in the Figure 4.4. Hence, the method 3 decreases the computational complexity by increasing the number of alternatives of method 2. The detailed PAPR analysis and computational complexity for all the schemes is done in the next section.

4.2 Results

The SLM technique requires a bank of modulation matrices to generate a set of candidate GFDM signals which leads to high computational complexity. In order to

reduce the complexity, the number of alternative symbols has to be minimized. In this work, we proposed three methods to alleviate high complexity associated with GFDM system. We consider PAPR performance and computational complexity as performance metrics for comparison between proposed methods and the conventional SLM scheme. To evaluate the PAPR performance of the GFDM system, we utilize complementary cumulative distribution function (CCDF), which is the measure of probability of a PAPR value exceeding a threshold level. The number of different phase vectors multiplied with original GFDM symbol is represented by U and the simulations are performed for all the proposed methods using Labview software of National Instruments. The parameters used for simulation are tabulated in Table 4.1.

Table 4.1: Parameters for simulated GFDM system

Parameter	**Value**
Number of sub carriers	64
Number of sub symbols	4
CP length	8
Prototyping filter	Root raised cosine
Filter roll off factor	0.9

4.2.1 Simulation results

The PAPR comparison of proposed method 1 with conventional scheme is illustrated in Figure. 4.5. We can observe the PAPR of the method 1 is higher than the traditional SLM scheme due to existence of correlations between the generated symbols. However, as the number of different phase sequence vectors U increase from 8 to 16 a significant reduction in PAPR can be observed. At a CCDF of 10^{-4} the GFDM system has a PAPR of 11.8 dB while, SLM technique for $U = 9$ and $U = 16$ has 7.9 dB and 6.8 dB as its PAPR values, whereas, the proposed method 1 has 8.5dB and 7.4 dB respectively. However, when compared with the conventional GFDM system, PAPR is reduced significantly by an amount of 3.3 dB. Even with the presence of correlations, we observe a significant PAPR reduction of 0.9 dB upon increasing the number of phase sequences from U =

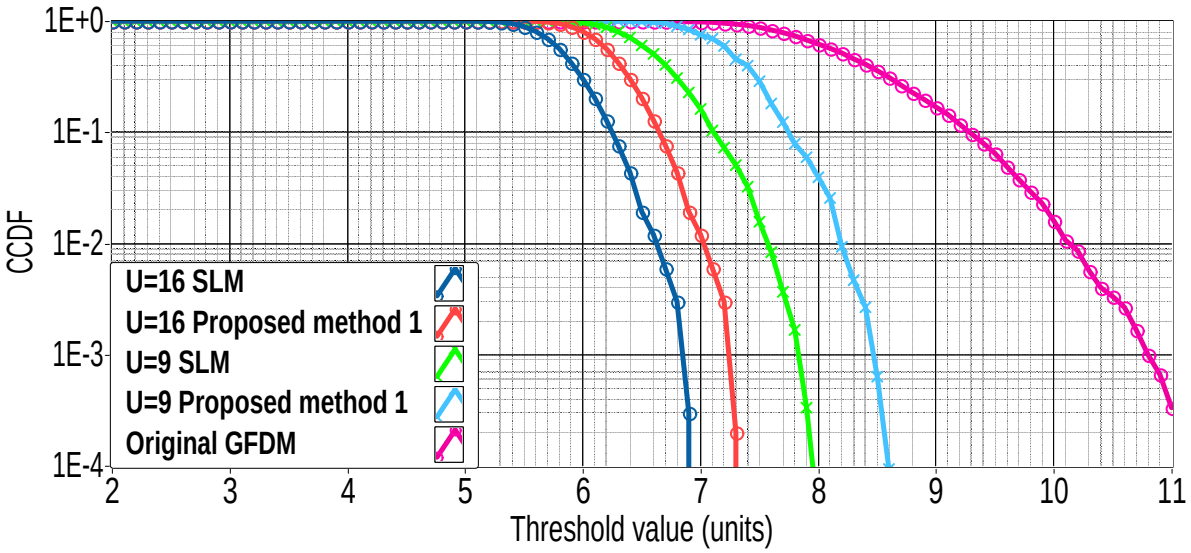

Figure 4.5: PAPR performance of the proposed method 1

8 to U = 16. The PAPR performance of the proposed method 2 is depicted in Figure 4.6, where we generate the phase rotation matrix of alternate symbol using a conversion matrix. From the figure it is clearly evident that, the performance of the method 2 closely matches with the conventional SLM scheme. In Figure 4.7, method 3 has almost

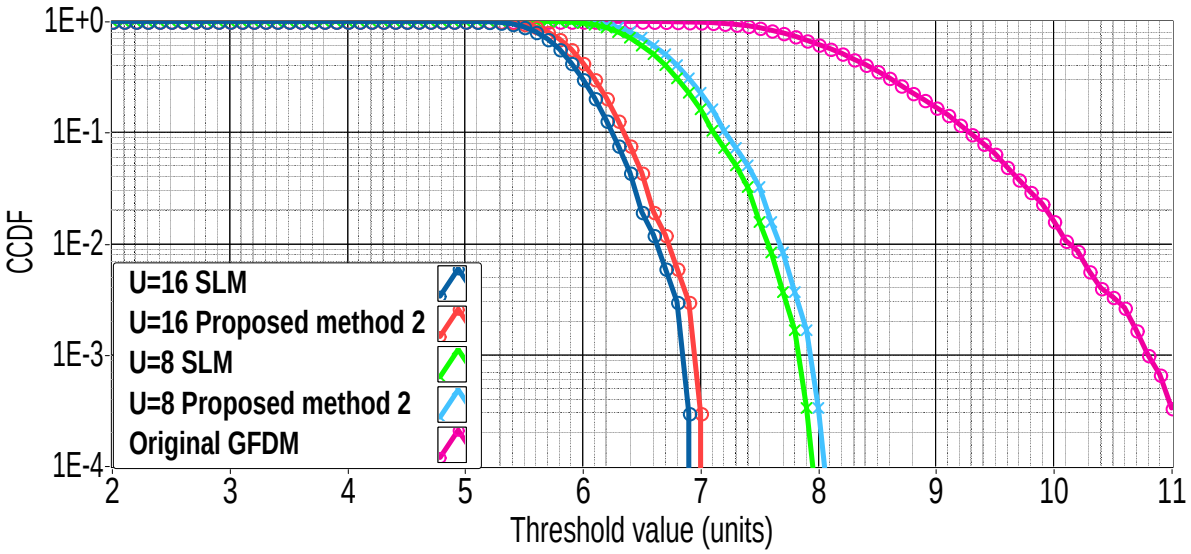

Figure 4.6: PAPR performance of the proposed method 2

same performance as traditional SLM scheme with same number of phase sequences. From inspection, we can draw a conclusion that, by using the proposed idea of cyclic shifts the computational complexity can be reduced without much compromise in PAPR reduction performance. The Figure 4.8 shows the comparisons between the three proposed

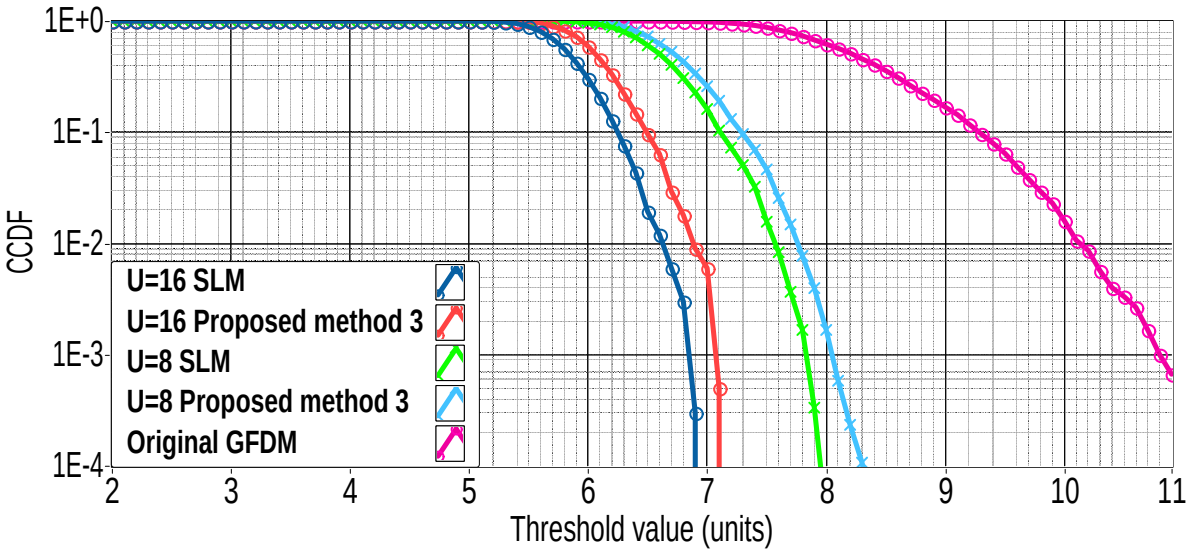

Figure 4.7: PAPR performance of the proposed method 3

methods. We can conclude that, the performance of the method 1 is inferior to that of other two methods at any arbitrary number of phase sequence vectors. Another interesting observation is, proposed method 2 delivers similar performance of method 3 at $U = 8$ but the performance deteriorates as the U increases. However, we conclude proposed method 3 as the best method since it has very less complexity when compared with method 2 and is an effective solution for trade-off between PAPR performance and computational complexity in the next subsection. The effect of varying the roll off factor alpha of the

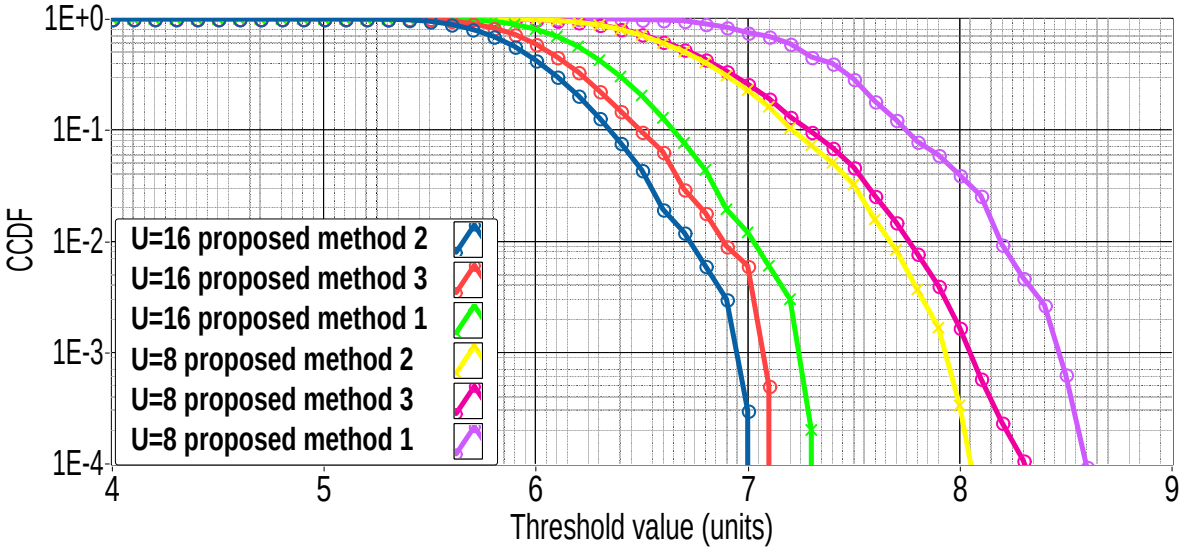

Figure 4.8: Comparison of PAPR performance between proposed methods

pulse shaping filter for the proposed technique is illustrated in Figure. **??**. The figure

evidences that upon increasing the roll off factor from 0.1 to 0.9, the PAPR reduces significantly in all the techniques. This is valid because, at a roll off factor of 0, the pulse shaping filter approaches the rectangular filter whose PAPR is higher. This can be clearly inferred from the figure, for roll off factor alpha = 0.9, at a CCDF of 10^{-3}, the attained PAPR is 7.8 dB, 6.7 dB for $U = 8$ and 16 for the SLM-imposed GFDM system. Whereas, at the same CCDF, for the same roll-off factor, and for the same set of phase sequences, the achievable PAPR is 7 dB and 8 dB for the proposed technique.

The Figure 4.9 shows the effect of roll off factor alpha on PAPR performance of the GFDM system employing method 3. It is evident that, upon increasing the alpha from 0.1 to 0.9 the PAPR is reduced by a significant amount. This is because, at a roll off factor of 0.1 the RRC filter approach to rectangular nature whose PAPR is high. It can be inferred from figure that, at an alpha=0.9 and CCDF of 10^{-4} the PAPR is 7.9 dB, 6.8 dB for U = 8 and 16 for conventional SLM-GFDM system, whereas at same value of CCDF and roll off factor 0.1 the achievable PAPR is 8.2 dB and 7.1 dB.

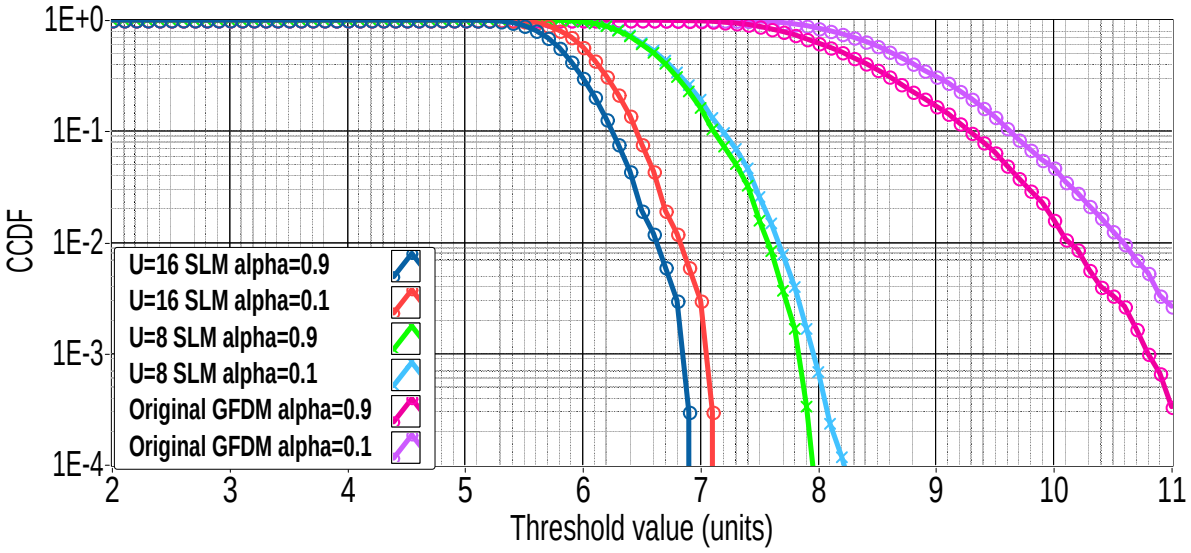

Figure 4.9: Effect of roll off factor on PAPR performance

4.2.2 Complexity analysis

In this work, we consider computational complexity of PAPR reduction schemes in terms of complex multiplications (CM) and complex additions (CA). Without loss in generality, we assume equal number of alternative symbols and compare computational

complexity of the three proposed methods. The computational complexity reduction ratio (CCRR) is defined as ratio between complexity of proposed scheme to the conventional SLM scheme

$$\text{CCRR} = \left(1 - \frac{\text{complexity of proposed scheme}}{\text{complexity of the conventional SLM}}\right) \times 100 \tag{4.19}$$

The computational complexity involved in computation of SLM scheme which generates U alternatives is $U(N\log_2 M + N + N \times \log_2 MK)$, where N is the size of the GFDM symbol. Since in the conventional SLM scheme, the transmitter needs to generate U different candidate signals the calculated complexity is multiplied with a factor of U. We need an additional NU CM for the search of peak power among U alternative GFDM signals. Hence a total number of $U(N\log_2 M + N + N \times \log_2 MK) + NU$ CM are required for the conventional SLM scheme. Additionally, we require $2U(N\log_2 M + N + N \times \log_2 MK)$ CA for the generation of U alternatives. In the proposed scheme 1, the amount of reduction in computational complexity can be achieved from generation of additional $U - \sqrt{U}$ alternative GFDM signal sequences from already known $\sqrt{U}$ alternative GFDM signal sequences without actual multiplication with modulation matrix. Hence, the complexity of initially known $\sqrt{U}$ alternate sequences remains the same and to generate extra $U - \sqrt{U}$ sequences we require an extra $N(U - \sqrt{U})$ CA.

We have proposed a low-complexity conversion matrix $\mathbf{R}$ in proposed method 2 to replace half the modulation matrices in the conventional SLM approach. These conversions use one GFDM signal to produce another signal without actual multiplication. Hence for generation of U alternative signal we require $U/2$ GFDM signal initially. To generate remaining $U/2$ matrices in proposed method 2 we require zero CM and 3N CA without any dependence on number of subsymbols. Hence, the computational complexity is high as it lacks in generation of number of alternatives. The proposed method 3 we require $U/2M$ GFDM signals for obtaining U GFDM representations. Additionally, the introduced circulant matrix $\mathbf{E}_i$ will require N multiplications and can generate M alternative signals. The complexity comparison of all the proposed schemes are shown in Table 5.1 and 4.3.

The complexity involved in CM is very high when compared with CA. The proposed method 3 not only has good PAPR reduction gain as shown in Figure. 4.7 but also contains low complexity among all the methods. From simulation results in previous section, we

Table 4.2: Number of complex multiplications for all the proposed methods

Method	**CM**
Conventional method	$UN(\log_2 M + \log_2 MK + 2)$
Proposed method 1	$\sqrt{U}N(\log_2 M + \log_2 MK + 1) + UN$
Proposed method 2	$\frac{UN}{2}(\log_2 M + \log_2 MK + 3)$
Proposed method 3	$\frac{UK}{2}(\log_2 M + \log_2 MK + 1) + NU$

Table 4.3: Number of complex additions for all the proposed methods

Method	**CA**
Conventional method	$2UN(\log_2 M + \log_2 MK + 1)$
Proposed method 1	$\sqrt{U}N(2\log_2 M + 2\log_2 MK + 1) + UN$
Proposed method 2	$UN(\log_2 M + \log_2 MK + 4)$
Proposed method 3	$UK(\log_2 M + \log_2 MK + 1) + 3UN$

Table 4.4: Comparison of complexity between proposed methods

Method	**CM**	**CA**	CCRR (CM)	CCRR (CA)
Conventional (U=16)	49,152	90,112	-	-
Proposed method 1 (U=16)	15,360	25,600	68.75	71.59
Proposed method 2 (U=16)	26,624	57,344	45.83	36.36
Proposed method 3 (U=16)	9,728	23,552	80.20	73.86

found the method 2 outperforms the method 3 at high values of U. However, we can observe that at a fixed $U = 16$ the proposed method 3 is having CCRR of 80.20 which is 1.65 times the proposed method 2. This indicates the high computational complexity of method 2 when compared with proposed method 3. Hence, we can conclude the proposed method 3 is effective solution for trade-off between PAPR performance and computational complexity.

4.3 Conclusion

In this work, we have proposed three modified SLM schemes for reducing high computational complexity of GFDM system. The proposed methods use the concepts of linearity, conversion matrix and shifting matrix by retaining the PAPR performance when compared with conventional SLM scheme. Since the CCRR increases with increase in number of phase sequences, all the proposed schemes are efficient and can be used in practical implementations of GFDM system depending on application. The effect of roll off factor on PAPR is provided for GFDM system with RRC as prototyping filter. We inferred from simulation results that, high roll off factor for RRC filters results in significant reduction in PAPR. Therefore, the proposed methods can make the GFDM system as an attractive physical layer waveform for the envisioned 5G applications. Depending on the choice of U, SLM transmitter generates U alternate forms of GFDM signals which may have different values of PAPR. It is to be remembered that, the computational complexity linearly increase upon increasing value of U. This scenario creates a trade-off between the achievable PAPR reduction and computational complexity employing SLM technique.

Chapter 5

Joint channel estimation and side information estimation for GFDM systems

As discussed in the previous chapter, in the conventional SLM technique, a combination of phase rotation vectors are generated to obtain modified form of GFDM signals. Among them, the signal corresponding to minimum PAPR is selected for transmission. As a result, the phase sequence vector which is leading to low PAPR must be transmitted to the receiver. It's necessity in conventional methodologies reduces the throughput efficiency and make the GFDM system unattractive for real time applications. In this chapter, authors implement a real time prototype of the GFDM system focussing on PAPR reduction and channel estimation using USRP. The idea of this contribution is to use the pilots associated with channel estimation for performing joint channel estimation and PAPR reduction. To address the practically encountered challenges, a modified SLM architecture by using the advantage of non orthogonal nature of GFDM system is proposed. The PAPR reduction in the proposed method is done using equispaced multiple pilots in each subsymbol, whose implementation is quite different from the traditional SLM. The primary difference is that the latter is a pilot-aided data decoding scheme with a self-channel mitigation mechanism which requires no SI estimation and only require pilots which are conventionally associated with channel estimation. To demonstrate the effectiveness of the proposed method, the metrics like PAPR and BER is evaluated and compared with the traditional SLM based GFDM that assumes perfect estimation of SI. Though there is a little compromise in PAPR reduction, the main advantage of the proposed method is reduction in complexity and achievement of blind SI estimation.

5.1 SLM technique

The fundamental idea of SLM technique is to produce different possible representation for the original GFDM signal representations and it can be easily interpreted from the name that, the symbol which yields the minimum PAPR among all shall be selected for transmission. We shall describe the GFDM SLM transceiver section below in detail.

5.1.1 Transmitter

The steps involved in SLM technique at the transmitter section are detailed in the previous chapter. In short,input data block $\mathbf{d}$ is multiplied with U non identical phase sequence vectors. Let $\bar{\boldsymbol{\phi}}(\mathbf{n})$ represent the vector which yields the minimum PAPR and its corresponding optimized GFDM signal is represented with $\bar{\mathbf{x}}$ i.e., mathematically, the optimized vector can be represented as $\bar{x} = \arg\min \mathrm{PAPR}(x^{(u)})$. since $\bar{x}$ is another GFDM signal, we can rewrite it as,

$$\bar{\mathbf{x}} = \mathbf{A}\bar{\mathbf{d}}, \tag{5.1}$$

where $\bar{\mathbf{d}}(\mathbf{n}) = \bar{\boldsymbol{\phi}}(\boldsymbol{n})\mathbf{d}(\mathbf{n})$ is the modified data vector. From (5.1) it is clearly evident that, the successful recovery of data is possible by having $\bar{\boldsymbol{\phi}}$ correctly known at the receiver.

5.1.2 channel

The multipath channel with its coefficients $\mathbf{h} = [h_0,\ h_1, \cdots h_{L-1}]$ extending for a length L where h_i is the complex baseband coefficient of $i+1$ path. We considered a complex Gaussian channel with circularly symmetric nature. we assume that all the coefficients of multipath components are uncorrelated with each other. The received signal $\mathbf{y_{cp}}$ is given as,

$$\mathbf{y_{cp}} = \mathbf{h} * \bar{\mathbf{x}} + \mathbf{w}. \tag{5.2}$$

where $\mathbf{y_{cp}}$ is of dimension $N_{cp} + N + L - 1$ and $\mathbf{w}$ is the AWGN channel with its variance of σ_w^2.

5.1.3 Receiver

At the receiver, to remove the effect of multipath components the first N_{cp} and last $L-1$ samples are removed from the received data packet, i.e, $\mathbf{y} = \mathbf{y}_{cp}(N_{cp}+1 : N_{cp}+MK)$ is selected for performing the demodulation. we utilize ZF receiver for data detection which is mathematically formulated as,

$$\mathbf{B} = (\mathbf{A^H A})^{-1}\mathbf{A^H}, \tag{5.3}$$

Here $\mathbf{B}$ is the GFDM demodulation matrix. Finally, the demodulated output is given by,

$$\mathbf{Z} = \boldsymbol{\phi}^* \cdot \mathbf{By}, \tag{5.4}$$

where $\mathbf{y}$ in (5.4) is the data after the removing the guard interval. The $\boldsymbol{\phi}^*$ is computed in the receiver by using the transported SI.

5.1.4 Channel estimation

In order to perform channel estimation, N_p pilots are adjusted in the data vector before convolving with prototype filter. Let us represent the $\mathbf{H_p}$ as the estimated channel response of pilot symbols, $\mathbf{Z_p}$ shows the pilots affected by the channel and $\mathbf{x_p}$ are the pilots inserted at the transmitter. Then we can obtain the estimated channel as,

$$\begin{aligned}\mathbf{H_p} &= \mathbf{x_p^{-1}Z_p} \\ &= \left[\frac{Z_p(0)}{x_p(0)}, \frac{Z_p(1)}{x_p(1)} \cdots, \frac{Z_p(N_p-1)}{x_p(N_p-1)}\right].\end{aligned} \tag{5.5}$$

For computing the complete channel response by using the channel coefficients $\mathbf{H_p}$, we use the concept of linear interpolation. Hence, actual data symbols can be obtained in the receiver by equalizing the demodulated with the interpolated channel response in the frequency domain.

5.2 Proposed method

We can observe that the compulsion of SI transportation led to reduction the throughput efficiency and make the GFDM system displeasing for 5G applications. The

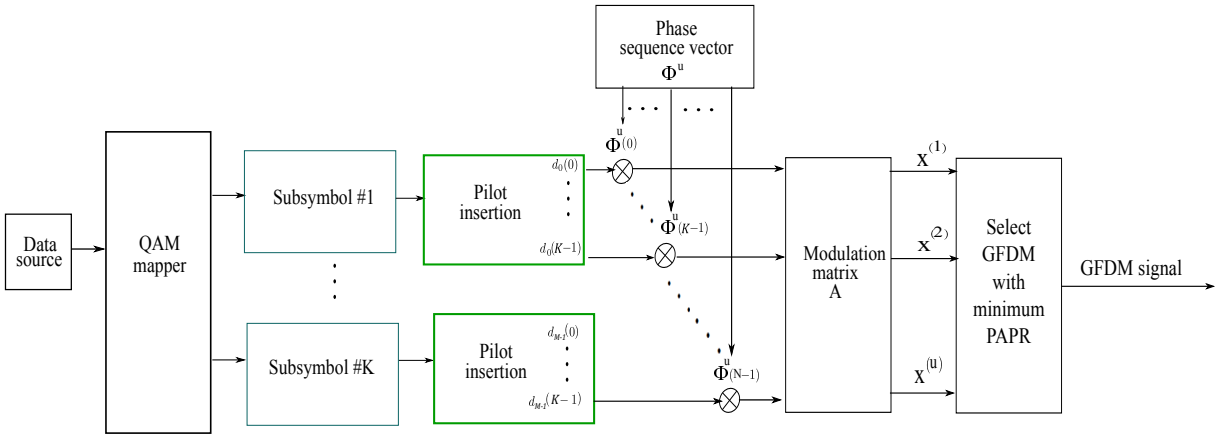

Figure 5.1: Modified GFDM-SLM modulator for the proposed method

fundamental principle of SI estimation for the proposed method is to use the pilots of the GFDM signal for performing joint SI and channel estimation. The pilots in the original GFDM system can be inserted with interleaving in practical systems for gaining the advantage of coherent detection. In the proposed method, we use the pilot symbols with even spacing in transmitter, where P is the space between the pilots. Hence, the total pilots in the GFDM symbol are $N_p = N/P$ and data will be present in $N - N_p$ indices. For instance, when $N_p = 2M$, on in the other way, let every subsymbol shall contain two pilots as shown in Figure. 5.1. This modification in the conventional SLM-GFDM architecture will provide us the opportunity to achieve the joint estimation. For the suggested equal pilot spacing for the subsymbols the arrangement in the data will be as,

$$\mathbf{d_m}(n) = \mathbf{d}(mM+n) = \begin{cases} \mathbf{d_m}(n_o) & = \mathbf{d}(mM+n_o) \\ \mathbf{d_m}(n_d) & = \mathbf{d}(mM+n_d). \end{cases} \tag{5.6}$$

Since we are considering two pilots for explaining the algorithm, let n_e and n_o denote the indices for the first and second pilots in each subsymbol and n_d is the data symbols. From (5.6), we use $\mathbf{d}$ and $\mathbf{d_m}$ interchangeably whenever required. The subsymbol data in its polar form can be represented as,

$$\mathbf{d_m}(n) = \mathbf{A_m}(n)\exp(j\theta_m[n]), \tag{5.7}$$

where $\mathbf{A_m}$ and θ_m are the magnitude and phase components of $\mathbf{d_m}$.

This polar representation is shown to utilize a common phase component in the process of SLM technique for all the subcarriers of a subsymbol. In other words, in the

proposed method we will update the phase on a subsymbol randomly by optimization. To detail, we perform phase modulation on subsymbol-to-subsymbol basis instead of sample-to-sample basis. By using the idea of SLM technique, the pilot subsymbols by the suggested arrangement on every subsymbol are rotated to minimize the PAPR of the GFDM block. This phase modulated subcarriers will need at least two pilots among them and a different phase can be assigned for different subsymbols. Since the pilots are equispaced, the locations of the pilots are easily known at the receiver. This will aid us in subsymbol based demodulation and hence justifying the concept of joint SI and channel estimation. Since we are using the pilots associated with channel estimation for performing the SI estimation we can achieve this without compromise in PAPR reduction. The only difference with the traditional method is that, the applied phase sequences are to be restricted to have same phase shift for all set of subcarriers in a subsymbol. Therefore, the proposed method effectively handles the main disadvantage of SLM technique mentioned in the previous section i.e., compulsion of SI transmission. Improper SI detection not only effects the PAPR reduction gain but also results in erroneous data detection. The central novelty of the proposed method lies in taking the advantage of flexible nature of GFDM to address the issues associated with traditional SLM technique. The main advantages of the proposed method lie in its effectiveness, as it does not require any SI estimation at the receiver side which will be described in detail below

5.2.1 Transmitter

For implementing the proposed method, we consider a subsymbol m will have the phase sequence vector represented as Θ_m. Just like the traditional method, the phase sequence vector is obtained by optimizing Θ_m from 0 to π. Hence, before modulation, data on each subsymbol is multiplied with the optimized $\hat{\Theta}_m$ as,

$$\begin{aligned}\lambda_{\mathbf{m}}(n) &= \mathbf{d_m}(n)\exp(\hat{\Theta}_m) \\ &= \mathbf{A_m}(n)\exp(j\theta_m[n] + \hat{\Theta}_m).\end{aligned} \tag{5.8}$$

From (5.8), it can be inferred that all the subcarriers in m^{th} subsymbol are with the identical phase value. For the optimized phase sequence vector, the GFDM signal

is obtained by multiplying the $\lambda_{\mathbf{m}}$ with the modulation matrix $\mathbf{A}$. As in the traditional method all the operations like adding CP must be performed.

5.2.2 Receiver

The received vector $\hat{\mathbf{Z}}$ after performing product with the demodulation matrix can be simplified as,

$$\begin{aligned}\hat{\mathbf{Z}}_{\mathbf{m}}(n) &= \mathbf{H}_{\mathbf{m}}(n)\lambda_{\mathbf{m}}(n) + \mathbf{w}_{\mathbf{m}}(n) \\ &= \mathbf{H}_{\mathbf{m}}(n)\mathbf{d}_{\mathbf{m}}(n)\exp(\hat{\Theta}_m) + \mathbf{w}_{\mathbf{m}}(n).\end{aligned} \tag{5.9}$$

The $\mathbf{H}_{\mathbf{m}}(n)$ is the channel attenuation of the subsymbol m, which can be termed as a channel applied on every sample of a subsymbol. The indices n_e, n_o of the first and second pilot in every subsymbol while the n_d is used for the data symbols. For $N_p = 2M$, the subchannel estimate of pilots $\hat{\mathbf{H}}_{\mathbf{m}}(n_e)$ and $\hat{\mathbf{H}}_{\mathbf{m}}(n_0)$ for a subsymbol m can be evaluated as,

$$\begin{aligned}\hat{\mathbf{H}}_{\mathbf{m}}(n_e) &= \hat{\mathbf{Z}}_{\mathbf{m}}(n_e)/\mathbf{d}_{\mathbf{m}}(n_e) \\ &= \left(\mathbf{H}_{\mathbf{m}}(n_e)\mathbf{d}_{\mathbf{m}}(n_e)\exp(\hat{\Theta}_m) + \mathbf{w}_{\mathbf{m}}(n_e)\right)/\mathbf{d}_{\mathbf{m}}(n_e) \\ &= \mathbf{H}_{\mathbf{m}}(n_e)\exp(\hat{\Theta}_m) + \hat{\mathbf{w}}_{\mathbf{m}}(n_e),\end{aligned} \tag{5.10}$$

where $\hat{\mathbf{w}}_{\mathbf{m}}(n_e) = \mathbf{w}_{\mathbf{m}}(n_e)/\mathbf{d}_{\mathbf{m}}(n_e)$ is shows the effect of noise. On the next pilot this operation would be simplified as,

$$\begin{aligned}\hat{\mathbf{H}}_{\mathbf{m}}(\mathbf{n_o}) &= \hat{\mathbf{Z}}_{\mathbf{m}}(n_o)/\mathbf{d}_{\mathbf{m}}(n_o) \\ &= \left(\mathbf{H}_{\mathbf{m}}(n_o)\mathbf{d}_{\mathbf{m}}(n_o)\exp(\hat{\Theta}_m) + \mathbf{w}_{\mathbf{m}}(n_o)\right)/\mathbf{d}_{\mathbf{m}}(n_o) \\ &= \mathbf{H}_{\mathbf{m}}(n_o)\exp(\hat{\Theta}_m) + \hat{\mathbf{w}}_{\mathbf{m}}(n_o),\end{aligned} \tag{5.11}$$

where $\hat{\mathbf{w}}_{\mathbf{m}}(n_o) = \mathbf{w}_{\mathbf{m}}(n_o)/\mathbf{d}_{\mathbf{m}}(n_o)$. At high SNR after neglecting the effect of subchannel coefficients can be reduced as,

$$\begin{aligned}\mathbf{H}_{\mathbf{m}}(n_o) &\approx \hat{\mathbf{H}}_{\mathbf{m}}(n_o)\exp(\hat{\Theta}_m) \\ \mathbf{H}_{\mathbf{m}}(n_e) &\approx \hat{\mathbf{H}}_{\mathbf{m}}(n_e)\exp(\hat{\Theta}_m).\end{aligned} \tag{5.12}$$

SI cancellation

We found the subchannel coefficients in the previous section. Now we further utilize one the channel estimates obtained in (5.12) for cancelling the Θ_m of every subsymbol. We denote $\mathbf{H_m}(n_e)$ of a subsymbol for performing the data estimation as follows,

$$\begin{aligned}\mathbf{Z_m}(n_d) &= \hat{\mathbf{Z}}_\mathbf{m}(n_d)/\mathbf{H_m}(n_e) \\ &= \frac{(\mathbf{H_m}(n_d)\mathbf{d_m}(n_d)\exp(\hat{\Theta}_m) + \mathbf{w_m}(n_d))}{(\mathbf{H_m}(n_e)\exp(\hat{\Theta}_m) + \hat{\mathbf{w}}_\mathbf{m}(n_e))}.\end{aligned} \tag{5.13}$$

After neglecting the noise by assuming high SNR the detected data $\mathbf{Z_m}(n_d)$ reduces into,

$$\begin{aligned}\mathbf{Z_m}(n_d) &\approx \frac{\mathbf{H_m}(n_d)}{\mathbf{H_m}(n_e)}\mathbf{d_m}(n_d) \\ &\approx \mathbf{R_m}(n_d)\mathbf{d_m}(n_d).\end{aligned} \tag{5.14}$$

The approximation in (5.14) is justifiable and the term $\mathbf{R_m}(n_d)$ is representing the normalized sub channel with respect to the n_e pilot of the subsymbol. If we can determine $\mathbf{R_m}(n_d)$ where n_d is representing the data symbols we can obtain the data symbols. The $\mathbf{R_m}$ at n_e index i.e., $\mathbf{R_m}(n_e)$ is $\frac{\mathbf{H_m}(n_e)}{\mathbf{H_m}(n_e)}$ which can be considered to unity at high SNR. The $\mathbf{R_m}$ in the case of n_o indexed pilot $\mathbf{R_m}(n_o)$ of every subsymbol shall be of the form,

$$\begin{aligned}\mathbf{R_m}(n_o) &= \frac{\mathbf{H_m}(n_e)\exp(\hat{\Theta}_m) + \mathbf{w_m}(n_e)}{\mathbf{H_m}(n_o)\exp(\hat{\Theta}_m) + \mathbf{w_m}(n_o)} \\ &\approx \frac{\mathbf{H_m}(n_e)}{\mathbf{H_m}(n_o)}.\end{aligned} \tag{5.15}$$

We can observe from the above equation (5.14) that SI cancellation is inherently present in the proposed method since Θ_m is unique for subsymbol. We can also observe that SI cancellation is present in both the numerator and denominator. Hence, the advantage of the proposed method lies in data estimation without either SI transmission or SI estimation.

Channel mitigation

Another important claim in the proposed method is the channel mitigation. It is well known that the traditional methods perform the channel estimation by interpolating the channel coefficients obtained from pilot symbols. The proposed method alleviates the

effect of $\mathbf{R_m}(n_d)$ of each subsymbol. Like traditional method, $\mathbf{R_m}(n_d)$ is obtained by interpolation between the subchannel at the both pilots $\mathbf{R_m}(n_e)$ and $\mathbf{R_m}(n_o)$ corresponding to the n_e and n_o indices of a subsymbol m which is denoted with $\hat{\mathbf{R}}_\mathbf{m}(n_d)$. The estimated data $\bar{\mathbf{Z}}_\mathbf{m}(n_d)$ can be given by,

$$\begin{aligned}\bar{\mathbf{Z}}_\mathbf{m}(n_d) &= \mathbf{Z_m}(n_d)/\hat{\mathbf{R}}_\mathbf{m}(n_d) \\ &= \mathbf{R_m}(n_d)\mathbf{d_m}(n_d)/\hat{\mathbf{R}}_\mathbf{m}(n_d). \end{aligned} \tag{5.16}$$

The standard minimum Euclidean distance algorithm is implemented for QAM demodulation of data on every subsymbol. The estimated data can be given as,

$$\hat{\mathbf{d}}_\mathbf{m}(n_d) = \min_{c_q \in \mathbb{Q}} |\bar{\mathbf{Z}}_\mathbf{m}(\mathbf{n_d}) - c_q|^2, \tag{5.17}$$

where $\mathbb{Q}$ is the set containing the constellation points c_q for $1 \leq q \leq Q$. $\hat{d} \in \mathbb{Q}$ is denoting the estimated data. The effectiveness of the proposed algorithm lies in choosing the value of N_p whose increment provides better channel estimation accuracy.

5.2.3 Results and discussion

The setup developed in the 1.8 is used for validating the concept of joint SI and channel estimation. The steps of implementation are shown in Figure (5.2).

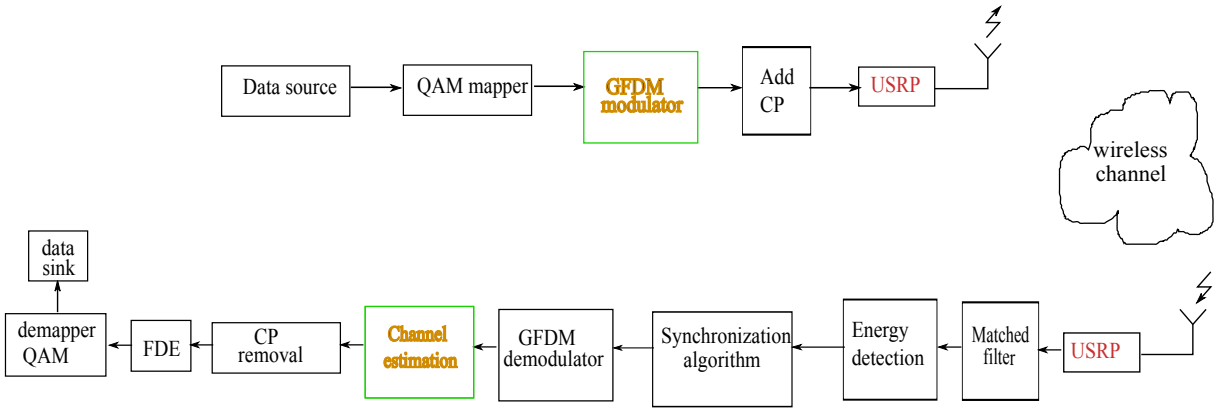

Figure 5.2: Block diagram of the GFDM transceiver system with National instrument USRPs

Initially, we present the simulated results which shall be validated using the developed test bed. The performance of the GFDM system in terms of PAPR is generally

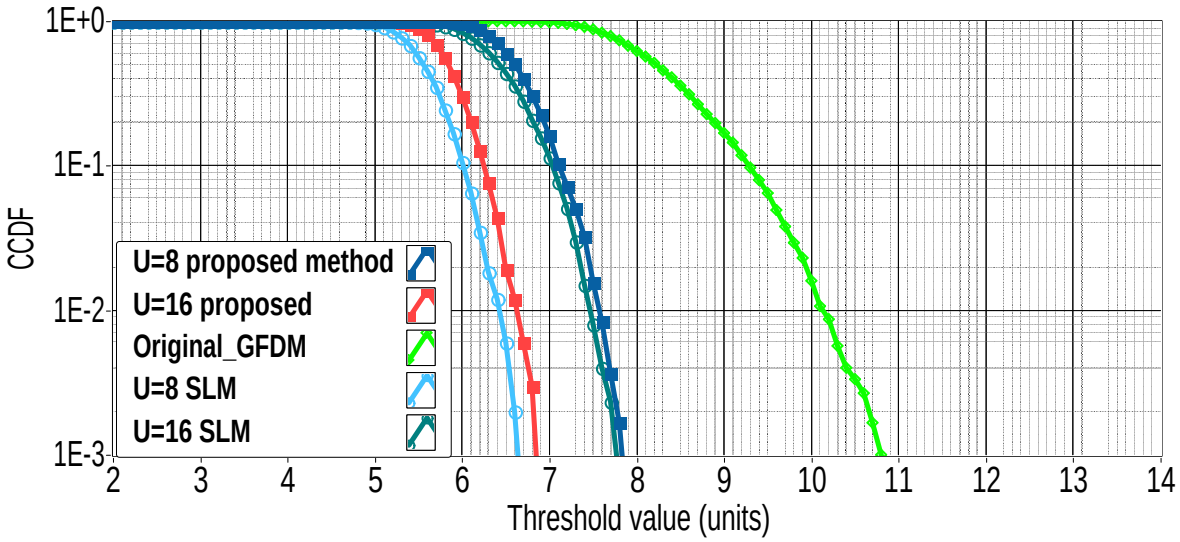

Figure 5.3: CCDF curve for $N_p = UM/4$

done by computing it's complementary cumulative distribution function (CCDF). CCDF is a measure of the probability of a PAPR value greater than a threshold. We use U for showing different number of phase vector vectors in a GFDM symbol and the CCDF curve obtained in simulations by comparing with the conventional SLM scheme is illustrated in Figure. 5.3. It is understandable from the figure that the PAPR performance of the proposed method is slightly worse than the traditional SLM scheme since the number of pilot symbols are restricted to $2M$. Additionally, when U is increased from 8 to 16, significant PAPR reduction can be observed. Even when $N_p = 2M$, the performance of the proposed method is much better than the original GFDM system. At a threshold CCDF of 10^{-3}, the conventional GFDM system has a huge PAPR of 10.8 dB while, SLM technique for $U = 8$ and $U = 16$ have a PAPR of 7.7 dB and 6.6 dB, whereas, the proposed technique results in a PAPR of 7.8 dB and 6.8 dB at $U = 8$ and $U = 16$ respectively. On comparison with conventional GFDM system, PAPR is reduced significantly by an amount of 3.2 dB. In addition, upon increasing the number of phase sequences from $U = 8$ to $U = 16$, PAPR reduction of around 1.1 dB is observed. Figure. 5.4, clearly depicts the advantage of increasing the number of pilot symbols from $N_p = 2M$ to $N_p = 4M$ as there is a significant reduction in PAPR in the proposed technique. But, this is at the cost of reduction in data efficiency. However, the obtained results closely follows the SLM technique.

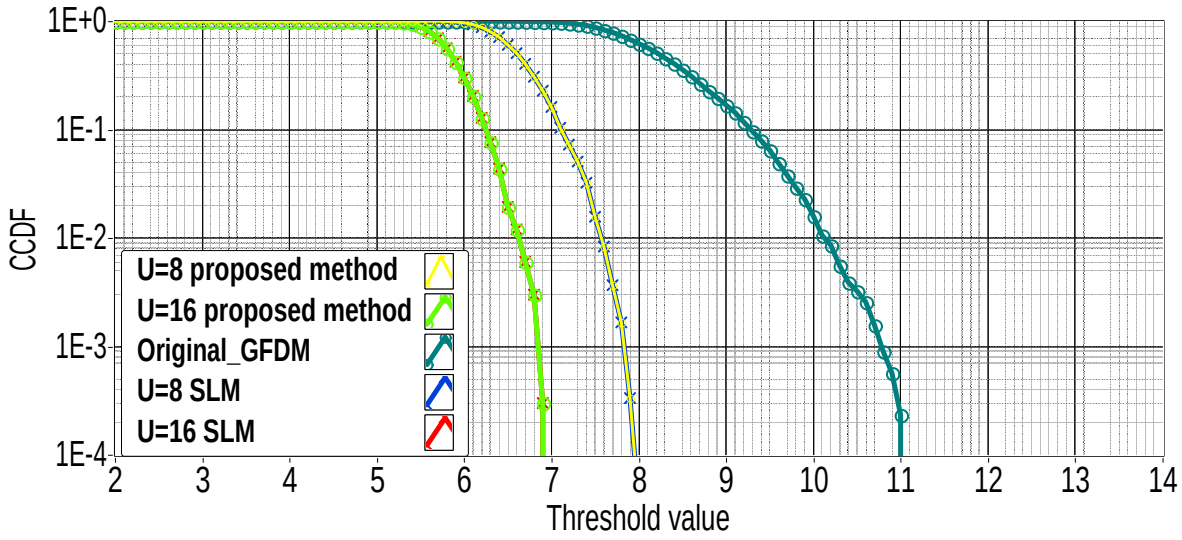

Figure 5.4: CCDF curve for $N_p = UM/2$

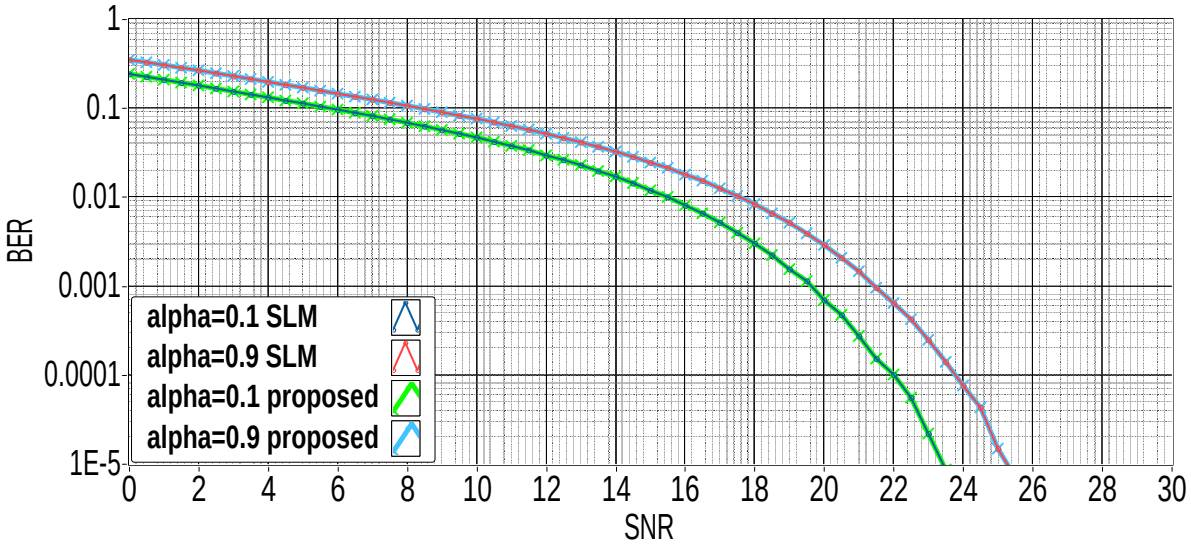

Figure 5.5: BER of traditional and proposed method in GFDM system in multipath channels

The reason behind the proposal of pilot aided based PAPR reduction methodology is to obtain not only PAPR reduction but also to effectively estimate the multipath time varying channel. So, in this regard, simulations are carried to obtain the performance of the system upon imposing channel estimation techniques. This is shown in Figure. 5.5, upon increasing the roll off factor alpha from 0.1 to 0.9 the BER performance deteriorates. It can be inferred from the results that, though GFDM is fundamentally non-orthogonal in nature the improvement in BER by decreasing alpha is due to the fact of improvement

in orthogonality. This improvement in BER may require a sacrifice in the achievable PAPR as depicted from Figure. 5.5, where the proposed method produce identical BER performance without requirement of any SI estimation. As a consequence, the proposed method may be considered as an effective alternative method to the conventional SLM-GFDM with the benefit that there is neither SI transmission nor SI detection.

The transmitted signal is captured by RX USRP as a constant stream of data from the air. RX USRP discards the incoming samples until the start of the data packet is detected by the energy detection algorithm, i.e., initial symbol detection will be performed after a reception of significant energy as shown in Figure. 5.2. The GFDM frame is prepended with an windowed preamble to perfrom coarse frequency correction by schimdl and cox algoritm to complete the synchronization [41]. The preamble in the header of the packet can be removed after correction of the initial coarse frequency offset. The indoor RF channel is often assumed to have slowly time varying nature. The concept of slow time varying means, the channel doesn't change during the real time measurement of its impulse response. The intention of authors in showing real time response is, the channel response is not destroyed by the proposed algorithm and it effectively reduces the PAPR performance as presented in simulation results. we have used correlation algorithm for determining the real time channel response [41]. Experimental results are analysed in terms of OOB control and estimated channel response using the developed testbed. These results only validate the proposed algorithm: the concept of joint data detection and PAPR reduction in indoor channel environments. The transmitted spectrum is shown in Figure. 5.6 where a OOB radiation of -46 dB has been observed. This advantage is achieved because of usage of prototype filter which performs localization in time and frequency. As a result, every subcarrier we would experience reduction in egress noise. This makes GFDM adaptable in scrambled spectrum applications like cognitive radio which was the major concern in OFDM systems [72]. The Figure. 5.8 depicts the received spectrum after enforcing traditional synchronization and proposed channel estimation algorithm suggest that the system performance is not destroyed. Despite of the non-orthogonal nature of GFDM, the received spectrum has not lost its shape, hence validating the effectiveness of the proposed algorithm. However, the spectrum is diminished in amplitude and frequency due to the indoor channel variations. The frequency response of the channel estimated by interpolation of the subchannels is depicted in Figure. 5.7 . The observed channel is

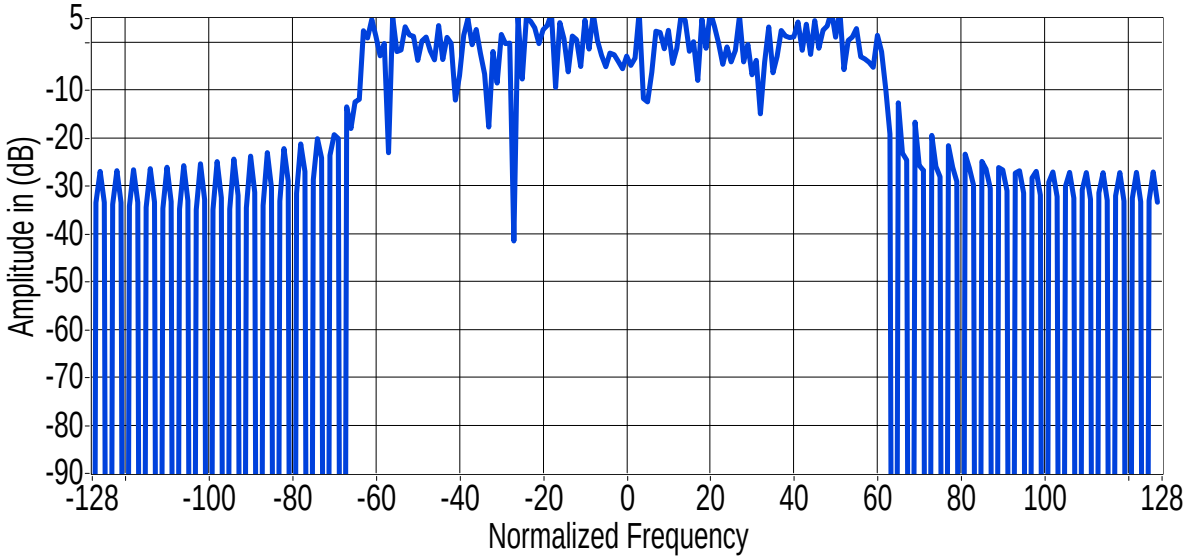

Figure 5.6: Transmitted signal spectrum from transmitter USRP

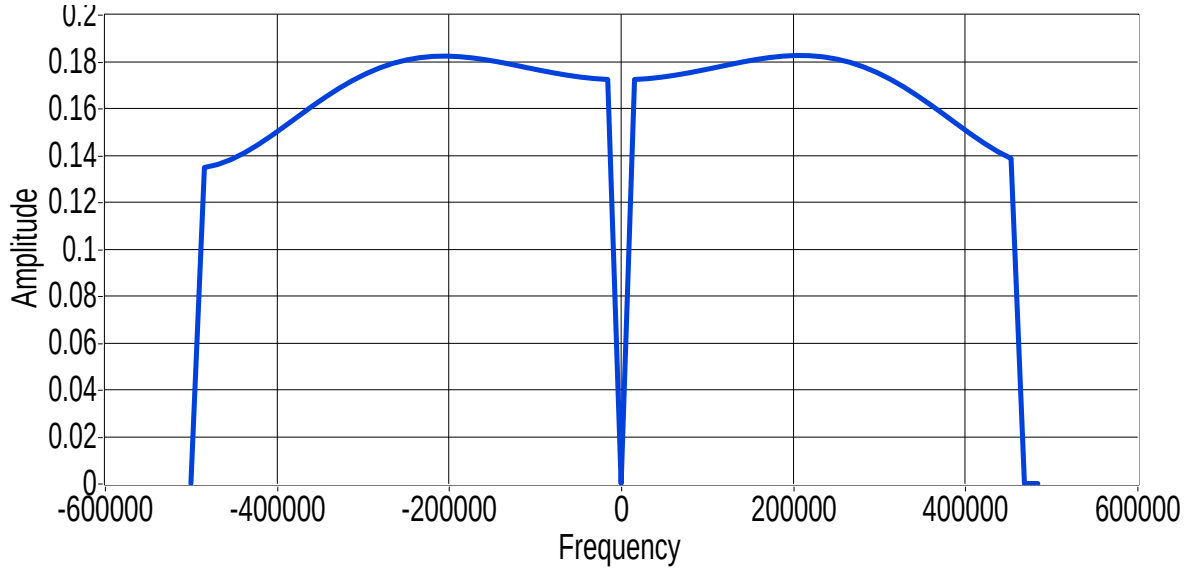

Figure 5.7: Indoor channel response using pilots

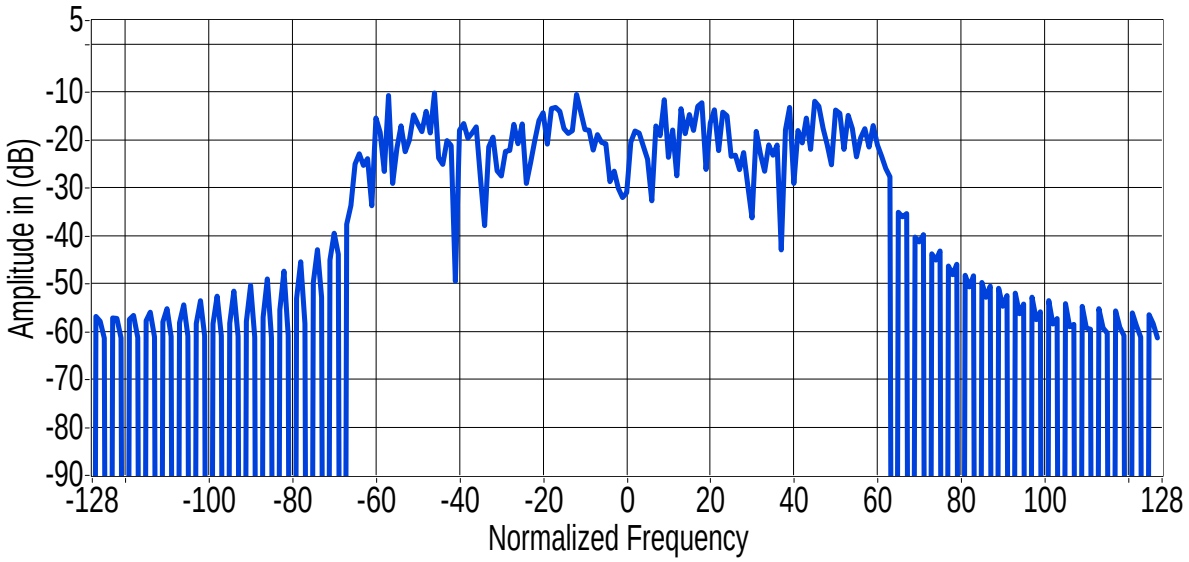

Figure 5.8: Received spectrum from receiver USRP

obtained when signal of frequency 2.4Ghz and the attenuation in magnitude introduced by indoor channel are measured as a function of frequency. We evidenced a bandpass nature over a bandwidth of range 50MHz. This primarily occurs due to reason that indoor channel exhibit a narrow band nature with flat frequency response.

5.3 Proposed method 2

The choice of phase sequence vector makes a significant impact on achievable PAPR reduction gain. In our first contribution of this chapter, SLM technique was implemented by using phase sequences which are randomly generated from the set $\{+1, +j\}$. The contribution of this method is to remove the need of SI transmission and further improve the PAPR reduction capability and bandwidth efficiency for SLM-GFDM system. To achieve this goal, we introduce the usage of the rows of normalised Riemann matrices as the phase sequence vectors for traditional SLM technique. The phase sequence in literature, often contain same magnitude but by using the rows of Riemann matrix we have some number of components with larger magnitude. This will aid in nullifying unwanted peaks and can facilitate better PAPR reduction gain. The optimal row vector of Riemann matrix is superimposed on the original data signals to avoid the SI transmission. To validate the proposed concept of PAPR reduction with no SI transmission, authors have

implemented a real time prototype of the GFDM system using USRP. After performing channel estimation, the superimposed Riemann sequence can be removed at the receiver which will also serve as SI. By proper selection of the power allocation, the suggested method provides PAPR performance without disturbing the demodulation procedure. The received spectral response from USRP authenticate the the proposed method by showing a good agreement with simulations.

The u^{th} alternative for GFDM system is obtained by using the resultant vector obtained after multiplication between phase vector $\phi^{(u)}$ with $\mathbf{d}$ as the data vector. The obtained GFDM signal is denoted as $\mathbf{x}^u$. We propose the utilization of the rows of Riemann matrix as $\phi^{(u)}$ for the traditional SLM scheme. The Riemann matrix can be simply obtained by removing the first row and column from the matrix defined as,

$$\begin{aligned} S(i,j) =& i-1 \qquad \text{if i divides j} \\ =& -1 \qquad \text{otherwise} \end{aligned} \tag{5.18}$$

The size of Riemann matrix is $N \times N$ and it can be normalised by using N to obtain the requires set of phase sequence vectors. Consider an example for $N = 4$ system where in, the 5×5 matrix $\mathbf{S}$ is,

$$S_{5\times5} = \begin{bmatrix} 0 & -1 & -1 & -1 & -1 \\ 1 & 1 & -1 & -1 & -1 \\ 2 & -1 & 2 & -1 & -1 \\ 3 & 3 & -1 & 3 & -1 \\ 4 & -1 & -1 & -1 & 4 \end{bmatrix} \tag{5.19}$$

The next step is to remove the first row and first column of the matrix as below,

$$S_{4\times4} \begin{bmatrix} 1 & -1 & -1 & -1 \\ -1 & 2 & -1 & -1 \\ 3 & -1 & 3 & -1 \\ -1 & -1 & -1 & 4 \end{bmatrix} \tag{5.20}$$

By using the proposed method for GFDM system, the phase sequence vectors can be

given as,

$$\begin{aligned}\phi^{(1)} &= [1 \quad -1 \quad -1 \quad -1]/4 \\ \phi^{(2)} &= [-1 \quad 2 \quad -1 \quad -1]/4 \\ \phi^{(3)} &= [3 \quad -1 \quad 3 \quad -1]/4 \\ \phi^{(4)} &= [-1 \quad -1 \quad -1 \quad 4]/4\end{aligned} \tag{5.21}$$

The size of Riemann matrix is $N \times N$ and it can be normalised by using N to avoid the loss in generality. In traditional phase sequence, all the elements are of same magnitude but the utilized Riemann matrix will have a small number of components with larger magnitude. This will help to nullify the peak and to obtain better PAPR reduction gain. In the SLM scheme, the absorbing point is, all the generated U vectors show the original GFDM symbol but every symbol is independent of each other. Let $\bar{\boldsymbol{\phi}}_{\mathbf{r}}(\mathbf{n})$ represent the vector with minimum PAPR among all the alternatives and its GFDM signal is represented with $\bar{\mathbf{x}}$ i.e., mathematically,

$$\bar{\mathbf{x}} = \arg\min \mathrm{PAPR}(\mathbf{x}^{\mathbf{u}}) \tag{5.22}$$

The optimized vector $\bar{\mathbf{x}}$ is also a GFDM signal and hence can be represented as,

$$\bar{\mathbf{x}} = \mathbf{A} \times \bar{\boldsymbol{\phi}}_{\boldsymbol{r}}(\boldsymbol{n}) \times \mathbf{d}(\mathbf{n}) \tag{5.23}$$

From (5.23) we can clearly understand, the successful data recovery is feasible by transporting $\bar{\boldsymbol{\phi}}_{\boldsymbol{r}}$ to the receiver. The optimized Riemann matrix row vector $\bar{\phi}_{\mathbf{r}}$ always require an extra SI which may require an extra $\log_2 U$ bits as an payload in the packet before transmission. It is quite obvious that, the SI is not known precisely at both, the transmitter and receiver. In addition, the traditional phase sequences are generally random in nature and hence it is mandatory to send the correct SI to the receiver side. Utmost care in SI transmission by using channel coding will be necessary since incorrect identification of SI information may force the complete GFDM block into error. We know Riemann matrix is a having a particular shape and hence can be received easily in multipath channel environments. The PAPR values of GFDM signals is highly related to autocorrelation of input sequences. Greater the autocorrelation of input sequences lower the side lobe value of its spectrum. The proposed SLM uses Riemann Matrix which has lower autocorrelation among them due to varying amplitudes when compared with traditional phase sequence

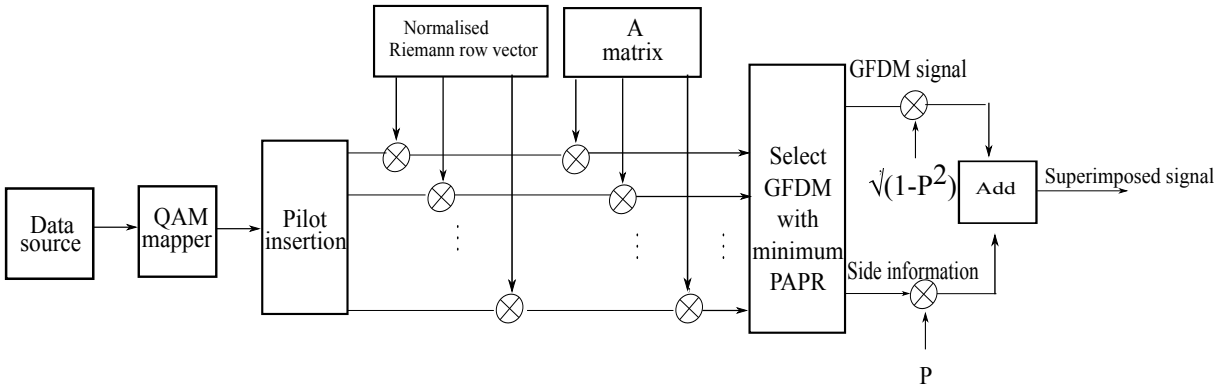

Figure 5.9: Block diagram of the GFDM-SLM modulator for proposed method

vectors. In addition, for achieving bandwidth efficiency without any compromise in PAPR reduction and BER performance, SI is superimposed with the GFDM modulated data before transmission. However, scaling the information is required in order to obtain a neat spectral response as it will be discussed in the result section. The rows of the Riemann matrix $\mathbf{S}$ are utilized as set as phase sequences. The phase sequence should be added as,

$$= P\bar{\boldsymbol{\phi}}_{\boldsymbol{r}} + \sqrt{(1-P^2)}\mathbf{x}^{(\mathbf{u})} \tag{5.24}$$

Here P is the power allocation factor. Ideally one want the power factor P to be very low since the maximum power must be provided to GFDM signal. For implementation, GFDM system is having good performance without any requirement of special hardware at the receiver when the P value is chosen between 0 to 0.1. Therefore, by choosing power appropriately, the phase sequences generated using Riemann matrix can effectively decrease the out of band radiation of GFDM system by omitting the concept of SI transmission as shown in Figure 5.9. However, channel estimation must be used to reinstate the transmitted signals in the receiver. After superimposing, we need to multiply the phase sequences $\bar{\boldsymbol{\phi}}_{\boldsymbol{r}}$ to obtain alternative signal $\mathbf{x}^{(\mathbf{u})}$ for $u = 1 \cdots U$. Hence, by using the proposed method over the traditional SLM scheme improves PAPR reduction and bandwidth efficiency. There is no additional complexity in the proposed method since it used only addition to obtain the superimposed signal. On contrary, the proposed phase sequence vector is having irregularity in the amplitude which may lead to spikes in the received response of the USRP as it will be detailed in the results section. The presence of spike reduces the potency of the traditional receiver since it is designed considering the multipath channels. Here P is the power allocation factor. Ideally one want the power factor P to be very low since the maximum power must be provided to GFDM signal. For

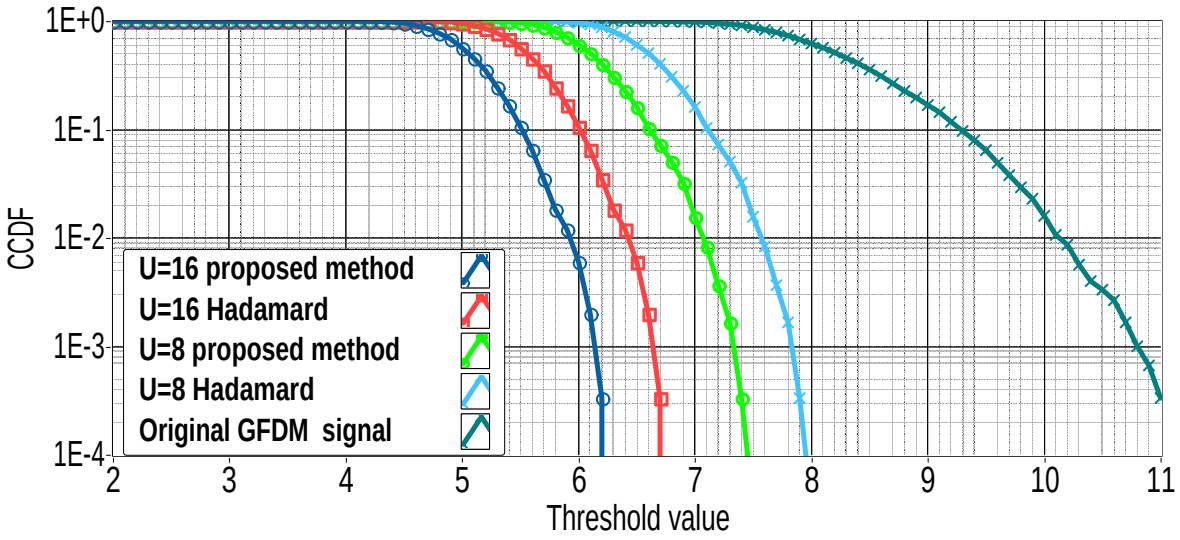

Figure 5.10: CCDF curve for comparison between traditional and proposed method

implementation, GFDM system is having good performance without any requirement of special hardware at the receiver when the P value is chosen between 0 to 0.1. Therefore, by choosing power appropriately, the phase sequences generated using Riemann matrix can effectively decrease the out of band radiation of GFDM system by omitting the concept of SI transmission as shown in Figure 5.1. However, channel estimation must be used to reinstate the transmitted signals in the receiver. After superimposing, we need to multiply the phase sequences $\bar{\boldsymbol{\phi}}_{\boldsymbol{r}}$ to obtain alternative signal $\mathbf{x}^{(\mathbf{u})}$ for $u = 1 \cdots U$. Hence, by using the proposed method over the traditional SLM scheme improves PAPR reduction and bandwidth efficiency. There is no additional complexity in the proposed method since it used only addition to obtain the superimposed signal.

5.3.1 Results and discussion

The different number of phase vector used for generation of alternative GFDM symbols is represented by U and the simulation results for the proposed method is compared with the existing Hadamard scheme as illustrated in Figure 5.10. For meaningful comparison, the Hadamard sequence and proposed Riemann sequence are generated by using similar parameters. From this figure it is clearly evident that, PAPR of the proposed method is very low when compared with Hadamard phase sequence vector because of presence of some number of components with larger magnitude. This will nullify unwanted

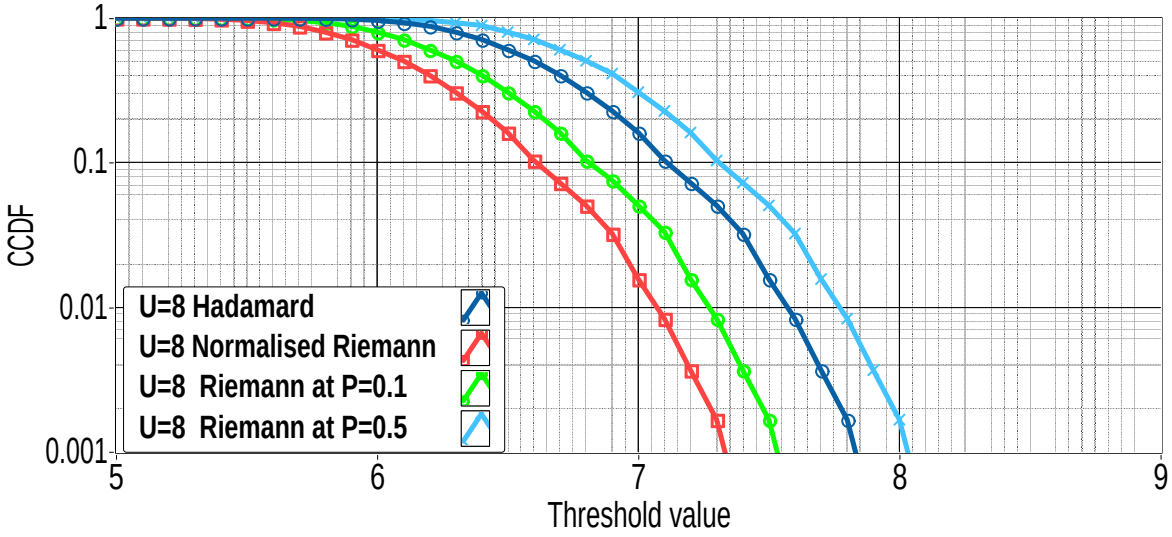

Figure 5.11: CCDF curve by varying power allocation to SI

peaks and can facilitate better PAPR reduction gain. Furthermore, we can observe the increase in the number of different phase sequences U from 8 to 16 provides a remarkable improvement in PAPR reduction gain. For instance, at a fixed threshold CCDF of 10^{-3}, the traditional GFDM system is having a huge PAPR of 10.8 dB while, the SLM using Hadamard coded sequence is having a PAPR of 7.8 dB and 6.6 dB for $U = 8$ and $U = 16$, while, the proposed technique has the PAPR values as 7.4 dB and 6.1 dB at $U = 8$ and $U = 16$ respectively. When compared with traditional GFDM system, PAPR is reduced by an amount of 4.7 dB. Another important observation is, upon increasing the U from 8 to 16, PAPR reduction of 1.3 dB is observed.

Figure 5.11 shows the PAPR curves at a fixed $U = 8$ by varying the power P on the superimposed transmitted signal. In Figure 5.10, we concluded that the presence of some components with larger amplitude contributed to better PAPR performance. However, when the SI with different amplitudes is superimposed on the transmitted vector the simulation results indicate an increase in PAPR due to its fundamental structure. Another important observation is, we can clearly observe there is an increment of 0.5 dB by increasing the power factor P from 0.1 to 0.5. The PAPR performance of the proposed method worsens than Hadamard phase sequences at higher P values.

Figure 5.12 illustrates the BER performance of the proposed superimposed GFDM-SLM system. We can observe the BER performance gets improved as the value of P

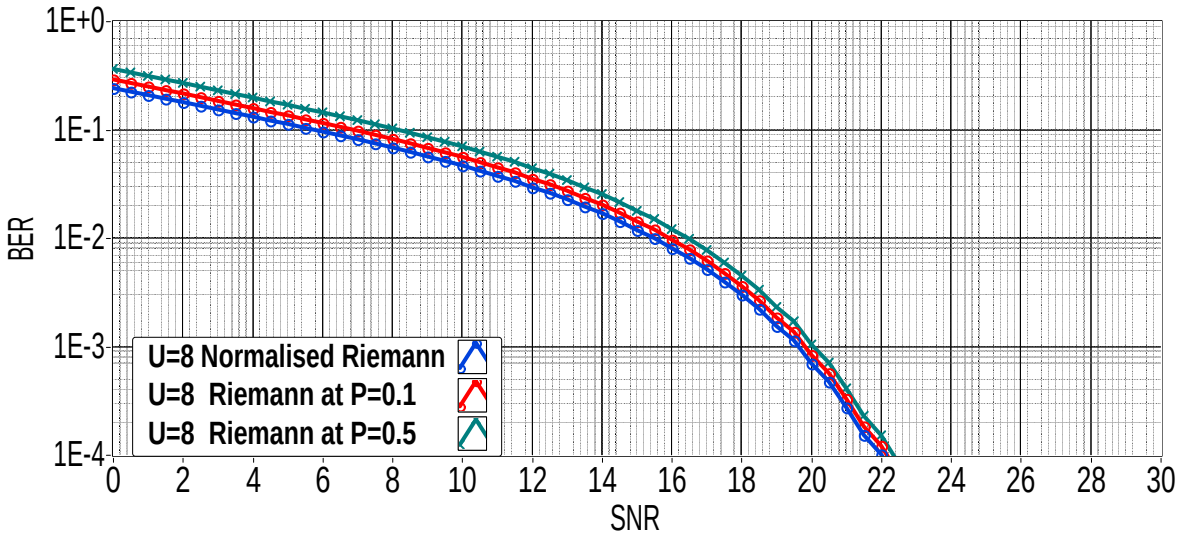

Figure 5.12: Effect of BER by varying power allocation to SI

increases. This advantage is achieved because increment in P leads to better SI estimation. The suggested scheme can achieve better BER than the traditional system using Hadamard phase sequence. Another reason for better BER is, existence of pattern in the proposed phase sequence vector. Hence, the value of P creates a scenario trade off between achievable PAPR and BER performance.

The superimposed signal is received in Rx USRP as a data stream in indoor channel environments. The Rx USRP abandon the samples until a appreciable energy is identified by using detection algorithm, i.e., STO estimation will be implemented as a first step as discussed in [73]. The windowed preamble appended in the header is utilized to perform CFO correction [73]. Later the channel impairments are equalised by estimating channel response using same pilots as presented in [55]. Experimental outcomes are examined in terms of spikes and OOB control in the received spectrum from the implemented test bed. These results are the proof of implementation of concept: superimposed SI transmission for GFDM-SLM system in indoor channel environments. The received spectrum with perfect SI estimation is shown in Figure 5.13 where a OOB radiation of 46 dB with no spikes can been observed. The prototype filter used will perform circular convolution which lead to localization in both time and frequency. This scenario lead to reduction in egress noise to achieve spectral response.

The received spectrum at $P = 1$, $P = 0.5$ and $P = 0.1$ are depicted in Figure 5.14,

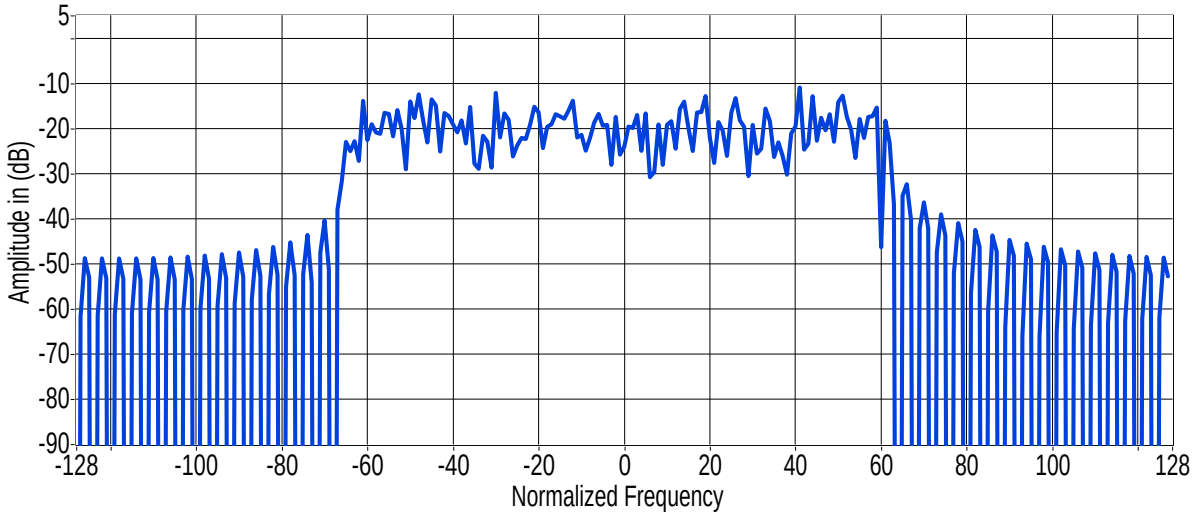

Figure 5.13: Received spectrum with perfect SI transmission

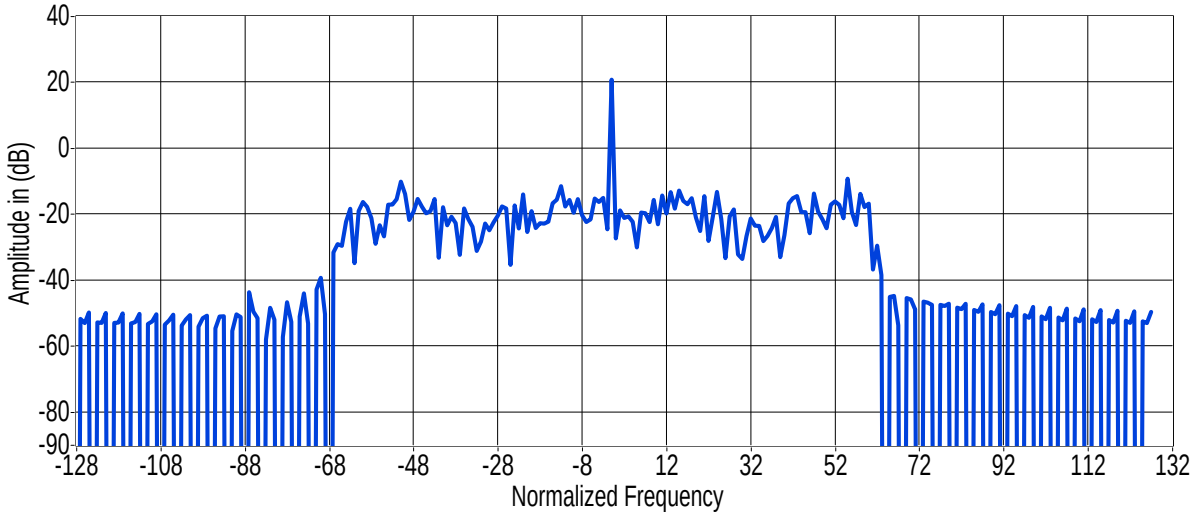

Figure 5.14: Received spectrum with P=1

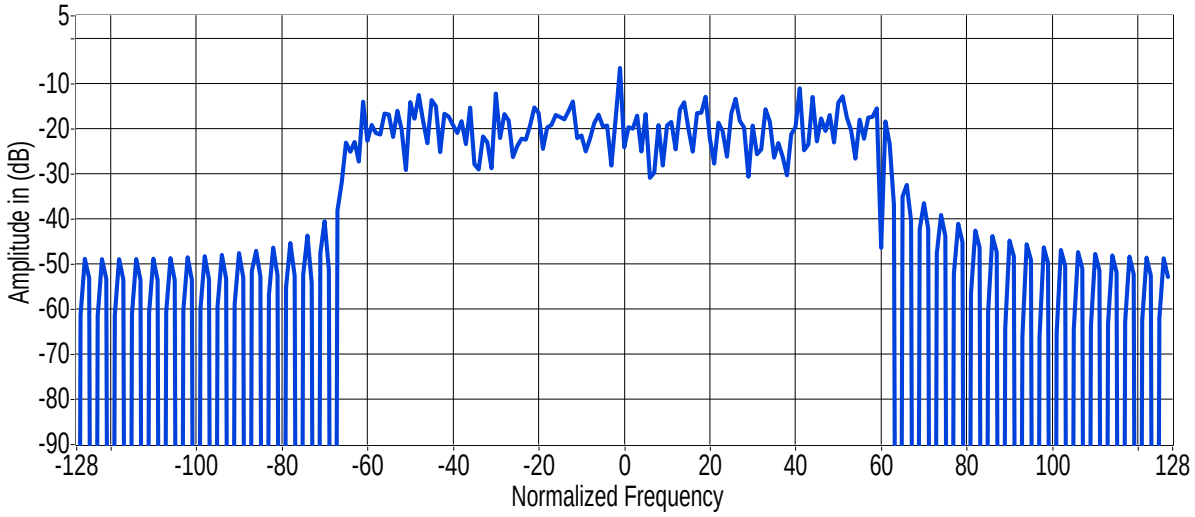

Figure 5.15: Received spectrum with P=0.5

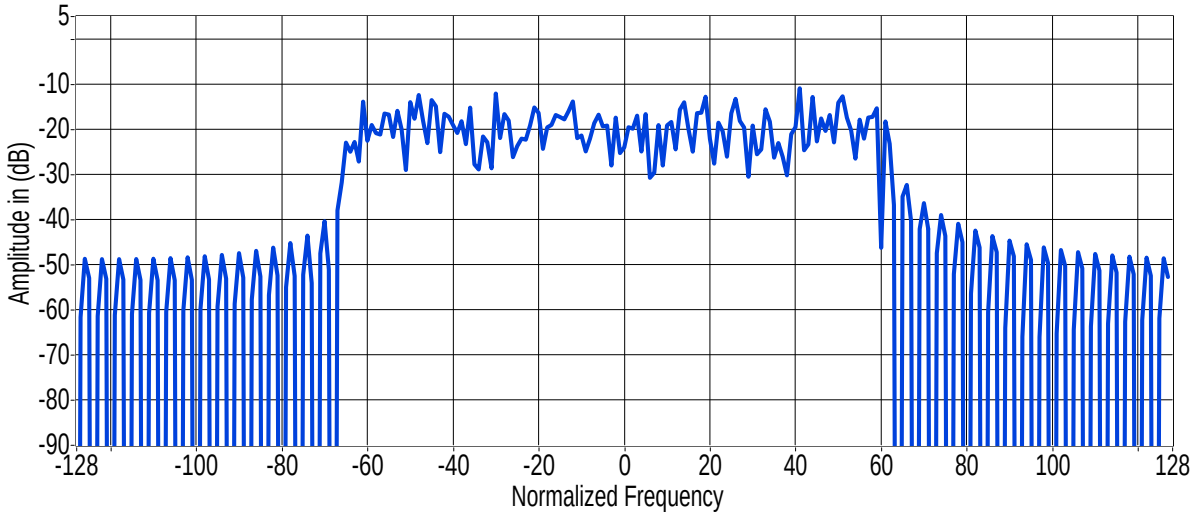

Figure 5.16: Received spectrum with P=0.1

Table 5.1: Real time results for Superimposed GFDM-SLM system

P value	**SNR=20dB**	spike(dB)	**SNR=10dB**	spike(dB)
0.05	0.003962	-20	0.046746	-20.8
0.1	0.004755	-14	0.0560953	-14.6
0.5	0.00594375	20	0.0701191	20.2

5.15 and 5.16 receptively. We can clearly observe a high peak occurs when the SI power is equal to the power of GFDM signal. This occurs due to the irregularity present in the superimposed SI. Hence, the receiver needs to use extra hardware in order to compensate these spikes. However, we can observe as P value decreases the received spectral response gradually approaches the ideal response in Figure 5.13. It can be inferred from previous discussion that as P decreases we achieve better PAPR and spectral response at the cost of BER. Hence, a good choice for trade-off would be to select P in the range of 0.05 to 0.1, where in, the proposed method outperforms the traditional method in terms of BER, PAPR and spectral response.The experimental values observed by varying SNR is tabulated in the Table 5.1. The PAPR values of GFDM signals is highly related to autocorrelation of input sequences. Greater the autocorrelation of input sequences lower the side lobe value of its spectrum. The proposed SLM uses Riemann Matrix will lower the autocorrelation of GFDM systems. It means that, applying the Riemann transformation to the modulation matrices helps in reduction of PAPR values.

5.4 Conclusion

This chapter of thesis investigates the concept of joint PAPR reduction and data decoding technique using subsymbol based phase modulation with a slight modification in the traditional SLM scheme. In comparison with the traditional SLM scheme the proposed method achieves identical performance at higher GFDM block sizes. In the receiver, the suggested subsymbol based data detection does not need any SI estimation. As a consequence, it eliminates the associated computational complexity. The simulation results show that the BER performance of the method is not degraded when compared with methods that use perfect SI estimation. For practical validation of the suggested

theory, an experimental setup is done using USRP RIO as a RF front end and Labview as software for baseband processing. The obtained experimental results suggest the significant reduction in out-of-band spectral leakage without disturbing the estimated channel response under indoor channel environments. Additionally, In this chapter, we propose the usage of normalised Riemann matrices as phase sequence vectors for traditional SLM technique without sending explicit SI to reduce PAPR in GFDM systems. The proposed modified SLM scheme has better PAPR performance than the traditional scheme. Additionally, SI is superimposed on to GFDM signals, in order to improve data rate for 5G applications. For the validation of suggested method, an experimental setup is done using USRP as a RF front end and Labview as software for baseband signal processing. The experimental results have shown significant reduction in OOB spectral leakage with appropriate power allocation to SI in the superimposed signal.

Chapter 6

Conclusions and future scope

6.1 Conclusions

ML estimation algorithm using pulse shaped multiple sets of identical data for correcting the time and frequency misalignments for GFDM systems is derived in the second chapter of the thesis. This is done to preserve the spectral advantage of the system. The CRLB for the frequency offset for an arbitrary pulse shape is also obtained. Simulations results obtained by modifying the preamble data in IEEE 802.11a standard, prove a little error floor due to noise enhancement in AWGN and multipath channels. The main advantage of this modified preamble occur in the real time results by reduction of slope and unwanted spikes in the spectrum characteristics. A new blind and simple time synchronization scheme based on the structure of UW-GFDM is proposed in the same chapter. The proposed method is not much dependent on SNR and mainly depends on the value of number of redundant subcarriers. We observed by increasing the number of redundant subcarriers we achieve effective synchronization and coding gain at the cost of PAPR and data efficiency. The intrinsic phase shift which has occurred between neighbouring samples of the oversampled GFDM symbol is exploited for offset estimation and correction. In noise less case we observed a straight forward reception whereas it leads to ML estimate of CFO in the presence of Gaussian noise. The real time results primarily focus on the time and spectral response using USRP hardware for indoor channel environment. The comparison of BER analysis between GFDM with RRC pulse shaping filter by varying the roll off factor is provided for the proposed method. We concluded that, with usage of

RRC filters with low roll off factor has high reduction in BER. Eventually the proposed algorithm in this work combats both channel induced distortions effects as well as effectively estimates the CFO. Additionally, in this chapter, the real time prototyping of the MGFDM system using windowed preamble is performed and the spectrum characteristics of multitaper filters are investigated. This chapter also provides an insight into impact of oversampling on jitter noise behaviour. We observed significant improvement in the performance due to mitigation of jitter noise power effect by oversampling in simulations and mathematical analysis. The constellation diagrams at the receiver validate the result by showing a good agreement with the obtained results.

We have proposed three modified SLM schemes for reducing high computational complexity of GFDM-SLM system. The proposed methods use the concepts of linearity, conversion matrix and shifting matrix by retaining the PAPR performance when compared with conventional SLM scheme. Since the CCRR increases with increase in number of phase sequences, all the proposed schemes are efficient and can be used in practical implementations of GFDM system depending on application. The effect of roll off factor on PAPR is provided for GFDM system with RRC as prototyping filter. We inferred from simulation results that, high roll off factor for RRC filters results in significant reduction in PAPR. This thesis investigates a joint PAPR reduction and data decoding technique using subsymbol based phase modulation with a slight modification in the traditional SLM scheme. In comparison with the traditional SLM scheme the proposed method achieves identical performance at higher GFDM block sizes. In the receiver, the suggested subsymbol based data detection does not need any SI estimation. As a consequence, it eliminates the associated computational complexity. The simulation results show that the BER performance of the method is not degraded when compared with methods that use perfect SI estimation. A good comparison of PAPR analysis between conventional GFDM with RRC pulse shaping filter by varying the roll off factor is provided. We concluded that, with usage of RRC filters with high roll off factor results in significant reduction in PAPR at the cost of BER performance. For practical validation of the above proposed theory, an experimental setup is done using USRP RIO as a RF front end and Labview as software for baseband processing. The obtained experimental results suggest the significant reduction in out-of-band spectral leakage without disturbing the estimated channel response under indoor channel environments. Therefore the proposed method

reduce PAPR in systems and makes the GFDM system more attractive as a contender for 5G communication.

6.2 Future scope

In this thesis several aspects, facts and issues related to the novel multicarrier technique GFDM are well investigated. The suggestions/opportunities for continuing research studies are mentioned below

- The short burst transmission which is possible with GFDM is a good sign for IoT applications but the complex receiver structure of GFDM is an concerning issue and it would be interesting to design a simpler receiver.
- Proving the effect of the log-normal shadowing mathematically with suitable parameter analysis could be a reasonable issue to be addressed. Meanwhile, handling interference and proposing methods for interference cancellation is another topic of interest worthy exploring.
- Another valuable research area that could be interesting is to propose different methodologies for allocating resources smartly to huge number of users within a GFDM block so as to minimize multiuser interferences of a network.
- Choosing variable block size structure optimally suitable for adverse channel conditions and exploring optimization methods for power allocations can be developed.
- The performance of GFDM can be improved by employing various diversity concepts and because of its ease in MIMO implementation compared to other 5G physical layer candidates.

Publications

List of International Journals:

1. **Sivaprasad Valluri**, Venkata Mani Vakamulla, "Joint channel mitigation and side information estimation for GFDM systems in indoor environments ", *AEU - International Journal of Electronics and Communications,* ***2018.*** *Vol.95, Pg.146-154* ***(SCI-Elsevier)***

2. ***Sivaprasad Valluri****, Venkata Mani Vakamulla, "A novel approach for reducing complexity in the SLM-GFDM system", Physical Communication,, 2019. Vol.34,, Pg.188-195* ***(SCI-Elsevier)***

3. ***Sivaprasad Valluri****, Venkata Mani Vakamulla, "Investigation of blind CFO estimation for GFDM System using USRP: Theory, Simulations and Experiments", IET Communications,* ***2019.*** *Vol.13,, Pg.1936-1944* ***(SCI-IET)***

List of International Conferences:

1. **S. P. valluri**, V.V. Mani,"A novel blind STO estimation for UW-GFDM systems," 2018 *International Conference on Advanced Technologies for Communications (ATC), Ho Chi Minh City, 2018, pp. 115-119.*

2. ***S. P. valluri****, V.V. Mani,"Demonstration of effect of oversampling on jitter removal for Multitaper GFDM system using SDR," 2018 International Conference on Advanced Technologies for Communications (ATC), Ho Chi Minh City, 2018, pp. 168-173.*

3. ***S. P. valluri**, V.V. Mani, "Receiver design for UW-GFDM systems," 2018 21st International Symposium on Wireless Personal Multimedia Communications (WPMC), Chiang Rai, Thailand, 2018, pp. 588-593.*

List of articles under review:

---

1. **Sivaprasad Valluri**, Venkata Mani Vakamulla, "Implementation of synchronized GFDM using USRP". **(First revision completed) AEU - International Journal of Electronics and Communications**

2. **Sivaprasad Valluri**, Venkata Mani Vakamulla, "An improved GFDM SLM modulator for 5G systems". **(under review) International Journal of Communication Systems**

Bibliography

[1] "Progress of multi-band antenna technology in mobile phone industry," in *IEE Wideband and Multi-band Antennas and Arrays 2005 (Ref. No. 2005/11059)*, Sep. 2005, pp. 1–5.

[2] Ji-Woong Choi and Yong-Hwan Lee, "Optimum pilot pattern for channel estimation in OFDM systems," *IEEE Transactions on Wireless Communications*, vol. 4, no. 5, pp. 2083–2088, Sep. 2005.

[3] T. Aoki and M. Sandell, "Analysis of pilots for residual frequency offset estimation in MIMO OFDM systems," *IEEE Transactions on Wireless Communications*, vol. 8, no. 3, pp. 1128–1132, March 2009.

[4] V. Kishore and V. Mani, "A DC biased optical generalised frequency division multiplexing for IM/DD systems," *Physical Communication*, vol. 33, pp. 115 – 122, 2019. [Online]. Available: `http://www.sciencedirect.com/science/article/pii/S1874490718303380`

[5] A. Toskala, *LTE and LTE Advanced in Releases 8-11*. John Wiley & Sons Ltd, 2015.

[6] R. Chen and J. Zheng, "Index-modulated MIMO-OFDM: Joint space-frequency signal design and linear precoding in rapidly time-varying channels," *IEEE Transactions on Wireless Communications*, vol. 17, no. 10, pp. 7067–7079, Oct 2018.

[7] 3GPP, "TS36.212: Evolved Universal Terrestrial Radio Access (E-UTRA); Multiplexing and channel coding (Release 10), V10.8.0," Tech. Rep., June, 2013.

[8] T. Hwang, C. Yang, G. Wu, S. Li, and G. Y. Li, "OFDM and Its Wireless Applications: A Survey," *IEEE Transactions on Vehicular Technology*, vol. 58, no. 4, pp. 1673–1694, May 2009.

[9] S. Gao, M. Zhang, and X. Cheng, "Precoded index modulation for multi-input multi-output OFDM," *IEEE Transactions on Wireless Communications*, vol. 17, no. 1, pp. 17–28, Jan 2018.

[10] M. M. Wang, L. Xiao, T. Brown, and M. Dong, "Optimal symbol timing for OFDM wireless communications," *IEEE Transactions on Wireless Communications*, vol. 8, no. 10, pp. 5328–5337, October 2009.

[11] M. Marey and O. A. Dobre, "Automatic identification of space-frequency block coding for OFDM systems," *IEEE Transactions on Wireless Communications*, vol. 16, no. 1, pp. 117–128, Jan 2017.

[12] S. Dang, G. Chen, and J. P. Coon, "Lexicographic codebook design for OFDM with index modulation," *IEEE Transactions on Wireless Communications*, vol. 17, no. 12, pp. 8373–8387, Dec 2018.

[13] K. Kim and H. Kim, "An ICI suppression scheme based on the correlative coding for alamouti SFBC-OFDM system with phase noise," *IEEE Transactions on Wireless Communications*, vol. 10, no. 7, pp. 2023–2027, July 2011.

[14] D. Na and K. Choi, "Intrinsic ICI-free alamouti coded FBMC," *IEEE Communications Letters*, vol. 20, no. 10, pp. 1971–1974, Oct 2016.

[15] Y. Chung and S. Phoong, "Channel estimation in the presence of transmitter and receiver I/Q mismatches for OFDM systems," *IEEE Transactions on Wireless Communications*, vol. 8, no. 9, pp. 4476–4479, Sep. 2009.

[16] J. G. Andrews, S. Buzzi, W. Choi, S. V. Hanly, A. Lozano, A. C. K. Soong, and J. C. Zhang, "What will 5G be?" *IEEE Journal on Selected Areas in Communications*, vol. 32, no. 6, pp. 1065–1082, June 2014.

[17] A. Osseiran, F. Boccardi, V. Braun, K. Kusume, P. Marsch, M. Maternia, O. Queseth, M. Schellmann, H. Schotten, H. Taoka *et al.*, "Scenarios for 5G mobile and

wireless communications: the vision of the METIS project," *IEEE Communications Magazine*, vol. 52, no. 5, pp. 26–35, 2014.

[18] Y. Niu, Y. Li, D. Jin, L. Su, and A. V. Vasilakos, "A survey of millimeter wave communications (mmwave) for 5G: opportunities and challenges," *Wireless Networks*, vol. 21, no. 8, pp. 2657–2676, Nov 2015.

[19] T. S. Rappaport, Y. Xing, G. R. MacCartney, A. F. Molisch, E. Mellios, and J. Zhang, "Overview of millimeter wave communications for fifth-generation (5g) wireless networks-with a focus on propagation models," *IEEE Transactions on Antennas and Propagation*, 2017.

[20] A. Kammoun, M. Debbah, M.-S. Alouini *et al.*, "Design of 5G Full Dimension Massive MIMO systems," *IEEE Transactions on Communications*, 2017.

[21] L. Lu, G. Y. Li, A. L. Swindlehurst, A. Ashikhmin, and R. Zhang, "An overview of massive MIMO: Benefits and challenges," *IEEE journal of selected topics in signal processing*, vol. 8, no. 5, pp. 742–758, 2014.

[22] S. K. Bandari, A. Drosopoulos, and V. V. Mani, "Exact ser expressions of GFDM in nakagami-m and rician fading channels," in *Proceedings of European Wireless 2015; 21th European Wireless Conference*, May 2015, pp. 1–6.

[23] N. Michailow, M. Matth, I. S. Gaspar, A. N. Caldevilla, L. L. Mendes, A. Festag, and G. Fettweis, "Generalized frequency division multiplexing for 5th generation cellular networks," *IEEE Transactions on Communications*, vol. 62, no. 9, pp. 3045–3061, Sept 2014.

[24] A. Farhang, N. Marchetti, and L. E. Doyle, "Low-complexity modem design for GFDM," *IEEE Transactions on Signal Processing*, vol. 64, no. 6, pp. 1507–1518, March 2016.

[25] V. Kishore and V. Mani, "An LED modelled GFDM for optical wireless communications," *AEU - International Journal of Electronics and Communications*, vol. 101, pp. 54 – 61, 2019. [Online]. Available: http://www.sciencedirect.com/science/article/pii/S143484111832137X

[26] S. K. Bandari, V. V. Mani, and A. Drosopoulos, "Multi-taper implementation of GFDM," in *2016 IEEE Wireless Communications and Networking Conference*, April 2016, pp. 1–5.

[27] M. Huemer, C. Hofbauer, A. Onic, and J. B. Huber, "Design and analysis of UW-OFDM signals," *AEU - International Journal of Electronics and Communications*, vol. 68, no. 10, pp. 958 – 968, 2014. [Online]. Available: http://www.sciencedirect.com/science/article/pii/S1434841114001149

[28] J. T. Dias and R. C. de Lamare, "Unique-word GFDM transmission systems," *IEEE Wireless Communications Letters*, vol. 6, no. 6, pp. 746–749, Dec 2017.

[29] S. P. Valluri and V. V. Mani, "Receiver design for UW-GFDM systems," in *2018 21st International Symposium on Wireless Personal Multimedia Communications (WPMC)*, Nov 2018, pp. 588–593.

[30] N. Michailow, M. Lentmaier, P. Rost, and G. Fettweis, "Integration of a GFDM secondary system in an OFDM primary system," in *2011 Future Network Mobile Summit*, June 2011, pp. 1–8.

[31] R. Datta, N. Michailow, M. Lentmaier, and G. Fettweis, "GFDM interference cancellation for flexible cognitive radio phy design," in *2012 IEEE Vehicular Technology Conference (VTC Fall)*, Sept 2012, pp. 1–5.

[32] D. Panaitopol, R. Datta, and G. Fettweis, "Cyclostationary detection of cognitive radio systems using GFDM modulation," in *2012 IEEE Wireless Communications and Networking Conference (WCNC)*, April 2012, pp. 930–934.

[33] R. Zakaria and D. Le Ruyet, "Theoretical analysis of the power spectral density for fft-fbmc signals," *IEEE Communications Letters*, vol. 20, no. 9, pp. 1748–1751, Sep. 2016.

[34] P. Wei, X. Xia, Y. Xiao, and S. Li, "Fast DGT-based receivers for GFDM in broadband channels," *IEEE Transactions on Communications*, vol. 64, no. 10, pp. 4331–4345, Oct 2016.

[35] B. Lim and Y. C. Ko, "SIR analysis of OFDM and GFDM waveforms with timing offset, CFO and phase noise," *IEEE Transactions on Wireless Communications*, vol. PP, no. 99, pp. 1–1, 2017.

[36] S. S. Das and S. Tiwari, "Discrete fourier transform spreading-based generalised frequency division multiplexing," *Electronics Letters*, vol. 51, no. 10, pp. 789–791, 2015.

[37] S. Tiwari, S. Sekhar Das, and K. K. Bandyopadhyay, "Precoded generalised frequency division multiplexing system to combat inter-carrier interference: performance analysis," *IET Communications*, vol. 9, no. 15, pp. 1829–1841, 2015.

[38] S. Tiwari and S. S. Das, "Low-complexity joint-mmse gfdm receiver," *IEEE Transactions on Communications*, vol. 66, no. 4, pp. 1661–1674, April 2018.

[39] R. O'Donnell, "Prolog to synchronization techniques for orthogonal frequency division multiple access (OFDMA): A tutorial review," *Proceedings of the IEEE*, vol. 95, no. 7, pp. 1392–1393, July 2007.

[40] J. J. van de Beek, M. Sandell, and P. O. Borjesson, "Ml estimation of time and frequency offset in OFDM systems," *IEEE Transactions on Signal Processing*, vol. 45, no. 7, pp. 1800–1805, Jul 1997.

[41] T. M. Schmidl and D. C. Cox, "Robust frequency and timing synchronization for OFDM," *IEEE Transactions on Communications*, vol. 45, no. 12, pp. 1613–1621, Dec 1997.

[42] B. Park, H. Cheon, C. Kang, and D. Hong, "A novel timing estimation method for OFDM systems," *IEEE Communications Letters*, vol. 7, no. 5, pp. 239–241, May 2003.

[43] H. Minn, V. K. Bhargava, and K. B. Letaief, "A robust timing and frequency synchronization for OFDM systems," *IEEE Transactions on Wireless Communications*, vol. 2, no. 4, pp. 822–839, July 2003.

[44] J. Mohammadi-Siahboomi, M. J. Omidi, and H. Saeedi-Sourck, "Low-complexity CFO compensation technique for interleaved OFDMA system uplink," *AEU - Inter-*

national Journal of Electronics and Communications, vol. 70, no. 5, pp. 718 – 726, 2016.

[45] P. S. Wang and D. W. Lin, "Maximum-likelihood blind synchronization for GFDM systems," *IEEE Signal Processing Letters*, vol. 23, no. 6, pp. 790–794, June 2016.

[46] I. Gaspar, A. Festag, and G. Fettweis, "Synchronization using a pseudo-circular preamble for generalized frequency division multiplexing in vehicular communication," in *2015 IEEE 82nd Vehicular Technology Conference (VTC2015-Fall)*, Sept 2015, pp. 1–5.

[47] T. Kim and S. Park, "A new symbol timing and frequency synchronization design for OFDM-based WLAN systems," in *The 9th International Conference on Advanced Communication Technology*, vol. 3, Feb 2007, pp. 1669–1672.

[48] M. M. U. Gul, X. Ma, and S. Lee, "Timing and frequency synchronization for OFDM downlink transmissions using zadoff-chu sequences," *IEEE Transactions on Wireless Communications*, vol. 14, no. 3, pp. 1716–1729, March 2015.

[49] J. J. Popoola and R. van Olst, "The performance evaluation of a spectrum sensing implementation using an automatic modulation classification detection method with a universal software radio peripheral," *Expert Systems with Applications*, vol. 40, no. 6, pp. 2165 – 2173, 2013. [Online]. Available: `http://www.sciencedirect.com/science/article/pii/S0957417412011712`

[50] D. Yang, J. Si, Z. Li, N. C. Beaulieu, J. Zhu, F. Zhou, and B. Hao, "Blind carrier frequency offset estimation for single carrier and orthogonal frequency division multiplexing signals using least-order cyclic moments," *IET Communications*, vol. 10, no. 6, pp. 669–676, 2016.

[51] S. Wu and Y. Bar-Ness, "A phase noise suppression algorithm for OFDM-based wlans," *IEEE Communications Letters*, vol. 6, no. 12, pp. 535–537, Dec 2002.

[52] W. Zhang and Q. Yin, "Blind carrier frequency offset estimation for tile-based orthogonal frequency division multiple access uplink with multi-antenna receiver," *IET Communications*, vol. 8, no. 8, pp. 1309–1316, May 2014.

[53] D. Gaspar, L. Mendes, and T. Pimenta, "GFDM BER under synchronization errors," *IEEE Communications Letters*, vol. 21, no. 8, pp. 1743–1746, Aug 2017.

[54] Z. Na, M. Zhang, M. Xiong, J. Xia, X. Liu, and W. Lu, "Pseudo-noise sequence based synchronization for generalized frequency division multiplexing in 5G communication system," *IEEE Access*, vol. 6, pp. 14 812–14 819, 2018.

[55] S. Valluri and V. Mani, "Joint channel mitigation and side information estimation for GFDM systems in indoor environments," *AEU - International Journal of Electronics and Communications*, vol. 95, pp. 146 – 154, 2018. [Online]. Available: http://www.sciencedirect.com/science/article/pii/S1434841118306915

[56] X. Zhu, J. Xia, H. Li, and H. Hu, "Ultimate performance of clipping and filtering techniques for PAPR reduction in OFDM systems," in *2013 IEEE 24th Annual International Symposium on Personal, Indoor, and Mobile Radio Communications (PIMRC)*, Sept 2013, pp. 782–785.

[57] M. F. Naeiny and F. Marvasti, "PAPR reduction of space-frequency coded OFDM systems using active constellation extension," *AEU - International Journal of Electronics and Communications*, vol. 65, no. 10, pp. 873 – 878, 2011. [Online]. Available: http://www.sciencedirect.com/science/article/pii/S1434841111000458

[58] R. J. Baxley and G. T. Zhou, "Comparing selected mapping and partial transmit sequence for PAR reduction," *IEEE Transactions on Broadcasting*, vol. 53, no. 4, pp. 797–803, Dec 2007.

[59] H. S. Joo, K. H. Kim, J. S. No, and D. J. Shin, "New PTS schemes for PAPR reduction of OFDM signals without side information," *IEEE Transactions on Broadcasting*, vol. 63, no. 3, pp. 562–570, Sept 2017.

[60] A. D. S. Jayalath and C. Tellambura, "SLM and PTS peak-power reduction of OFDM signals without side information," *IEEE Transactions on Wireless Communications*, vol. 4, no. 5, pp. 2006–2013, Sept 2005.

[61] W.-W. Hu, "PAPR reduction for pilot-aided OFDM systems with the parametric minimum cross-entropy method," *AEU - International Journal of Electronics*

and Communications, vol. 70, no. 3, pp. 367 – 371, 2016. [Online]. Available: http://www.sciencedirect.com/science/article/pii/S1434841115003337

[62] J. Park, E. Hong, and D. Har, "Low complexity data decoding for SLM-based OFDM systems without side information," *IEEE Communications Letters*, vol. 15, no. 6, pp. 611–613, June 2011.

[63] E. Hong, H. Kim, K. Yang, and D. Har, "Pilot-aided side information detection in SLM-based OFDM systems," *IEEE Transactions on Wireless Communications*, vol. 12, no. 7, pp. 3140–3147, July 2013.

[64] S. H. Han and J. H. Lee, "An overview of peak-to-average power ratio reduction techniques for multicarrier transmission," *IEEE Wireless Communications*, vol. 12, no. 2, pp. 56–65, April 2005.

[65] D.-W. Lim, S.-J. Heo, J.-S. No, and H. Chung, "On the phase sequence set of SLM OFDM scheme for a crest factor reduction," *IEEE Transactions on Signal Processing*, vol. 54, no. 5, pp. 1931–1935, May 2006.

[66] G. H. Golub and C. F. V. Loan, *Matrix Computation*, 2nd ed. Baltimore, MD: The Johns Hopkins Univ. Press, 1989.

[67] S. P. valluri and V. V. Mani, "A novel blind STO estimation for UW-GFDM systems," in *2018 International Conference on Advanced Technologies for Communications (ATC)*, Oct 2018, pp. 115–119.

[68] T. J. Lee and Y. C. Ko, "Channel estimation and data detection in the presence of phase noise in MIMO-OFDM systems with independent oscillators," *IEEE Access*, vol. 5, pp. 9647–9662, 2017.

[69] L. Yang, P. Fitzpatrick, and J. Armstrong, "The effect of timing jitter on high-speed OFDM systems," in *2009 Australian Communications Theory Workshop*, Feb 2009, pp. 12–16.

[70] J. Woo, H. S. Joo, K. Kim, J. No, and D. Shin, "PAPR analysis of class-iii SLM scheme based on variance of correlation of alternative OFDM signal sequences," *IEEE Communications Letters*, vol. 19, no. 6, pp. 989–992, June 2015.

[71] M. Matthe, I. Gaspar, D. Zhang, and G. Fettweis, "Reduced complexity calculation of LMMSE filter coefficients for GFDM," in *2015 IEEE 82nd Vehicular Technology Conference (VTC2015-Fall)*, Sept 2015, pp. 1–2.

[72] M. Danneberg, R. Datta, A. Festag, and G. Fettweis, "Experimental testbed for 5G cognitive radio access in 4g lte cellular systems," in *2014 IEEE 8th Sensor Array and Multichannel Signal Processing Workshop (SAM)*, June 2014, pp. 321–324.

[73] S. P. valluri and V. V. Mani, "Demonstration of effect of oversampling on jitter removal for multitaper GFDM system using SDR," in *2018 International Conference on Advanced Technologies for Communications (ATC)*, Oct 2018, pp. 168–173.